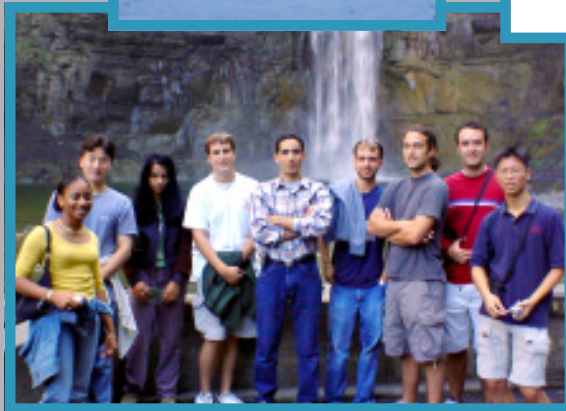
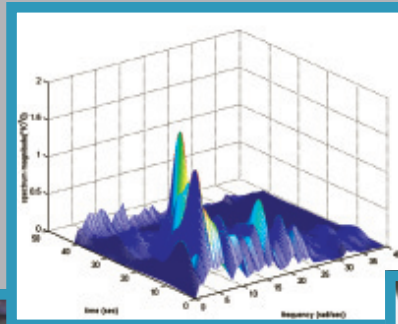
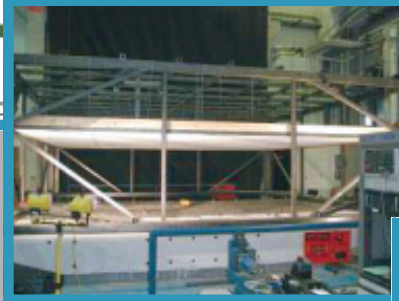
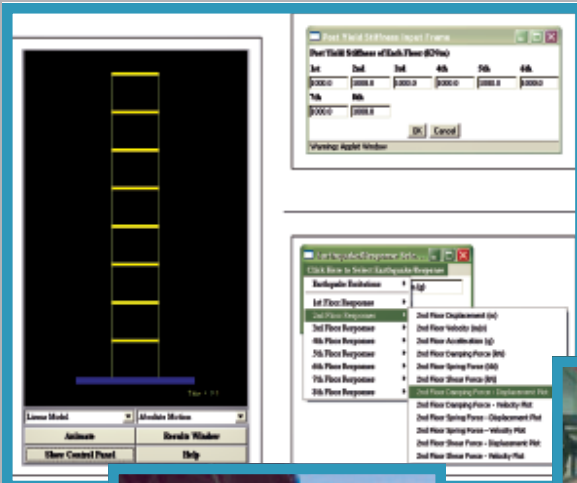
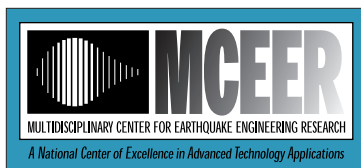


Student Research Accomplishments 2002 – 2003





The Multidisciplinary Center for Earthquake Engineering Research

The Multidisciplinary Center for Earthquake Engineering Research (MCEER) is a national center of excellence in advanced technology applications that is dedicated to the reduction of earthquake losses nationwide. Headquartered at the University at Buffalo, State University of New York, the Center was originally established by the National Science Foundation (NSF) in 1986, as the National Center for Earthquake Engineering Research (NCEER).

Comprising a consortium of researchers from numerous disciplines and institutions throughout the United States, the Center's mission is to reduce earthquake losses through research and the application of advanced technologies that improve engineering, pre-earthquake planning and post-earthquake recovery strategies. Toward this end, the Center coordinates a nationwide program of multidisciplinary team research, education and outreach activities.

Funded principally by NSF, the State of New York and the Federal Highway Administration (FHWA), the Center derives additional support from the Federal Emergency Management Agency (FEMA), other state governments, academic institutions, foreign governments and private industry.

Student Research Accomplishments

2002-2003

Multidisciplinary Center for Earthquake Engineering Research
University at Buffalo, State University of New York

Edited by Ramiro Vargas and Benedikt Halldorsson

November 2003

MCEER-03-SP06

Red Jacket Quadrangle, Buffalo, New York 14261

Phone: (716) 645-3391; Fax: (716) 645-3399

E-mail: mceer@mceermail.buffalo.edu

World Wide Web: <http://mceer.buffalo.edu>

Foreword

The Student Leadership Council (SLC) is a formal incarnation of the students who are involved in performing MCEER research under a faculty advisor. Since its inception, MCEER has included and encouraged student efforts throughout its research program and in all of the disciplinary specialties concerned with earthquake engineering.

Throughout the years, students have been an integral component in advancing research in earthquake hazard mitigation. Many former students are now employed in academia, professional practice or government agencies applying knowledge gained during their exposure to MCEER research. While associated with MCEER, students participate in Center annual meetings, attend conferences, workshops and seminars, and have the opportunity to make presentations at these events. The SLC was formed in the year 2000 to formalize these programs and to afford students from many different institutions the opportunity to meet with each other and develop/improve interaction.

The idea for the *Student Research Accomplishments* was conceived by the SLC and features the work of some of MCEER's current students. Topics range from traditional civil and lifeline engineering to applications of advanced technologies to social impacts and economic modeling.


This issue was coordinated and edited by Ramiro Vargas and co-edited by Benedikt Halldorsson, both Ph.D. candidates in the Department of Civil, Structural & Environmental Engineering at the University at Buffalo. Past editors were Diego Lopez Garcia, Department of Civil, Structural and Environmental Engineering, University at Buffalo, and Gauri Guha, Department of Energy, Environmental and Mineral Economics, the Pennsylvania State University.

This year marked the first *Best Student Article Competition*. Members of MCEER's Industry Advisory Board (IAB) judged the 16 submissions, and selected a winner and three honorable mentions. We congratulate Michael Pollino, University of Buffalo, who was awarded first prize, and Hiram Badillo-Alvarez, University of Buffalo, Zehra Cagnan, Cornell University and Yong Gao, University of Illinois at Urbana-Champaign, who received honorable mentions for their outstanding efforts. All four students were invited to present their research at the 2004 MCEER Annual Meeting. Our thanks go to Sreenivas Alampalli, New York State Department of Transportation, Paul Hough, Armstrong World Industries, Jeremy Isenberg, Weidlinger Associates, Amarnath Kasalanati, Dynamic Isolation Systems, Jon Mochizuki, City of Los Angeles Dept. of Water and Power, and Jean-Robert Pierre, Transenergie Hydro Quebec for their reviews and recommendations.


Finally, MCEER wishes to extend its thanks to the Student Leadership Council for its endeavors, and in particular to Jeffrey Berman, current president, and A. Natali Sigaher, past president, for their able guidance of the SLC.


Best Student Article Competition: 2003

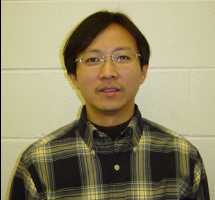
Winner

| | |
|---|---|
|  | Michael Pollino |
| | <i>Graduate Student, Department of Civil, Structural & Environmental Engineering, University at Buffalo</i> <i>Research Supervisor: Michel Bruneau, Professor and Director of MCEER</i> Seismic Retrofit of Bridge Steel Truss Pier Anchorage Connections page 51 |

Honorable Mentions

| | |
|--|---|
|  | Hiram Badillo-Almaraz |
| | <i>Graduate Student, Department of Civil, Structural & Environmental Engineering, University at Buffalo</i> <i>Research Supervisor: Andrew S. Whittaker, Associate Professor</i> Seismic Fragility Testing of Suspended Ceiling Systems page 67 |

| | |
|---|--|
|  | Zehra Cagnan |
| | <i>Graduate Student, School of Civil and Environmental Engineering, Cornell University</i> <i>Research Supervisor: Rachel Davidson, Assistant Professor</i> Post-Earthquake Lifeline Service Restoration Modeling page 101 |

| | |
|---|---|
|  | Yong Gao |
| | <i>Graduate Student, Department of Civil & Environmental Engineering, University of Illinois at Urbana-Champaign</i> <i>Research Supervisor: Billie F. Spencer, Jr., Nathan M. Newmark Professor</i> Java-Powered Virtual Laboratory for Nonlinear Structural Dynamic Analysis page 9 |

Contents

Seismic Design and Analysis of Structures

| | | |
|---|--|----|
| 1 | Cyclic Testing of Light-Gauge Steel Plate Sheer Walls <i>Jeffrey W. Berman, University at Buffalo</i> | 1 |
| 2 | Java-Powered Virtual Laboratory for Nonlinear Structural Dynamic Analysis <i>Yong Gao, University of Illinois at Urbana-Champaign</i> | 9 |
| 3 | Response of Elastic and Inelastic Structures with Damping Systems to Near-Field and Soft-Soil Ground Motions <i>Eleni Pavlou, University at Buffalo</i> | 15 |
| 4 | Advanced Time-Frequency Analysis Applications in Earthquake Engineering <i>Nikolaos P. Politis, Rice University</i> | 23 |
| 5 | Experimental and Analytical Study of Seismically Isolated Structures with Uplift Prevention <i>Panayiotis C. Roussis, University at Buffalo</i> | 31 |
| 6 | Evolutionary Power Spectrum Estimation using Harmonic Wavelets <i>Jale Tezcan, Rice University</i> | 37 |
| 7 | Seismic Response of Single Degree of Freedom Systems with Structural Fuses <i>Ramiro E. Vargas, University at Buffalo</i> | 43 |

Seismic Design and Analysis of Bridges

| | | |
|---|--|----|
| 8 | Seismic Retrofit of Bridge Steel Truss Pier Anchorage Connections <i>Michael Pollino, University at Buffalo</i> | 51 |
| 9 | Performance Estimates in Seismically Isolated Bridge Structures <i>Gordon P. Warn, University at Buffalo</i> | 59 |

Seismic Design and Analysis of Nonstructural Building Components

| | | |
|----|---|----|
| 10 | Seismic Fragility Testing of Suspended Ceiling Systems <i>Hiram Badillo-Almaraz, University at Buffalo</i> | 67 |
| 11 | Seismic Behavior of Welded Hospital Piping Systems <i>Elliott Goodwin, University of Nevada, Reno</i> | 73 |

Contents (Cont'd)

| | | |
|----|--|----|
| 12 | Advanced Composite Multi-infill Panels for Seismic Retrofitting <i>Wooyoung Jung, University at Buffalo</i> | 81 |
| 13 | Seismic Performance Assessment by Fragility and Loss Estimation <i>Cagdas Kafali, Cornell University</i> | 89 |

Seismic Design and Analysis of Lifeline Systems

| | | |
|----|---|-----|
| 14 | Issues of Seismic Response and Retrofit for Critical Substation Equipment <i>Ali Ashrafi, New Jersey Institute of Technology</i> | 95 |
| 15 | Post-earthquake Lifeline Service Restoration Modeling <i>Zehra Cagnan, Cornell University</i> | 101 |
| 16 | Fragility Analysis of Water Supply System <i>Anita Jacobson, Cornell University</i> | 107 |

Cyclic Testing of Light-Gauge Steel Plate Shear Walls

Jeffrey W. Berman

Graduate Student, Department of Civil, Structural & Environmental Engineering, University at Buffalo

Research Supervisor: Michel Bruneau, Professor and Director of MCEER

Summary

This paper describes the prototype design, specimen design, experimental set-up, and experimental results of tests on three light-gauge steel plate shear wall (SPSW) concepts. Prototype light-gauge steel plate shear walls are designed as seismic retrofits for a hospital structure in an area of high seismicity and emphasis is placed on minimizing their impact on the existing framing. Three single story test specimens are designed using these prototypes as a basis, two specimens with flat infill plates (thicknesses of 0.9 mm) and a third using a corrugated infill plate (thickness of 0.7 mm). Connection of the infill plates to the boundary frames is achieved through the use of bolts in combination with industrial strength epoxy or welds, allowing for mobility of the infills if desired. Testing of the systems is done under quasi-static conditions. It is shown that one of the flat infill plate specimens, as well as the specimen utilizing a corrugated infill plate, achieve significant ductility and energy dissipation while minimizing the demands placed on the surrounding framing. Experimental results are compared to monotonic pushover predictions from computer analysis using a simple model and good agreement is observed.

Introduction

Light-gauge steel plate shear walls could provide engineers with an effective option for the seismic retrofit of older buildings. The concept is to create a system that is strong enough to resist the necessary seismic forces and yet light enough to avoid having to heavily reinforce existing framing due to the increased demands the retrofit strategy may place on it. Furthermore, an interest exists in creating systems that could be installed with minimum disruption to the function and occupants of an existing building, and, in the context of the seismic retrofit of hospitals, that could be modular to facilitate relocation of the light-gauge infills as floor plans are rearranged (something that often occurs in hospitals). This paper describes the design and quasi-static testing of three such light-gauge steel plate shear wall systems. Specimen design is based on accepted analytical representations for steel plate shear walls which, when allowed to buckle in shear and form a diagonal tension field, have been shown to be a useful seismic energy dissipation system. (Timler and Kulak, 1983, Driver et al., 1997, Elgaaly 1998, Rezaei 1999, etc.)

Prototype Design

Two prototype light-gauge steel plate shear walls were designed as seismic retrofit options for a prototype demonstration hospital (Yang and Whittaker, 2002). This hospital is a four-story steel framed building with plan dimensions of 83.5 meters in the east-west direction and 17.2 meters in

the north-south direction. The test specimens were designed to retrofit the north-south frames and they included the flexible web-angle beam-to-column connections. To minimize the forces applied to the existing framing by the yielding infill plates (i.e., to avoid having to strengthen the existing columns), it was decided that every line of gravity framing in the north-south direction would be retrofitted. The middle bay (between framing lines 3 and 4) was arbitrarily chosen as the location for the retrofit on each frame line.

The equivalent lateral force procedure of FEMA 302 (FEMA 1997) was used to calculate a design base shear. Tributary gravity loads for one bay of north-south framing were determined. These and a portion of the design live load were used as the active seismic weight for a single gravity frame line. The resulting seismic coefficient, C_s , was determined to be 0.58 and the corresponding base shear tributary to one of the gravity frames was approximately 1420 kN.

For the calculated design base shear, plate thicknesses for both flat and corrugated plate scenarios were found using the procedure described in Berman and Bruneau (2003a). This procedure is based on development of the plastic collapse mechanisms for the strip model, formulated by Timler and Kulak (1983), and implemented in a steel design standard (Figure 1). Minimum required plate thicknesses at the first floor level were found to be 22 Gauge (0.75 mm or 0.0295 in) for the corrugated infill plate (assuming a corrugation profile equal to that of Type B steel deck), and 20 Gauge (1.0 mm or 0.0396 in.) for the flat infill plates. A yield stress of 380 MPa (55 ksi) was assumed in both cases. Note that tension field action can only develop in the direction parallel to the corrugations, and that pairs of retrofitted bays (with corrugations oriented in opposite directions) are required to implement this system.

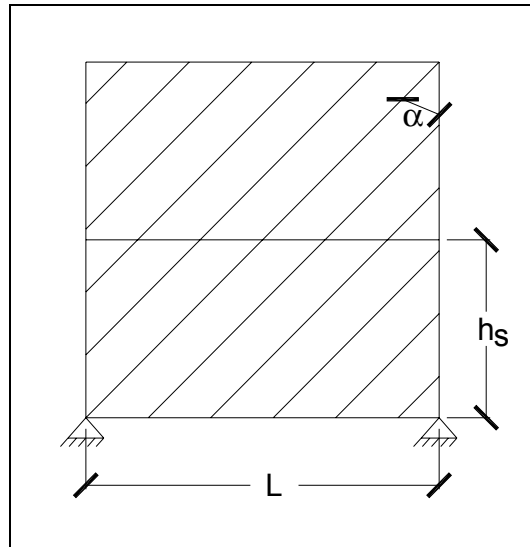


Figure 1. Example of Generic Strip model

Test Specimen Design

Using the prototype designs as a basis, three light-gauge steel plate shear wall specimens were designed for quasi-static testing in the Structural Engineering and Earthquake Simulation Laboratory

(SEESL) at the University at Buffalo (two flat infill plate specimens with different infill-to-boundary frame connections, and one corrugated specimen). The infill plate thicknesses for the specimens were selected to be identical to those for the prototype retrofits for the demonstration hospital. The 2:1 (L:h) aspect ratio of the prototype was also maintained for the specimens. The bay width and story height of the specimens were designed to be 3660 mm (12 ft.) and 1830 mm (6 ft.), respectively (i.e., approximately 1/2 scale from the prototypes).

Strip models of each specimen using a yield stress of 380 MPa for the infill material were developed and, using the results of pushover analyses, boundary frames for the infills were designed to remain elastic with a safety factor of 2.5, resulting in W 310 x 143 columns and W 460 x 128 beams. The beam-to-column connections using L 203 x 102 x 12.7 angles on both sides of the beam web were welded to the beam and bolted to the column flanges.

Connecting the infill plates to the surrounding frame members proved difficult and a number of different options were explored, some of which are detailed in Berman and Bruneau (2003b). In the case of the flat infills, two alternatives were developed which resulted in Specimens F1 and F2. To test the effectiveness of SPSW with corrugated infills, Specimen C1 was developed, in which the corrugated infill is connected to the boundary frame using the Hysol 9460 epoxy and intermediate L 152 x 102 x 19 angles. For more detailed information on the specimen design and infill connections used, see Berman and Bruneau (2003b).

The test setup is shown in Figure 2. Specimens are mounted on large clevises attached to a foundation beam, itself tensioned to the strong floor of the SEESL. Lateral load was applied at the top of the wall by a servo-controlled hydraulic actuator mounted between the specimen and a reaction frame. ATC 24 (ATC 1992) testing protocol was followed and Figures 3 and 4 show specimens F1 and C1 prior to testing.

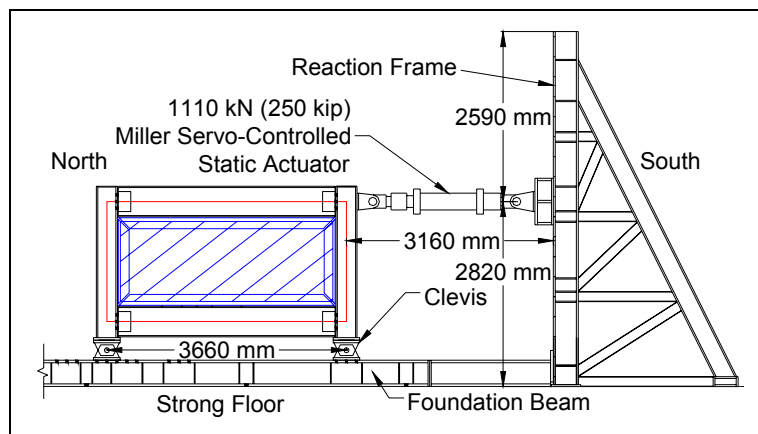


Figure 2. Test setup

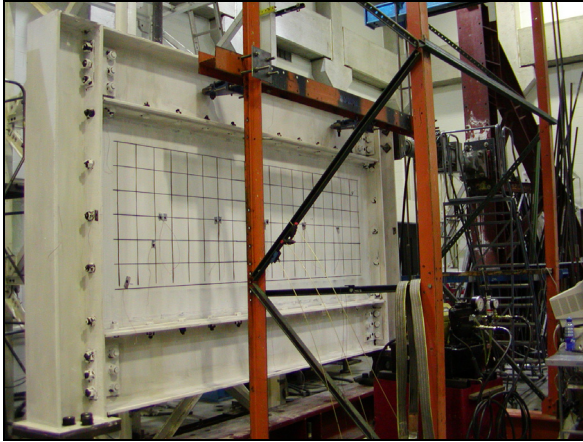


Figure 3. Specimen F1

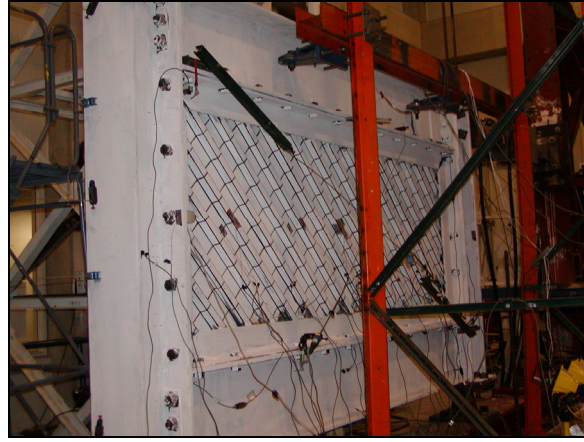


Figure 4. Specimen C1

Experimental Results

Despite the numerous ancillary tests that were performed to select an adequate connection configuration and epoxy, Specimen F1 suffered a premature failure of the epoxy during Cycle 7 at 0.25% drift while still exhibiting elastic behavior. The epoxy failed in the connection along the top beam of the specimen and the poor epoxy coverage is shown in Figure 5. Epoxy was directly applied to the infill plate only and not to the WT's, which could have contributed to cause this insufficient coverage. Qualitatively, this hypothesis was verified by the successful testing of Specimen C1, in which epoxy was applied to both the infill plate and intermediate angles.

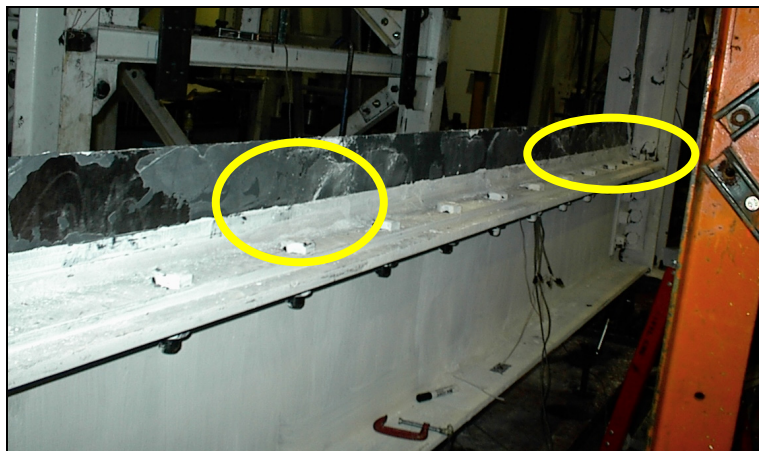


Figure 5. Poor epoxy coverage – Specimen F1

The hysteresis curves for Specimen C1 are shown in Figure 6 along with the monotonic pushover curve obtained from a strip model of the specimen using the measured material properties. Quantitative values of displacement ductility ratio, μ , and other key hysteretic response parameters are presented in Table 1. As shown, Specimen C1 reached a μ of 3 prior to losing substantial strength. Contribution of the infill to the total initial stiffness exceeded 90%. As expected, tension field action developed only in the direction parallel to the corrugations, resulting in unsymmetric hysteresis loops. Pinching of the hysteresis due to permanent plastic deformations of the infill is also apparent. This hysteretic behavior is similar to that of a braced frame with a single slender brace (Bruneau et al., 1997).

The epoxy connection of the infill plate to the boundary frame of specimen C1 cracked in some locations; however, according to strain gauge data, the entire plate yielded. This shows that epoxy connections are capable of developing yield forces in thin steel plates, although more research is needed to determine the reliability of such connections.

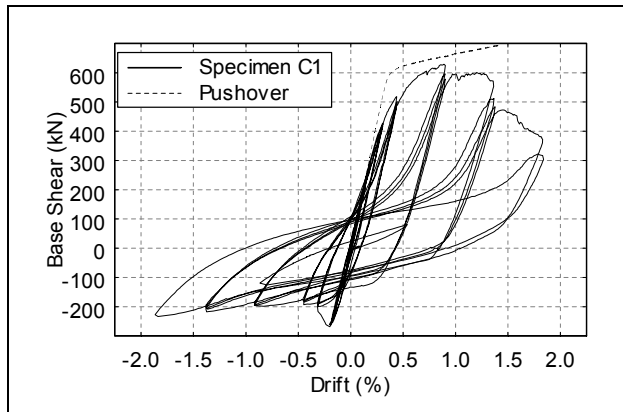


Figure 6. Specimen C1 hysteresis and pushover

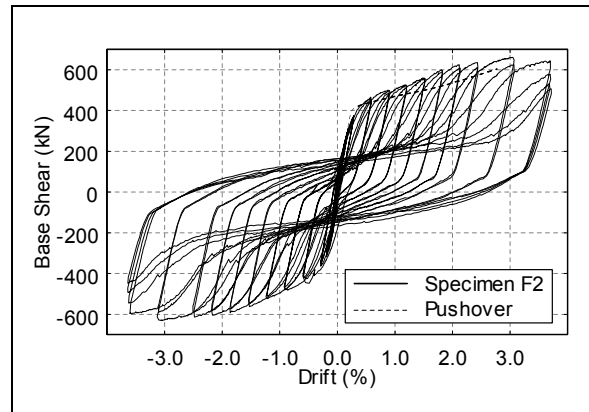


Figure 7. Specimen F2 hysteresis and pushover

Table 1. Hysteretic response values for all specimens

| Specimen ID | Total Initial Stiffness [kN/mm] | Initial Stiffness w/o Boundary Frame [kN/mm] | Yield Base Shear [kN] | Yield Disp. [mm] | Max Drift [%] | μ | Total Energy Diss. [kN-m] | Energy Diss. Infill Only [kN-m] |
|-------------|---------------------------------|--|-----------------------|------------------|---------------|-------|---------------------------|---------------------------------|
| F1 | 84 | 73 | 372 | 4.6 | 0.25 | 1 | NA | NA |
| C1 | 93 | 86 | 518 | 8 | 1.4 | 3 | 73 | 50 |
| F2 | 106 | 96 | 364 | 5.3 | 3.7 | 12 | 444 | 212 |

Stable and ductile behavior was observed in Specimen F2 as shown by the hysteresis loops of Figure 7. Also shown in Figure 7 is the monotonic pushover curve obtained from a strip model of the specimen. Reasonable agreement in terms of initial stiffness and yield base shear are evident. Specimen F2 reached a ductility ratio of 12 and drift of 3.7%, as shown in Table 1, prior to losing significant strength. Additionally, from the data presented in Table 1, the infill of Specimen F2 contributed approximately 90% of the initial stiffness of the system. The pinching exhibited by the hysteresis loops of Figure 7 is again due to the accumulation of non-recoverable plastic strains, a hysteretic behavior comparable to that of a concentrically braced frame having slender braces.

Conclusions

Three light-gauge steel plate shear wall specimens were designed and tested using quasi-static loading. Two of the specimens had flat infill plates, one with an epoxy connection to the boundary frame and one with a welded connection, while the third was designed with a corrugated infill plate and also utilized an epoxy connection to the boundary frame. Specimen design was based on prototype light-gauge steel plate shear walls, themselves designed as seismic retrofit options for a demonstration hospital. Two of the three specimens were shown to achieve the goals of increased stiffness, energy dissipation capability, and ductility of the existing framing, while using bolted connections detailed in a manner that provides a possibility to relocate the infills elsewhere in the building.

Though the hysteretic curves of the specimens were pinched, they were stable and provided significant energy dissipation in the cases of the specimens with the corrugated infill and the flat infill in which the welded connection was used (the former being significantly more ductile). Furthermore, the adequacy of the strip model in predicting the monotonic behavior of light-gauge steel plate shear walls into the nonlinear range was found to be acceptable through comparison with the experimental results. For more information, see Berman and Bruneau (2003b).

Acknowledgements

This research was carried out under the supervision of Dr. Michel Bruneau, and supported by the Earthquake Engineering Research Centers Program of the National Science Foundation, under award number EEC-9701471 to the Multidisciplinary Center for Earthquake Engineering Research.

References

- ATC (1992): *Guidelines for seismic testing of components of steel structures*. Report 24, Applied Technology Council, Redwood City, CA.
- Berman J, Bruneau M (2003a): Plastic analysis and design of steel plate shear walls. *Journal of Structural Engineering*, ASCE, **129**, (11), 1148-1156.
- Berman JW, Bruneau M (2003b): *Experimental investigation of light-gauge steel plate shear walls for the seismic retrofit of buildings*. Technical Report MCEER-03-0001, Multidisciplinary Center for Earthquake Engineering Research, Buffalo, NY.
- Bruneau M, Uang CM, and Whittaker A (1997): *Ductile design of steel structures*. McGraw-Hill, Inc., New York, NY.

Driver RG, Kulak GL, Kennedy DJL, and Elwi AE (1997): *Seismic behavior of steel plate shear walls*. Structural Engineering Report No. 215, Department of Civil Engineering, University of Alberta, Edmonton, Alberta, Canada.

Elgaaly M (1998): Thin steel plate shear walls behavior and analysis. *Thin Walled Structures*, **32** (1-3), 151-180.

FEMA (1997): *FEMA 302 NEHRP recommended provisions for seismic regulations for new buildings and other structures. Part-1-Provisions*, Building Seismic Safety Council for the Federal Emergency Management Agency, Washington, D.C.

Rezai M (1999): *Seismic behavior of steel plate shear walls by shake table testing*. Ph.D. Dissertation, University of British Columbia, Vancouver, British Columbia, Canada.

Timler PA, Kulak GL (1983): *Experimental study of steel plate shear walls*. Structural Engineering Report No. 114, Department of Civil Engineering, University of Alberta, Edmonton, Alberta, Canada.

Yang TY, Whittaker A (2002): *MCEER demonstration hospitals - Mathematical models and preliminary results*. Technical Report. Submitted to the Multidisciplinary Center for Earthquake Engineering Research, University at Buffalo, Buffalo, NY.

Java-Powered Virtual Laboratory for Nonlinear Structural Dynamic Analysis

Yong Gao

Graduate Student, Department of Civil & Environmental Engineering, University of Illinois at Urbana-Champaign

Research Supervisor: Billie F. Spencer, Jr., Nathan M. Newmark Professor

Summary

A Java-Powered Virtual Laboratory (VL) has been developed for conducting nonlinear dynamic analysis of buildings and has been made available on the internet (<http://cee.uiuc.edu/sstl/java>). This virtual laboratory provides students and practitioners with a means to interactively gain fundamental understanding and intuition about earthquake engineering and structural dynamics. By accessing this on-line software, remote users are able to analyze buildings with a different number of stories using various structural models and design parameters. Dynamic analysis of the structure can be performed using four historical earthquakes, as well as a sinusoidal excitation. Animation of the structural responses is also provided to visualize the dynamic behavior of the building.

Introduction

Educators must always strive to better prepare the next generation of structural engineers to understand and effectively deal with the design of earthquake resistant structures to reduce the associated human and financial losses. One of the challenges of teaching students about the fundamentals of earthquake engineering is giving them an intuitive understanding of the dynamics of structures. Demonstrating the concepts of dynamics using static chalk boards or books is difficult. The best approach is through hands-on laboratories. Unfortunately, few instructors have the necessary facilities readily available to demonstrate structural dynamic concepts. This Java-Powered Virtual Laboratory (VL) provides a means for online interactive experiments and is intended to increase understanding and provide a conceptual “feel” of dynamic analysis and design (Dargush et al., 2003).

In this nonlinear structural dynamic analysis VL, users are provided wide flexibility to perform dynamic analysis. Users can choose the number of stories, as well as select the floor mass, stiffness, and damping coefficients for each story. Four nonlinear models are provided to portray the behavior of the structure. The same type of nonlinearity is employed for all stories, but the parameters defining this nonlinearity can be varied for each story. Sinusoidal and four historical earthquake excitations can be chosen for conducting the dynamic analysis. Additional features of this VL include graphically comparing dynamic analysis results of different nonlinearities and animating the response using a virtual building. The user friendly interface helps the participants to understand advanced topics more easily and effectively.

Methodology

This VL was programmed using Java. The Java programming language (Newman 1996) offers significant advantages because of its minimal dependence on the operational platform. Therefore, this VL can be accessed universally through internet. The Java language also requires a minimum amount of administration maintenance for the VL once it has been developed and published on the internet. If additional updates are required, they can be made locally and put on the internet. When remote users access this software the next time, they will automatically download and run the updated version. In addition, the VL's interactive interface, optimized with Java programming, significantly increases the efficiency of presenting and, in turn, understanding of a wide range of topics in earthquake engineering.

Four types of nonlinear models are provided in this VL to describe the structural dynamic behavior. These nonlinearities (shown in Figure 1) include: (i) linear stiffness and linear viscous damping; (ii) linear stiffness and nonlinear power-law damping; (iii) hysteretic stiffness using the Bouc-Wen model and linear viscous damping; and (iv) hysteretic bilinear stiffness and linear viscous damping. For the first two types of nonlinearities, buildings behave as linear elastic structures. However, damping remains linear for type (i), and type (ii) follows the nonlinear power-law with respect to the velocity. The Bouc-Wen model and hysteretic bilinear nonlinear model are widely employed for modeling nonlinear behavior of concrete and steel structures. By choosing various nonlinearities, users are able to analyze different types of structures using this software.

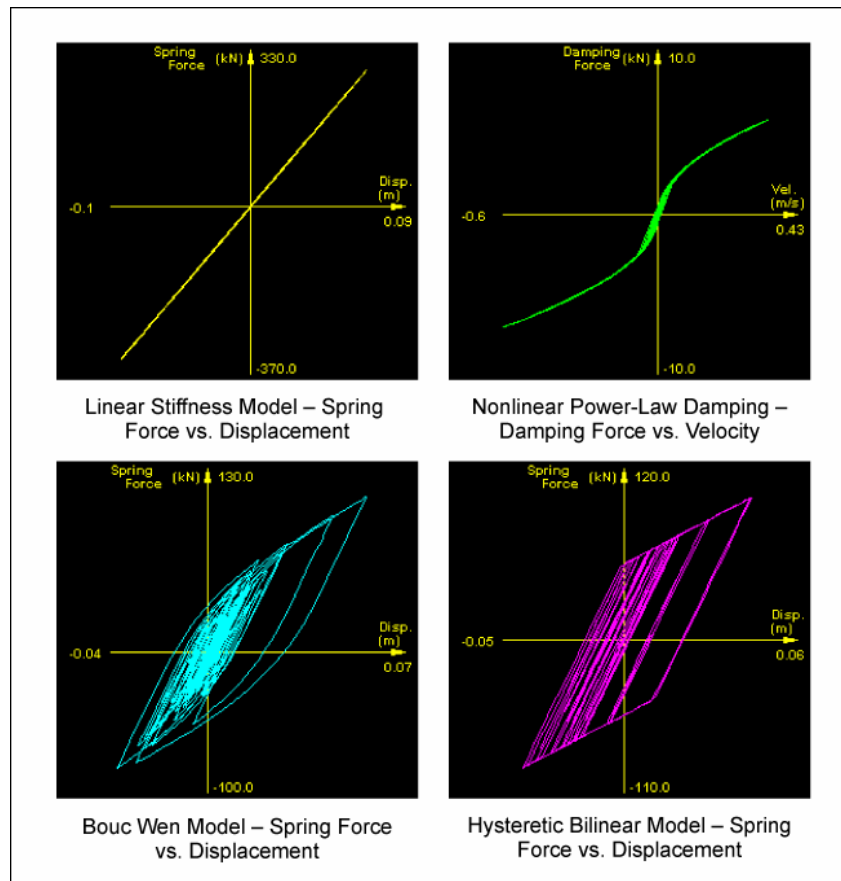


Figure 1. Typical relationship between force and response for different nonlinearities

Computational analysis of the dynamic problems in this virtual simulation utilizes several state-of-the-art numerical algorithms. The Generalized α method was employed to solve the hysteretic bilinear stiffness problem, and the Runge-Kutta method was applied to handle all other linear and nonlinear analysis (Tedesco et al., 1998; Belytschko and Hughes, 1983; Berg, 1989). These computation algorithms were first verified by programming in Matlab and then translated into Java. The book, *Numerical Recipes* (Press et al., 1987), was very helpful for this translation. It is worth noting that the time step of numerical algorithms is important in conducting an accurate dynamic analysis. A smaller time step might be needed as the number of stories increases. The time step in this VL can be specified and the earthquake data are re-sampled when the time step is changed. Accurate results have been obtained by using these numerical methods.

Virtual Laboratory Overview

The interface of the VL is provided in Figure 2. There are four response frames on the left of the user interface. On the right, there is a panel to control the structural analysis and input parameters. There is also an animation panel which provides the animated response. This panel is shown in Figure 3. The control panel and animation panel are interchanged with each other by clicking the “Show Virtual Model” or “Show Control Panel” button located at the lower corner of each panel. A description of each of these components is given below.

The control panel allows users to design and analyze the structure. The number of stories in the building can be changed, and the time step can be modified as well, depending on the calculation requirements. A few default time steps have been preset for different story numbers as a

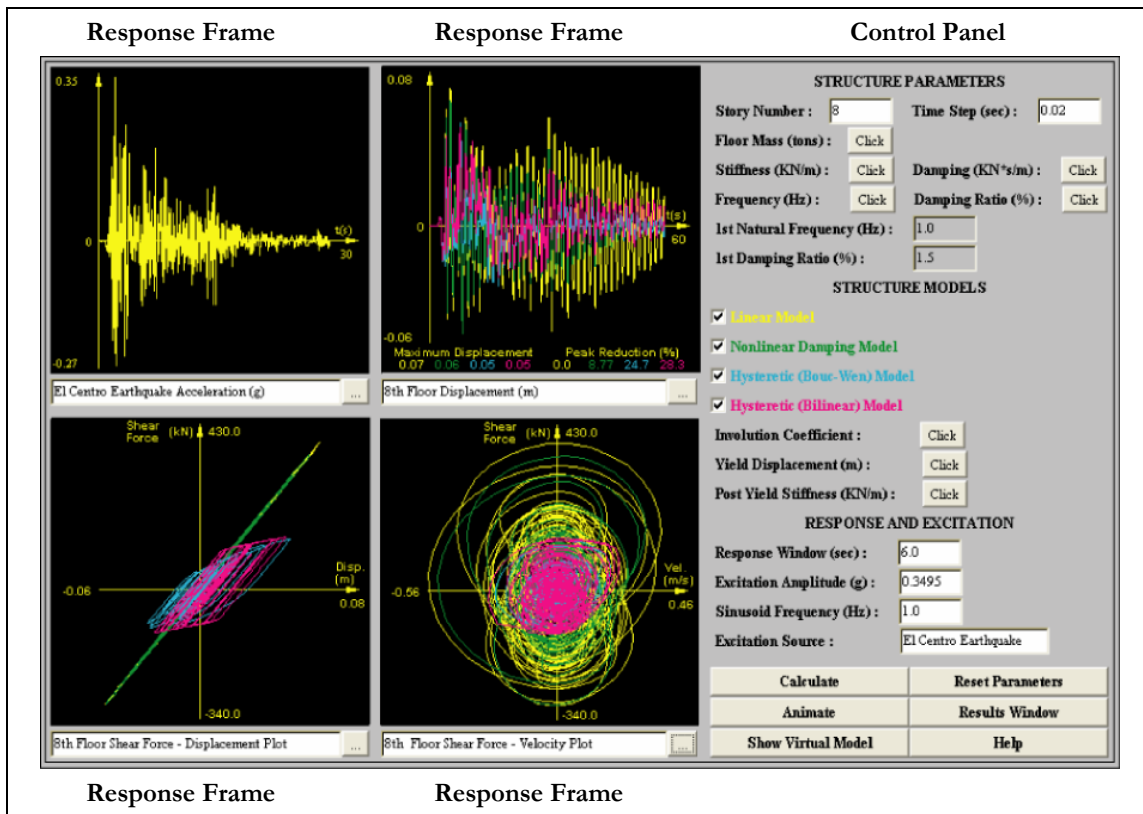


Figure 2. Java-powered virtual laboratory

guideline. Structural parameters, including floor mass, story stiffness and damping coefficients, can be varied by clicking the selection button following the label. A dialogue box (Figure 4) will open when the selection button is pushed. Modal properties, including natural frequency and damping ratio, are automatically computed when structural parameters are changed. These properties can be found by clicking the selection button following the label as well. For convenience, the first natural frequency and the damping ratio are also shown in the control panel.

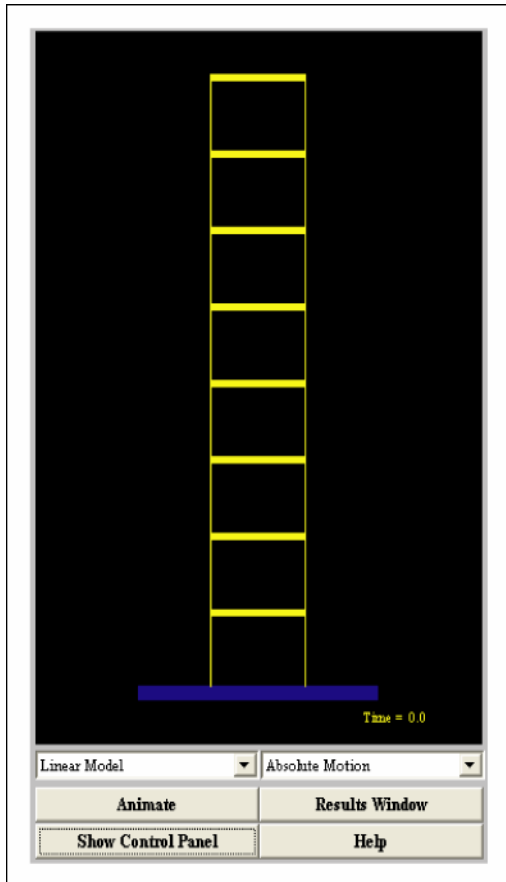


Figure 3. Animation panel

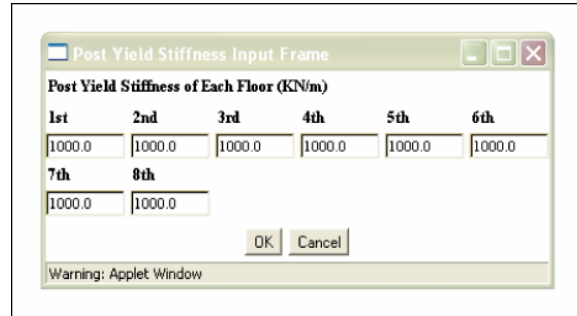


Figure 4. Post yield stiffness input dialogue box

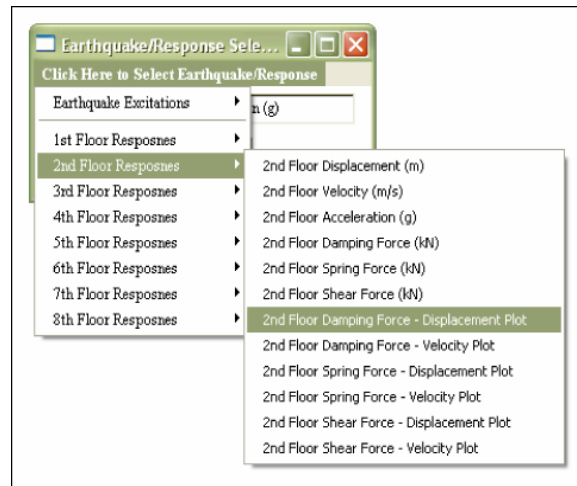


Figure 5. Response selection dialogue box

Users can describe the structure using four different analytical models, which can be selected by clicking the check box under the label “Structural Models,” and they can choose either one or multiple nonlinearities to conduct dynamic analysis. The associated parameters for these models, including an involution coefficient for nonlinear damping model, yield displacement and post yield stiffness for nonlinear stiffness model, can be changed in the dialogue box brought up by clicking the selection button (see Figure 4).

Users are also able to control the excitations and the manner in which animation is shown by modifying the related parameters in the control panel. The excitation amplitude can be changed, and

the frequency component of the sinusoidal excitation is also variable. The value in the “Response Window” controls how many seconds of the response/earthquake will be displayed during the animation in response frames. The name of the current excitation is always displayed following the label “Excitation Source” in the control panel.

After all the parameters have been input, users can push the “Calculate” button at the lower left corner of the control panel to conduct the dynamic analysis. An animation button is also provided to show the time history of the response. All parameters in the control panel are reset to the default values by clicking the button “Reset Parameters.” By pushing the “Show Virtual Model” button, users can toggle between the control panel and the animation panel to help visualize the dynamic response using an animated virtual building. Other important buttons provided are “Result window” and “Help.”

Calculated results are shown in the response frames. The functions of these response frames are identical, except that the top left frame can also display the earthquake excitation. There is a selection button at the lower right corner of each frame. For the top left frame, this selection button brings up a dialog box (shown in Figure 5) for the user to select the earthquake excitation or response to display. For the other three response frames, the selection button brings up a similar dialog box for a response selection only. The currently displayed signal is shown in the text field under the plot in each of these frames.

Various analytical results can be displayed in these response frames. The top right response frame shows an example of the time history response. In this example, the 8th floor inter-story drifts for all the selected structural models are displayed simultaneously. It also shows the maximum response values and the corresponding peak reduction factors, which is the reduction relative to the linear elastic case. By seeing the time history and peak reduction factor for different nonlinearities simultaneously, users can easily appreciate the difference between these nonlinearities under the current excitation. Similar time history plots for relative velocity, absolute acceleration, spring force, damping force and shear force are also readily displayed by clicking the selection button in each of the four frames. The bottom two response frames demonstrate relationships between shear force and displacement, and between shear force and velocity. Similar plots for spring force and damping force can also be shown by clicking the selection button in any one of these four frames.

Conclusions

A unique Java-Powered Virtual Laboratory has been developed to facilitate the understanding of a wide range of topics in earthquake engineering and dynamic analysis. Participants are expected to gain fundamental understanding of these topics by conducting online numerical experiments using this interactive software. This virtual laboratory provides an excellent alternative way for students and practitioners to develop their knowledge of earthquake engineering. By designing this virtual laboratory using Java programming, this software can be accessed universally through the internet. Other available virtual laboratories, including structural control using tuned mass dampers (TMD) and hybrid mass dampers (HMD), and base isolation using linear and nonlinear devices, can be found at <http://cee.niuc.edu/sst/java>.

Acknowledgements

This research was primarily supported by the Earthquake Engineering Research Centers Program of the National Science Foundation, under award number EEC-9701471 to the Multidisciplinary

Center for Earthquake Engineering Research. The author thanks Professor Billie F. Spencer for his excellent supervision during this project. In addition, the author would like to thank Prof. Yozo Fujino of the University of Tokyo for his help in securing the Kobe and Hachinohe earthquake records.

References

Belytschko T, Hughes TJ (1983): *Computational methods for transient analysis*. North-Holland.

Berg GV (1989): *Elements of structural dynamics*. Prentice Hall.

Dargush AS, Abdullah MM, Agrawal AK, Purasinghe R, and Spencer Jr. BF (2003): The MCEER interface between research and education. *Research Progress and Accomplishments 2002 – 2003*, MCEER-03-SP01, Multidisciplinary Center for Earthquake Engineering Research, University at Buffalo, Buffalo, NY.

Newman A (1996): *Special edition using Java*. Que Cooperation, Indianapolis, IN.

Press WH, Flannery BP, Teukolsky SA, and Vetterling WT (1987): *Numerical recipes: the art of scientific computing*. Cambridge University Press.

Tedesco JW, McDougal WG, and Ross CA (1998): *Structural dynamics: theory and applications*. Addison-Wesley.

Response of Elastic and Inelastic Structures with Damping Systems to Near-Field and Soft-Soil Ground Motions

Eleni Pavlou

Graduate Student, Department of Civil, Structural & Environmental Engineering, University at Buffalo

Research Supervisor: Michael C. Constantinou, Professor and Chairman

Summary

The effect of near-field and soft-soil ground motions on structures with viscous-damping systems was examined. Damping modification factors for damping ratios up to 100% of critical were obtained for sets of near-field and soft-soil ground motions and compared to the values presented in 2000 NEHRP Recommended Provisions. A study was carried out for the ductility demand in structures without and with damping systems, where the damped buildings were designed for a smaller base shear than conventional buildings in accordance with the 2000 NEHRP Provisions. Nonlinear response-history and simplified methods of the 2000 NEHRP Provisions were used to analyze single-degree-of-freedom systems and 3-story moment frames with linear and nonlinear viscous damping systems to acquire knowledge on the influence of near-field and soft-soil ground motions on the accuracy of simplified methods of analysis.

Introduction

FEMA's *National Earthquake Hazard Reduction Program (NEHRP) Recommended Provisions for Seismic Regulations for New Buildings and Other Structures* of year 2000 (BSSC 2001) and the upcoming Provisions for year 2003 contain the first simplified methods for analysis and design of buildings with damping systems. These procedures are largely based on studies that excluded the effects of near-field and soft-soil seismic excitations (Ramirez et al., 2001, 2002a, 2002b, 2003; Whittaker et al., 2003). This paper concentrates on a systematic assessment of the validity of these methods for these special classes of seismic excitations.

Recently, Ramirez et al. (2001, 2002a, 2002b, 2003) evaluated the accuracy of simplified methods of analysis of buildings with damping systems. Particularly, the simplified analysis methods of 2000 NEHRP Recommended Procedures (BSSC 2001) have been evaluated and shown to produce results of acceptable accuracy. However, the studies did not consider near-field and soft-soil earthquake motions, so the conclusions presented in the Ramirez et al. papers do not necessarily apply to such conditions.

To shed some light on these issues, structures with linear and nonlinear viscous damping systems were employed to examine how the response to near-field and soft-soil ground motions differs from that to far-field motions. This paper presents: (1) a comparison of the values of damping coefficients obtained through analyses with the near-field and soft-soil motions, and the values listed in the 2000

NEHRP Provisions to modify the 5-percent damped response spectrum for the effects of higher damping; (2) a comparison of ductility demands in structures without and with damping systems, where the damped buildings are designed for a smaller base shear than conventional buildings; (3) results of the simplified method of analysis for single-degree-of-freedom structures with linear viscous and nonlinear viscous damping systems along with the results of nonlinear response history analysis; and (4) a comparison of results of dynamic response history analysis and of simplified analysis of 3-story frames with linear and nonlinear viscous damping systems.

A set of ten near-field ground motions assembled by Somerville (1997) and seven soft-soil earthquake histories (Lord 1996) were utilized in the analysis of ductile systems with and without supplemental viscous damping. The single-degree-of-freedom system considered in this study had perfect non-degrading bilinear hysteretic behavior and was characterized by the elastic period with values of $T_e=0.5$ to 2.0 sec, the ductility-based portion of R-factor with values of $R_\mu = 2.0, 3.33,$ and 5.0 and the post-yielding to elastic stiffness ratio with values of $a=0.05, 0.15, 0.25, 0.50,$ and 1.00. In addition, analyses were conducted for 3-story special steel moment resisting frames with linear and nonlinear viscous damping systems. These frames were designed to have base shear strength of $0.75V, V,$ and $0.8V,$ respectively, where V is the base shear for the building frame without a damping system for seismic excitation described by the NEHRP spectrum with parameters $S_{DS} = 1.0, S_{D1} = 0.6,$ and $T_s = 0.6$ seconds. Damping systems were then added to these frames and proportioned in accordance with the 2000 NEHRP Recommended Provisions to satisfy the drift criteria. Detailed description of the above systems is presented in Ramirez et al. (2001).

Modification of Response Spectrum for High Damping

In order to reduce the elastic spectral demands for increases in damping, the damping coefficient is used. Linear response-history analyses were carried out for the two sets of earthquake motions to calculate values for the damping coefficient for damping ratios up to 100% of critical. The value of the damping coefficient B for a particular period is obtained as the ratio of the average 5%-damped spectral acceleration, $S_a(T,0.05)$, to the average spectral acceleration for a different damping ratio β , $S_a(T,\beta)$. Figure 1 shows the calculated damping coefficients and the coefficients presented in 2000 NEHRP, for the near-field (fault-normal components) and the soft-soil ground motions for damping ratios up to 50% of critical.

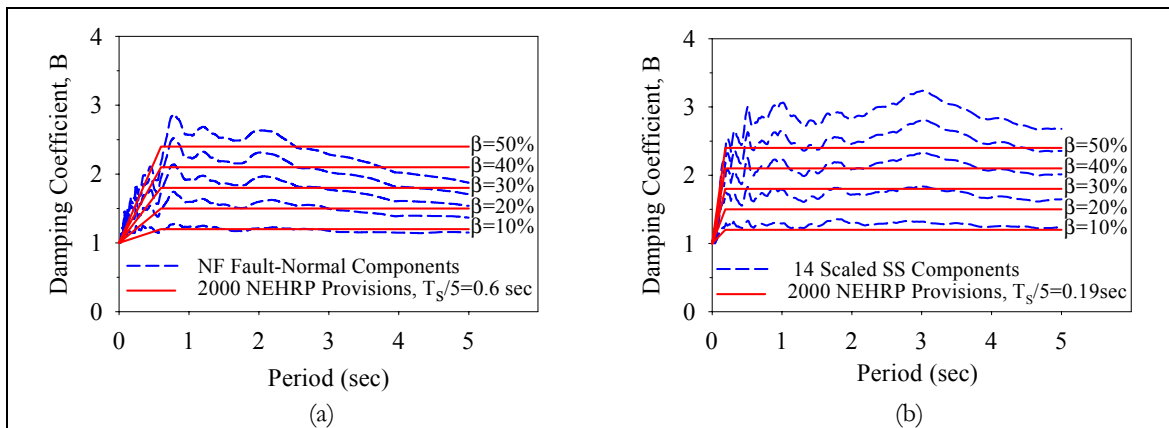


Figure 1. Calculated and NEHRP B coefficient for (a) near-field and (b) soft-soil ground motions

Evaluation of Displacement Ductility Demands in Structures with Viscous Damping Systems

Furthermore, in order to establish values of the displacement ductility demand for the near-field and soft-soil ground motions, nonlinear time history analyses were performed on the ductile single-degree-of-freedom framing systems with and without supplemental linear viscous damping. Figure 2 compares the calculated average displacement ductility ratio for the undamped and the damped systems for the two ground motion sets.

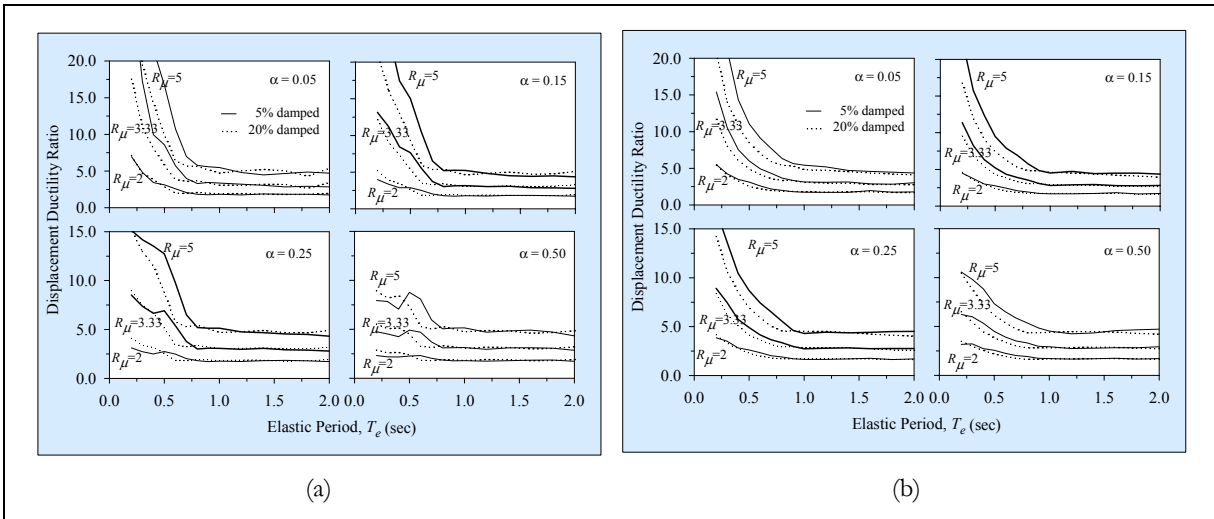


Figure 2. Comparison of average displacement ductility ratio for 5%- and 20%-damped systems for (a) near-field and (b) soft-soil ground motions

Results of Simplified Method of Analysis and Comparison to Results of Nonlinear Response History Analysis

Single-degree-of-freedom Structures

In addition, nonlinear response history analyses for the near-field and soft-soil ground motions were performed to investigate the accuracy of the simplified methods of the 2000 NEHRP Provisions. Figure 3 presents a comparison of the results of nonlinear history analysis and the results of the simplified method of analysis. Graphs of the peak displacement, peak velocity and peak acceleration are presented by plotting the average results of the nonlinear history analyses on the vertical axis against the results of the simplified method of analysis on the horizontal axis for systems with linear viscous damping devices, $\beta_v = 0.15$.

3-story Building Frames

To further examine the influence of near-field and soft-soil ground motions on the accuracy of simplified methods of analysis, multi-degree-of-freedom systems were considered. Nonlinear response-history analysis of the 3-story frames was performed using computer program IDARC2D (Valles 1996). Indicative results of the simplified methods of analysis and nonlinear response-history

analysis are tabulated in Tables 1 and 2 for minimum, maximum, average, and average plus one standard deviation ($\text{avg} + 1\sigma$) responses for the 3-story frame 3S-75 with linear viscous damping system to provide 10% viscous damping ratio. Included in the table are (a) peak interstory drifts, (b) peak interstory velocities, (c) peak damper forces, and (d) maximum story shears (including the viscous component). The results reported in Tables 1 and 2 attest to the accuracy of the equivalent lateral force (ELF) and the modal analysis (RSA) procedures of 2000 NEHRP Recommended Procedures for buildings with damping systems. Both methods provided conservative estimates of drift and predictions for damper forces and member actions in good overall agreement with the average of results of nonlinear response-history analysis.

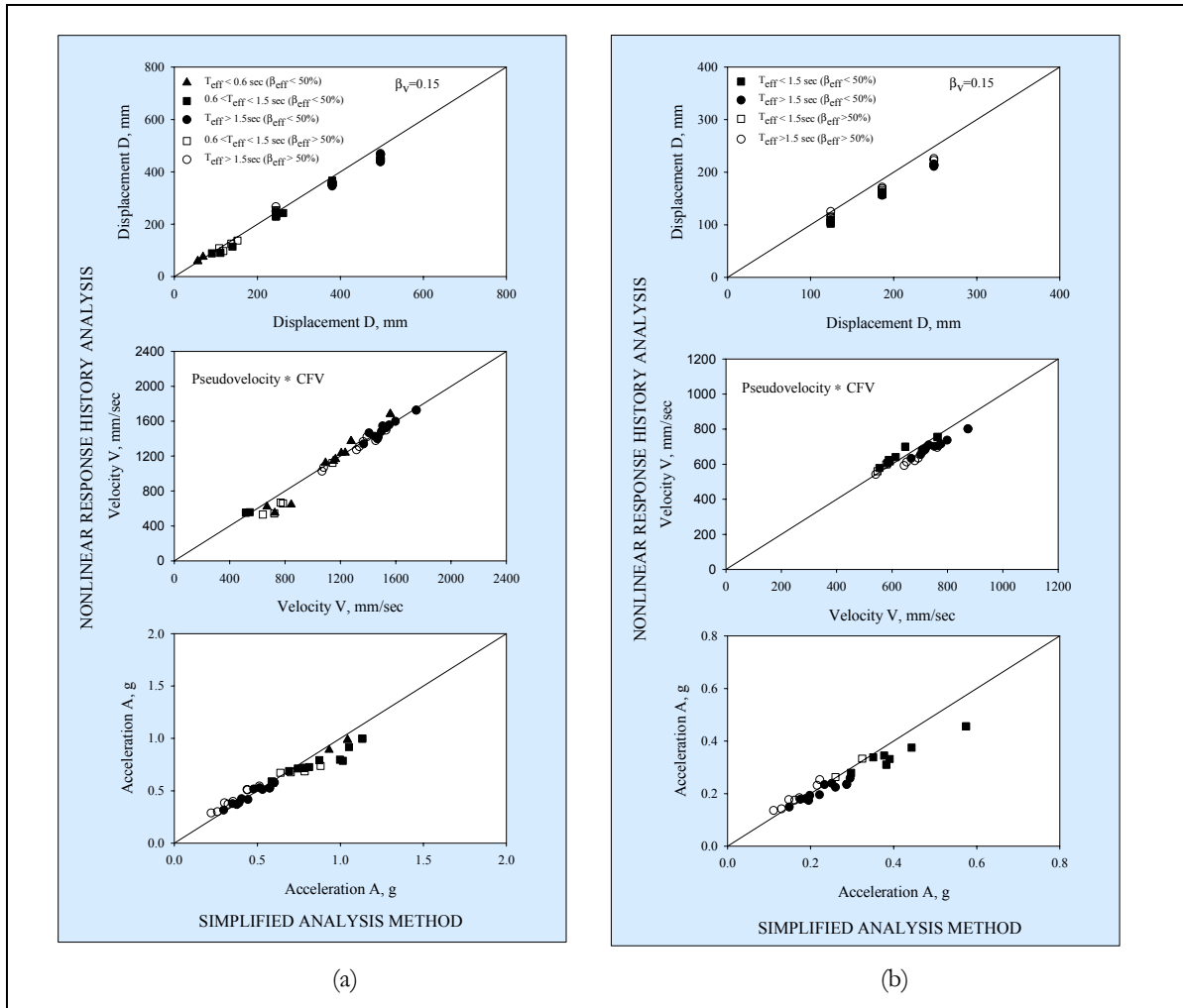


Figure 3. Comparison of response history analysis to simplified method of analysis for systems with linear viscous damping devices, $\beta_v = 0.15$ for (a) near-field and (b) soft-soil ground motions

Table 1. Comparison of results of simplified methods of analysis to results of nonlinear response-history analysis: 3-story frame 3S-75 with linear viscous damping system to provide 10% viscous damping ratio – near-field, fault-normal components

| Response Quantity | S T O R Y | Simplified Methods of Analysis NEHRP (2003) | | | | Nonlinear Time History Analysis IDARC2D, version 5.0 | | | |
|------------------------------|-----------------------|--|-------------|------|-------------|---|---------|----------------|------|
| | | ELF | | RSA | | Min. | Average | Avg+1 σ | Max. |
| Story Drift (mm) | 3 | 112 | | 113 | | 61 | 98 | 131 | 151 |
| | 2 | 133 | | 127 | | 67 | 112 | 150 | 184 |
| | 1 | 89 | | 80 | | 39 | 78 | 112 | 152 |
| Interstory Velocity (mm/sec) | 3 | 468 | 460 | 577 | 515 | 287 | 526 | 660 | 694 |
| | 2 | 555 | 546 | 435 | 472 | 340 | 484 | 577 | 625 |
| | 1 | 499 | 435 | 331 | 324 | 237 | 348 | 426 | 453 |
| Damper Force (kN) | 3 | 373 | 367 | 460 | 411 | 229 | 420 | 528 | 554 |
| | 2 | 443 | 436 | 347 | 377 | 271 | 386 | 461 | 500 |
| | 1 | 398 | 347 | 264 | 258 | 189 | 278 | 341 | 362 |
| Max. Story Shear (kN) | 3 | 717 | 709 | 881 | 856 | 513 | 706 | 841 | 936 |
| | 2 | 1161 | 1165 | 1157 | 1165 | 963 | 1239 | 1384 | 1446 |
| | 1 | 1638 | 1623 | 1517 | 1513 | 1172 | 1665 | 1905 | 1980 |

Note: Values in **bold** indicate results obtained using the revised velocity correction factors from Table 6 of Ramirez et al., (2002a).

Table 2. Comparison of results of simplified methods of analysis to results of nonlinear response-history analysis: 3-story frame 3S-75 with linear viscous damping system to provide 10% viscous damping ratio – soft-soil scaled components

| Response Quantity | S T O R Y | Simplified Methods of Analysis NEHRP (2003) | | | | Nonlinear Time History Analysis IDARC2D, version 5.0 | | | |
|------------------------------|-----------------------|--|-------------|------|-------------|---|---------|----------------|-------------|
| | | ELF | | RSA | | Min. | Average | Avg+1 σ | Max. |
| Story Drift (mm) | 3 | 105 | | 108 | | 50 | 89 | 110 | 119 |
| | 2 | 125 | | 121 | | 66 | 103 | 128 | 150 |
| | 1 | 82 | | 76 | | 45 | 68 | 92 | 121 |
| Interstory Velocity (mm/sec) | 3 | 408 | 415 | 561 | 494 | 186 | 511 | 408 | 415 |
| | 2 | 484 | 492 | 410 | 443 | 200 | 484 | 484 | 492 |
| | 1 | 419 | 377 | 318 | 307 | 117 | 341 | 419 | 377 |
| Damper Force (kN) | 3 | 325 | 331 | 448 | 394 | 149 | 408 | 325 | 331 |
| | 2 | 386 | 392 | 327 | 354 | 160 | 386 | 386 | 392 |
| | 1 | 334 | 300 | 253 | 245 | 93 | 273 | 334 | 300 |
| Max. Story Shear (kN) | 3 | 655 | 653 | 877 | 852 | 341 | 659 | 655 | 653 |
| | 2 | 1134 | 1142 | 1162 | 1169 | 873 | 1213 | 1134 | 1142 |
| | 1 | 1521 | 1513 | 1519 | 1515 | 1278 | 1591 | 1521 | 1513 |

Note: Values in **bold** indicate results obtained using the revised velocity correction factors from Table 6 of Ramirez et al., (2002a).

Concluding Remarks

The study conducted to investigate the effects of near-field and soft-soil ground motions on the response of yielding structures with viscous damping devices has led to the following conclusions:

- The damping coefficient values in 2000 NEHRP are accurate or conservative for near-field and soft-soil ground motions for periods up to 5 seconds and 3 seconds, respectively.
- The ductility demand in damped structures with lower stiffness and strength is comparable to, or less than, the ductility demand in undamped structures for near-field and soft-soil ground motions.
- The 2000 NEHRP simplified method of analysis for single-degree-of-freedom systems produces results on displacement and acceleration that are generally accurate or conservative for near-field and soft-soil ground motions. Moreover, the use of previously established correction factors for velocity on the basis of analyses with far-field motions produces very good estimates of peak structural velocity in near-field and soft-soil motions.
- The application of the simplified methods of analysis of 2000 NEHRP Recommended Procedures to steel moment frames with linear and nonlinear viscous damping systems provided conservative estimates of drift and predictions for damper forces and member actions in good overall agreement with the average of results of nonlinear response-history analysis.

Acknowledgments

Financial support for this project was provided by the Multidisciplinary Center for Earthquake Engineering Research, Task on Rehabilitation Strategies for Buildings, which is primarily supported by the Earthquake Engineering Research Centers Program of the National Science Foundation, under award number EEC-9701471. The work was performed under the direction of Technical Subcommittee 12, Base Isolation and Energy Dissipation, of the Building Seismic Safety Council, which was tasked with developing analysis and design procedures for inclusion in the 2000 and 2003 editions of the *NEHRP Recommended Provisions for Seismic Regulations for New Buildings and Other Structures*. The work of Technical Subcommittee 12 was supported by the Federal Emergency Management Agency.

References

Building Seismic Safety Council (BSSC) (2001): *NEHRP recommended provisions for seismic regulations for new buildings and other structures, 2000 Edition*. Report Nos. FEMA 368 and 369. Federal Emergency Management Agency, Washington, DC.

Lord JA (1996): Personal communication with Michael C. Constantinou.

Ramirez OM, Constantinou MC, Gomez JD, Whittaker AS, Chrysostomou CZ (2002): Evaluation of simplified methods of analysis of yielding structures with damping systems. *Earthquake Spectra*; **18**(3): 501-530.

Ramirez OM, Constantinou MC, Gomez JD, Whittaker AS, and Chrysostomou CZ (2002): Elastic and inelastic seismic response of buildings with damping systems. *Earthquake Spectra*; **18**(3): 531-547.

Ramirez OM, Constantinou MC, Kircher CA, Whittaker AS, Johnson MW, Gomez JD, Chrysostomou CZ (2001): *Development and evaluation of simplified procedures for analysis and design of buildings with passive energy dissipation systems, Revision 1*. Report No. MCEER 00-0010,. Multidisciplinary Center for Earthquake Engineering Research, University at Buffalo, Buffalo, NY.

Ramirez OM, Constantinou MC, Whittaker AS, Kircher CA, Johnson MW, Chrysostomou CZ (2003): Validation of the 2000 NEHRP provisions equivalent lateral force and modal analysis procedures for buildings with damping systems. *Earthquake Spectra*; to appear.

Somerville P, Smith N, Punyamurthula, S, Sun J (1997): *Development of ground motion time histories for phase 2 of the FEMA/SAC steel project*. Report No. SAC/BD-97-04, Sacramento, CA.

Valles RE, Reinhorn AM, Kunnath SK, Li C, Madan A (1996): *IDARC2D Version 4.0: A computer program for the inelastic damage analysis of buildings*. Report No. NCEER-96-0010. National Center for Earthquake Engineering Research, University at Buffalo, Buffalo, NY. Information on Version 5.0 of IDARC2D can be found at <http://civil.eng.buffalo.edu/idarc2d50/>.

Whittaker AS, Constantinou MC, Ramirez OM, Johnson MW, Chrysostomou CZ (2003): Equivalent lateral force and modal analysis procedures of the 2000 NEHRP provisions for buildings with damping systems. *Earthquake Spectra*; to appear.

Advanced Time-Frequency Analysis Applications in Earthquake Engineering

Nikolaos P. Politis

Graduate Student, Department of Civil and Environmental Engineering, Rice University

Research Supervisor: Pol D. Spanos, L.B. Ryon Chair in Engineering

Summary

Future design procedures for civil structures, especially those to be protected from extreme and blast related loads, will need to account for temporal evolution of their frequency content. Separate time analysis and frequency analysis by themselves do not fully describe the nature of these nonstationary dynamic loads. In the past few years, significant effort has been devoted to wavelets and time-frequency analysis. This article attempts to briefly present certain techniques which are currently available, and suggests possible applications in the area of earthquake engineering. Further, it gives an outline of current research topics, some preliminary results on earthquake signal representation using time-frequency analysis techniques, and possible future research directions in this area. To comply with the space limitations of this article, only references that are readily available in the form of books are cited.

Introduction

Spectral analysis using the Fourier Transform has been one of the most important and most widely used tools in earthquake engineering. Over the past few years, however, researchers have become aware of the limitations of this technique, especially in the case of nonstationary signals, and of nonlinear systems.

Monte Carlo simulations are often used in the design of a structure subjected to earthquake excitations. These simulations require the generation of artificial earthquake signals, compatible with a design power spectrum, for input into the structural system. Further, the techniques used for the generation of the artificial earthquake signals must account for their inherent nonstationary frequency characteristics. Also, capturing evolutionary and localized features of the response of linear and nonlinear dynamic systems subject to nonstationary inputs is not feasible within the limits of traditional spectral analysis. It is clear that other techniques need to be developed.

In this direction, significant effort has been devoted in the development of Time-Frequency (TF) methods, which allow a temporal representation of the spectral characteristics of the signal. Such TF methods involve the short-time Fourier transform (STFT), the wavelet transform (WT), the Wigner-Ville distribution (WVD), the best basis search algorithm using wavelet packets or Malvar-Wilson wavelets, and the matching pursuit (MP) algorithm using Gabor atoms or chirplets (Hubbard 1998).

Fourier Analysis and Wavelets

Fourier analysis is based on the notion that any regular periodic function and certain nonperiodic functions with finite integral can be expressed as a sum of trigonometric functions in an infinite time framework (Boggess and Narcowich, 2001). Fourier transform gives a unique representation of the signal in the frequency domain and provides information about which frequencies appear in the signal but not about the time instants in which these frequencies are encountered. The time information is not lost through the transform but it is hidden in the phases. Thus, it is able to yield a perfect and unique reconstruction of the signal. There are many signals in nature for which the Fourier transform is not just a mathematical artifact but whose frequencies correspond to actual physical waves that make the signal. The physical interpretation of the signal is then simple. However, there are cases for which the Fourier analysis does not provide results that can be physically interpreted. As a result of Whittaker's sampling theorem of 1935, its subsequent application in communication theory by Shannon in 1949, and the discrete fast Fourier transform algorithm by Cooley and Tukey in 1965, the improved computational efficiency of the Fourier analysis has made it the most widely used mathematical tool in a vast field of applications. However, Fourier analysis and regular power spectra representations are not suitable for all kinds of problems and signals. The natural phenomena are usually nonlinear and the majority of the signals have changing frequency contents.

For the aforementioned reasons, other methods that account for joint time-frequency representation of the signals have been developed. The most widely used one is the short-time Fourier transform (STFT). The basic concept in this method is to divide the signal into small segments (windows) of the same width and perform Fourier analysis on each of them to get the frequencies present in each segment (Cohen 1995). If good localization in time is desired, then a narrow window in the time domain has to be chosen. However, if good frequency localization is desired, a narrow window in the frequency domain has to be chosen. Thus, there is a trade-off between time and frequency localization governed by Heisenberg's uncertainty principle. Related to the STFT is the Gabor transform. In 1946, Gabor gave a new perspective of the STFT by introducing a tiling of the time-frequency domain as shown in Figure 1c. Gabor expansion is the best way to compute the inverse discrete STFT (Qian and Chen, 1996).

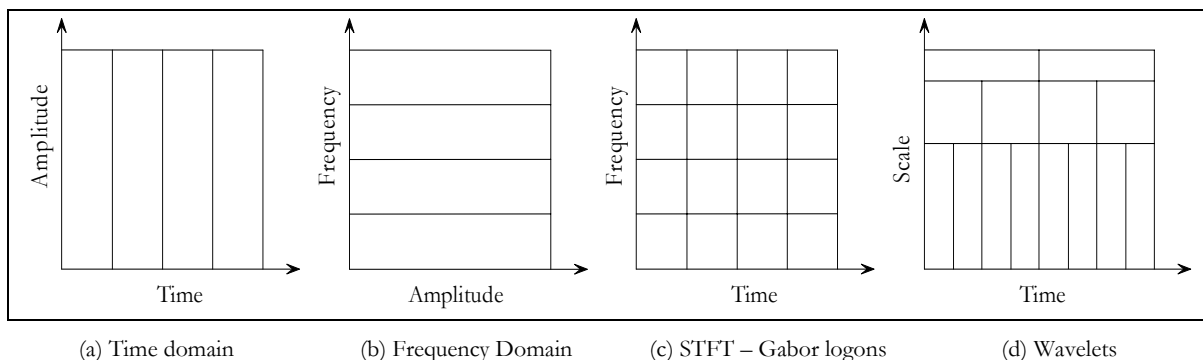


Figure 1. Time and frequency domain representations and tiling

Wavelets are a natural extension of the Fourier analysis (Daubechies 1992). A wavelet is small wave whose energy is concentrated in time (Figure 2). In order to detect the characteristics of a signal, we compare it to a given elementary function. When the scaled and time-shifted elementary functions are used for this purpose, the resulting representation is called wavelet analysis and the elementary function is known as a mother wavelet. From another perspective, instead of having a constant window as in the case of STFT, wavelet analysis considers variable size windows, allowing for the use of long time segments for capturing the low frequency contents, and narrow time segments for capturing high frequency contents (Figure 1d). Although wavelet analysis is a time-scale analysis technique, connection to the time-frequency analysis can be made. Low scales correspond to compressed wavelets which are capable of capturing rapidly changing features of the signal linked to high frequencies. On the other hand, high scales correspond to dilated wavelets that are able to capture the slowly changing features of the signal linked to low frequencies. As in the case of Fourier analysis, we have continuous and discrete transforms. The discrete transforms can be redundant, orthogonal, or biorthogonal. There are infinitely many wavelets in the sense that any function concentrated in time can serve as an analyzing function. A plethora of wavelets has been developed to best suit several problems in science and engineering related to transient, time-variant, or nonstationary phenomena. This gives the method a great flexibility. However, this can also be a disadvantage since one has to choose the best wavelet for the application in hand. For instance, although wavelets have been successfully used in the solution of nonlinear differential equations, they have not provided a straightforward method for the solution of differential equations the way the Fourier analysis has. Wavelets have become a common language for people in different fields that had been using the same techniques under different names. This has brought a revolution in the field of time-frequency analysis. A great amount of literature has been developed on wavelets in the past few years, both on the mathematical foundation of the method and on their applications in numerous fields.

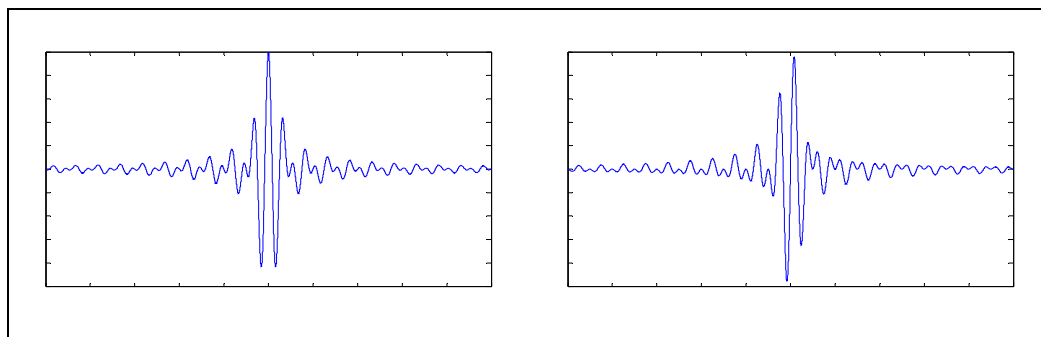


Figure 2. Real and imaginary part of the harmonic wavelets

The STFT and WT are based on the concept of finding the similarity between the signal and the analyzing functions and have the disadvantage that Heisenberg's uncertainty principle restrains their time-frequency resolution. Another approach, the Wigner-Ville distribution (WVD), based on time-frequency density function, yields better time-frequency resolutions. The WVD can be used to derive the instantaneous frequency function and the spectrogram. Disadvantages of the WVD include the cross-terms that affect the time-frequency resolution, and the negative values that the distribution can take (Cohen 1995).

Best Basis and Matching Pursuit Algorithms

Both Fourier and wavelet analysis have limitations. Fourier analysis gives good results for regular periodic signals (Figure 3a) and wavelet analysis is suitable for highly nonstationary signals that possess sudden picks and discontinuities (Figure 3c). Other approaches have been examined, and several algorithms and analyzing functions have been proposed (Jaffard et al., 2001). These include the best basis, and the matching pursuit algorithms. The best basis search algorithm uses wavelet packets, Malvar-Wilson wavelets, or generalized Malvar-Wilson wavelets. The matching pursuit (MP) algorithm uses Gabor atoms, or chirplets.

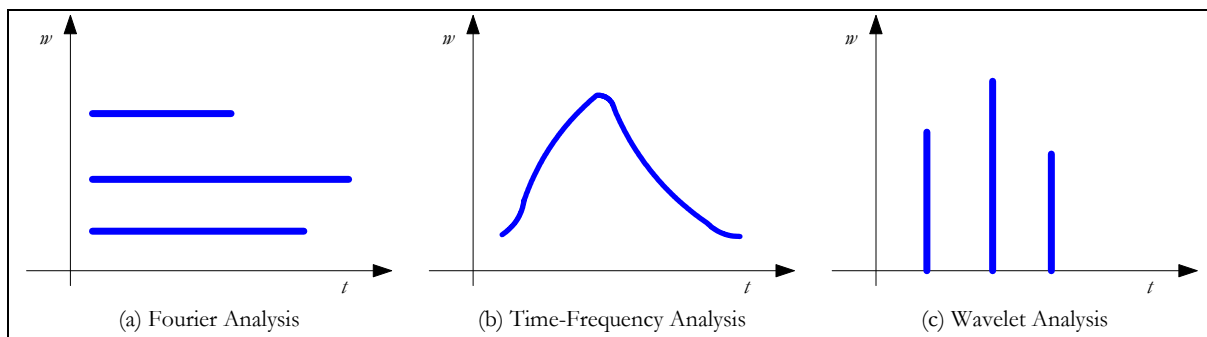


Figure 3. Time-Frequency plane representations and suitable types of analysis.

In the first approach, the signal is expressed as a linear combination of time-frequency atoms. The atoms are obtained by dilations of the analyzing functions, and are organized into dictionaries as wavelet packets, or Malvar-Wilson wavelets. Wavelet packet atoms are waves indexed by time, scale, and frequency (Figure 4a). For any orthogonal analyzing function, it is possible to generate a dictionary of wavelet packet bases. The Malvar-Wilson wavelets are functions which have the form of Figure 4b. They are characterized by an attack period, a stationary period, and a decay period whose duration can be arbitrarily and independently chosen. A modified version of the Malvar-Wilson wavelets that takes into account a linear modulation of the frequencies can be found in Jaffard et al., 2001.

The best basis algorithm described in Wickerhauser (1994) uses a minimum entropy criterion and gives the most concise description for a signal for the dictionary in hand. The representation of the signal depends on the size of the dictionary, thus leading to large dictionaries and high computational cost to account for more kinds of signals and achieve high time-frequency resolution. The application of the best basis search for the wavelet packet dictionary is equivalent to an optimal filtering of the signal, whereas, the Malvar-Wilson wavelets dictionary is equivalent to an optimal segmentation of the signal. For any given signal, the best basis algorithm decides which base represents the signal more efficiently.

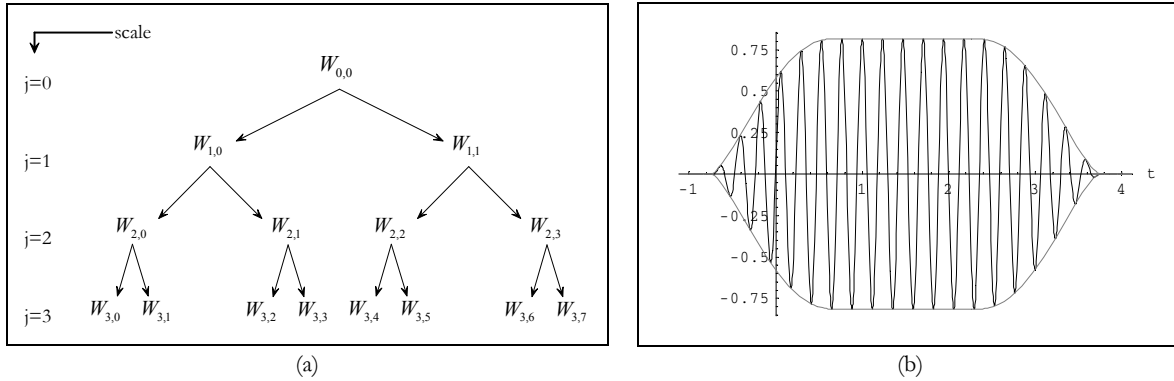


Figure 4. (a) Wavelet packets tree structure, (b) Malvar-Wilson wavelets

A chirplet function is shown in Figure 5 along with its WVD. Chirplets have a short smooth Gaussian envelope and a linear frequency modulation. They are characterized by four parameters which allow for localization and modulation: the time center, the frequency center, the variance, and the frequency change rate. Since they are derived from the Gaussian function, they always have a nonnegative WVD. A signal can be adaptively expanded in terms of chirplet atoms using the matching pursuit algorithm and the adaptive spectrogram that can be derived by taking the WVD of the signal. The Gabor atoms can be derived from the chirplets by setting the frequency change rate to zero. Chirplets and Gabor atoms do not form bases and their dictionaries are redundant. The Matching Pursuit algorithm allows for the decomposition of the signals into elementary functions that do not form bases. It is a basic component of the adaptive Gabor expansion, and the adaptive chirplet transform; a detailed description of the algorithm can be found in (Qian 2001).

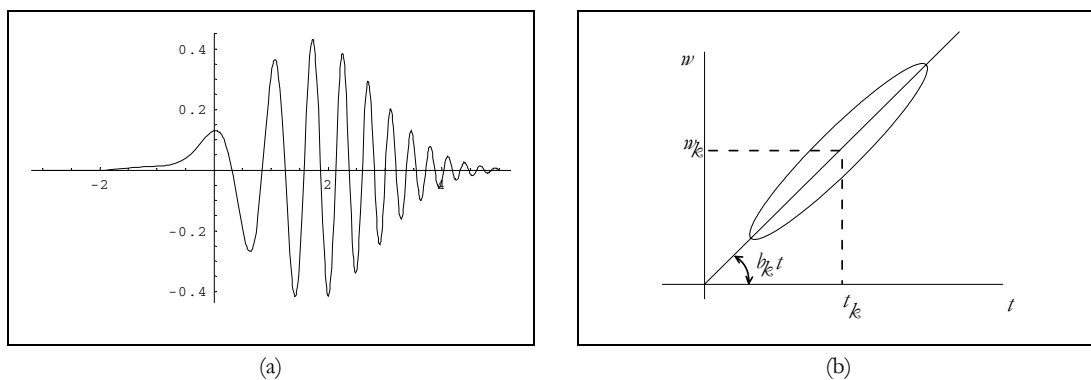


Figure 5. Gaussian chirplet and its WVD

Current Research and Future Work

The adaptive Gabor expansion and the adaptive chirplet transform have been implemented to obtain representations of earthquake records. Preliminary results show that, in terms of signal

expansion, the two methods give almost the same results. In this regard, the level of sophistication of the analyzing function used to capture the physics of the seismic records is examined. Comparisons with other methods of analysis such as wavelet analysis using harmonic wavelets (Figure 2), and classic Fourier analysis have been conducted. As expected, the adaptive methods give better results.

Further, effort is devoted in the direction of transition from individual spectrograms, derived by the WVD of the expanded signal, to evolutionary power spectrum. The spatial variation of earthquake records will be of interest as well. Thus, the extension to the multivariate case, which inevitably leads to the concept of the cross-power spectrum, is attempted and efficient expressions for the evolutionary coherency functions are pursued. In addition, a methodology allowing for the simulation of artificial, nonstationary signals, such as earthquakes, and other extreme loads (blast, wind, ocean waves, etc.) based on these evolutionary power spectra, is being developed.

Finally, capturing of the evolutionary and localized features of the response of linear and nonlinear dynamic systems subject to nonstationary inputs will also be pursued, especially in conjunction with the design of critical structures which may be exposed to extreme, low probability loads. Advanced time-frequency analysis techniques are used to observe the shifting of the natural frequencies of nonlinear structures and the changes on modal damping. It is clear that these techniques can become useful in health monitoring and structural control.

Concluding Remarks

The classic spectral analysis in the frequency domain has been discussed, and several limitations that derive from the use of Fourier analysis have been pointed out. Also, the alternative of employing short-time Fourier transform has been considered. Then, modern techniques of time-frequency analysis have been discussed. In this regard, wavelet transform has been presented. A plethora of applications of wavelet transform in earthquake engineering is available in the literature. Several issues regarding the interpretation of the results, since wavelet transform is a time-scale transform, need further attention. Alternatives to the wavelets-based scheme have been presented. Applications of these techniques to earthquake engineering include the derivation of evolutionary power spectra of dynamic loads, and the capturing of the changing frequency content of the response. In this context, it is believed that stochastic dynamics and time-frequency analysis merit additional attention.

Acknowledgements

This research has been carried out under the supervision of professor P. D. Spanos at Rice University and was partially supported by the Earthquake Engineering Research Centers Program of the National Science Foundation, under award number EEC-9701471 to the Multidisciplinary Center for Earthquake Engineering Research. The support of this research in the areas of signal processing, stochastic processes, and nonlinear dynamics by National Science Foundation grants is gratefully acknowledged.

References

Bogges A, Narcowich FJ (2001): *A first course in wavelets with Fourier analysis*. Prentice Hall. Upper Saddle River, NJ.

Cohen L (1995): *Time-frequency analysis*. Prentice Hall PTR. Englewood Cliffs, NJ.

Daubechies I (1992): *Ten lectures on wavelets*. Society for Industrial and Applied Mathematics. Philadelphia, Pa.

Hubbard BB (1998): *The world according to wavelets: the story of a mathematical technique in the making*. A.K. Peters. Wellesley, MA.

Jaffard S, Meyer Y, and Ryan RD (2001): *Wavelets: tools for science & technology*. Society for Industrial and Applied Mathematics. Philadelphia.

Qian S (2001): *Introduction to time-frequency and wavelet transforms*. Prentice Hall. Upper Saddle River, NJ.

Qian S, Chen D (1996): *Joint time-frequency analysis: methods and applications*. PTR Prentice Hall. Upper Saddle River, N.J.

Wickerhauser MV (1994): *Adapted wavelet analysis from theory to software*. A.K. Peters. Wellesley, MA.

Experimental and Analytical Study of Seismically Isolated Structures with Uplift Prevention

Panayiotis Roussis

Graduate Student, Department of Civil, Structural & Environmental Engineering, University at Buffalo

Research Supervisor: Michael C. Constantinou, Professor and Chairman

Summary

Experimental and analytical studies of a seismically isolated five-story model structure are conducted to understand the behavior of a novel uplift-prevention Friction Pendulum isolator. Shake table testing on the earthquake simulator at the University at Buffalo involves a number of simulated ground motions with a variety of frequency content and amplitude. A comprehensive analytical model is developed to predict the dynamic response of the model structure. The computer program 3D-BASIS-ME is enhanced to include an element representative of the mechanical behavior of the new isolator and used for comparison with experimental results. The experimental results generated demonstrate the effectiveness of the new isolator in uplift prevention and provide satisfactory evidence for the validity of the new element incorporated in 3D-BASIS-ME.

Introduction

With its appealing conceptual simplicity and its proven effectiveness, seismic isolation has become the epitome of seismic-resistant engineering in recent years. Having found a plethora of applications in many parts of the world over the past couple of decades, seismic isolation has emerged as a pragmatic approach to providing earthquake resistance to structural systems.

The fundamental strategy underlying the seismic isolation technique involves decoupling the structure from the damaging horizontal ground motion, by means of additional flexibility and energy dissipation capability, thus mitigating structural vibration and damage during seismic events.

Research developments in the areas of analytical modeling and experimental validation techniques have been paralleled by notable advances in seismic isolation device hardware. Advocated herein is a novel uplift-prevention Friction Pendulum isolator, abbreviated hereafter as XY-FP. While a conventional Friction Pendulum in principle (Zayas et al., 1987; Mokha et al., 1990; Constantinou et al., 1993), the proposed isolator is morphed into two perpendicular opposing concave beams. Furthermore, the configuration through which the two parts are interconnected permits tension to develop in the bearing, thereby preventing uplift in case of large overturning moments.

This paper presents an experimental and analytical study on seismic isolation of a five-story frame building with large overturning effects incorporating the new XY-FP isolator. The objectives of this study are to: (a) generate experimental results that demonstrate the effectiveness of the XY-FP

isolator in uplift prevention; (b) modify the computer program 3D-BASIS-ME (Tsopelas et al., 1994) to include an element representative of the mechanical behavior of the new isolator; and (c) assess the validity and accuracy of analytical methods to predict the behavior of such systems.

Model Description

The shake-table testing on the earthquake simulator at the University at Buffalo involved a five-story single-bay moment-resisting steel frame. A schematic and a photograph of the quarter-scale model structure are illustrated in Figure 1. The structure is square in plan with a dimension of 52 inches. The story heights are 43 inches for the first story and 47 inches for the remaining stories, for a total height of 231 inches. The member layout is identical for all stories. The floors are comprised of MC 6x12 channel sections. In conforming to the similitude laws, artificial mass, in the form of steel plates and lead blocks, was added to the structure at all floor levels. The structure was mounted on a 6.9-kip steel plate, for a total weight of 24 kips.

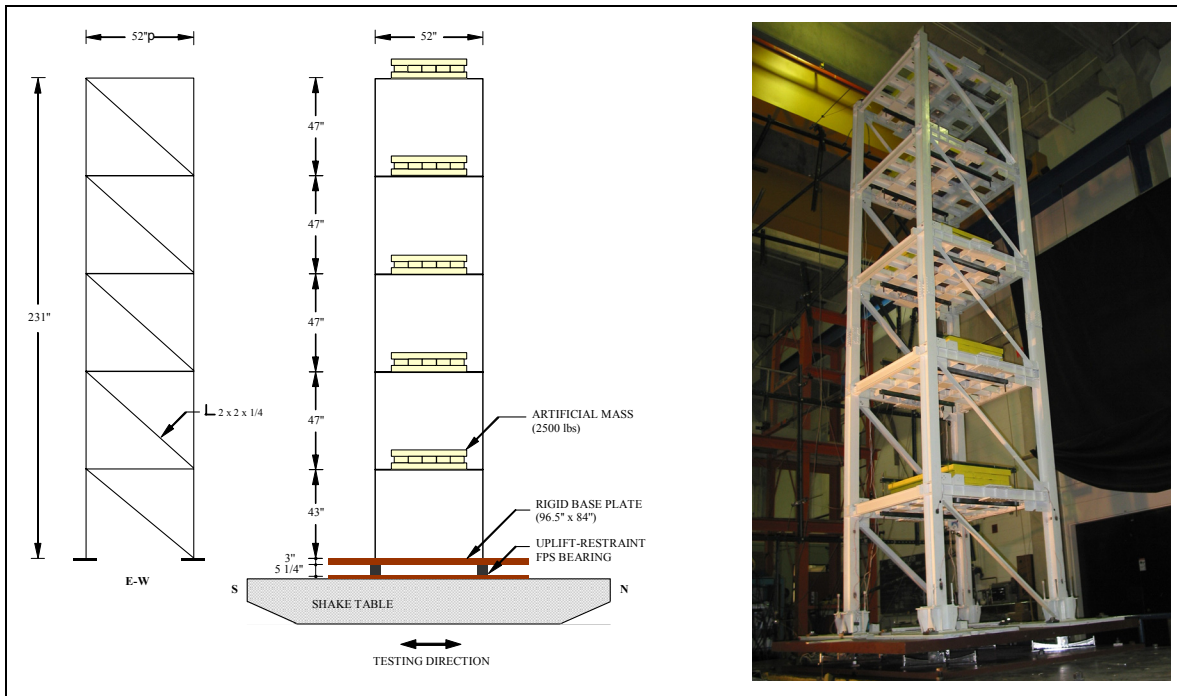


Figure 1. Seismically isolated five-story model on seismic simulator of the University at Buffalo

Installed beneath the base plate, the isolation system is comprised of four XY-FP bearings. While a conventional Friction Pendulum in principle, the XY-FP bearing consists of two perpendicular stainless steel concave beams with their concave surfaces opposing each other (Figure 2). Under the imposed constraint to remain mutually perpendicular, the two beams can move independently relative to each other. Furthermore, the configuration through which the two parts are interconnected permits tension to develop in the bearing, thereby preventing uplift in case of large overturning moments. The isolator at hand has a radius of curvature of 39 inches and is designed to have a displacement capacity of 8 inches.

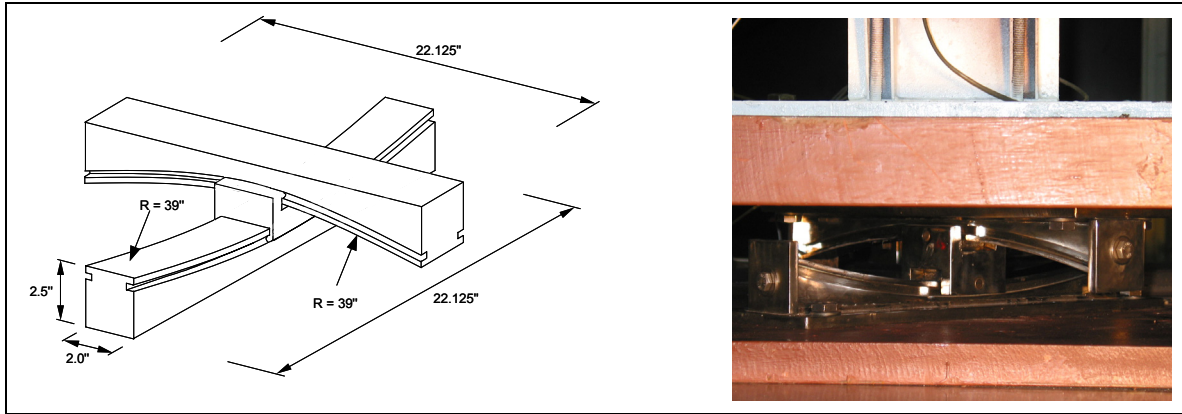


Figure 2. Uplift-prevention XY-FP bearing

Testing Program

The shake-table testing on the earthquake simulator at the University at Buffalo utilized the slender five-story model structure described above. The testing program involved a number of simulated ground motions having a variety of frequency content and amplitude. Each record was compressed in time by a factor of two to conform to similitude requirements. The bearings were rotated below the base plate for testing in different directions. Specifically, tests were done at 0-degree, 45-degree, and 90-degree angle of bottom bearing beam with respect to the excitation direction.

The instrumentation of the five-story model structure consisted of accelerometers and displacement transducers which recorded, respectively, the horizontal accelerations and displacements of the frame at floor levels, the base plate, and the shake table. In addition, the first-story columns were calibrated with strain gauge load cells to measure the first-story shear. To assess the accuracy of important recordings, measurements were contrasted with corresponding calculated quantities. For instance, to check the direct acceleration measurements, recorded floor absolute displacements were double-differentiated to obtain floor acceleration histories. In addition, first-story shear was calculated by summing up floor inertia forces (product of floor mass and floor acceleration) and compared to the recorded first-story shear.

Analytical Prediction of Response

A comprehensive analytical model has been developed to predict the dynamic response of the model structure. The computer program 3D-BASIS-ME (Tsopelas et al., 1994) has been enhanced and used for comparison with experimental results.

Assumed to remain elastic at all times, the five-story superstructure model in 3D-BASIS-ME utilized the shear-type representation. Each floor mass is lumped into a single point mass having three degrees of freedom (two lateral and one torsional) in the horizontal plane. The isolation system was modeled with spatial distribution and explicit nonlinear force-displacement characteristics of the individual isolation devices. To accommodate the mechanical behavior of the new XY-FP isolator, a new hysteretic element (TYPE8) was incorporated into the program. Contrary to the conventional FP isolator (TYPE6), the new element is capable of providing uplift prevention.

The analysis accounted for: (a) the variability of axial load in isolators due to overturning moment effects; (b) the dependency of friction on velocity (Constantinou et al., 1990); (c) the dependency of friction parameter f_{max} on bearing pressure (Constantinou et al., 1993); and (d) the initial displacement of the isolators, namely the permanent displacement from the immediate previous test.

Comparison of Analytical and Experimental Results

The validity of the 3D-BASIS model, especially with reference to the newly introduced XY-FP isolators, was investigated by comparison of the analytical predictions with experimental results.

Figure 3 depicts a comparison between experimental and analytical results for bearing direction of 45 degrees with respect to the excitation direction for two input ground motions. The comparison was made in terms of histories of the isolation system displacement, the first-story shear, and the bearing axial force, as well as in terms of shear force-displacement loops for the isolation system. The presented experimental results attest to the accuracy of the analytical model incorporated in 3D-BASIS-ME.

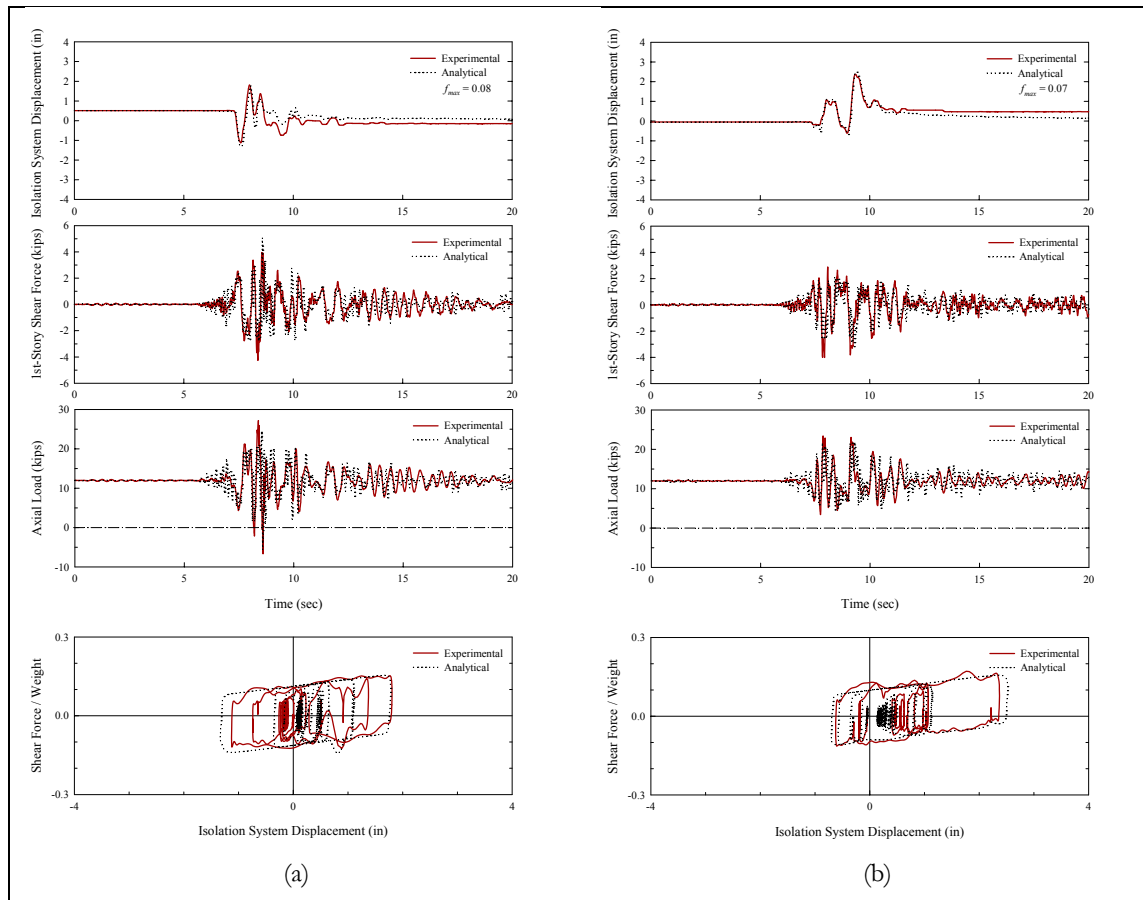


Figure 3. Comparison between experimental and analytical results for (a) Newhall 360, and (b) Sylmar 90 excitation.

Of particular interest are the axial force histories associated with the isolators, herein plotted per isolator pair. Due to the slenderness of the structure (height to width aspect ratio approximately 4.5), large overturning moment effects were induced on the bearings under strong lateral shaking. For the most severe motions, the fluctuations in the vertical bearing loads caused by the overturning moments were large enough to cause reversal of the bearing axial force from compression to tension (Figure 3a).

Concluding Remarks

Experimental and analytical studies of a seismically isolated building were conducted to understand the behavior of a novel uplift-prevention Friction Pendulum isolator. The shake-table testing on the earthquake simulator at the University at Buffalo utilized a five-story model structure having a slender configuration. The testing program involved a number of simulated ground motions with a variety of frequency content and amplitude.

A comprehensive analytical model was developed to predict the dynamic response of the model structure. The computer program 3D-BASIS-ME was enhanced to include an element representative of the mechanical behavior of the new XY-FP isolator and used for comparison with experimental results.

This investigation led to the following conclusions:

1. The experimental results generated demonstrate the effectiveness of the new XY-FP isolators in uplift prevention.
2. Satisfactory experimental evidence has been provided for the validity of the new XY-FP isolator model incorporated in 3D-BASIS-ME.
3. The response of the isolated structures subjected to severe earthquakes can be accurately predicted by analytical procedures.

Acknowledgments

This research was carried out under the supervision of Professor Michael C. Constantinou and primarily supported by the Earthquake Engineering Research Centers Program of the National Science Foundation, under award number EEC-9701471 to the Multidisciplinary Center for Earthquake Engineering Research.

References

Constantinou MC, Mokha AS, and Reinhorn AM (1990): Teflon bearings in base isolation II: modeling. *Journal of Structural Engineering, ASCE*, **116** (2), 455-474.

Constantinou MC, Tsopelas PC, Kim Y-S, and Okamoto S (1993): *NCEER-TAISEI corporation research program on sliding seismic isolation systems for bridges: experimental and analytical study of friction pendulum system (FPS)*. Report No. NCEER-93-0020. National Center for Earthquake Engineering Research, University at Buffalo, Buffalo, NY.

Mokha AS, Constantinou MC, and Reinhorn AM (1990): *Experimental study and analytical prediction of earthquake response of a sliding isolation system with spherical surface*. Report No. NCEER-90-0020. National Center for Earthquake Engineering Research, University at Buffalo, Buffalo, NY.

Tsopelas PC, Constantinou MC, and Reinhorn AM, (1994): *3D-BASIS-ME: Computer program for nonlinear dynamic analysis of seismically isolated single and multiple structures and liquid storage tanks*. Report No. NCEER-94-0010. National Center for Earthquake Engineering Research, University at Buffalo, Buffalo, NY.

Zayas V, Low SS, and Mahin SA (1987): *The FPS earthquake resisting system, experimental report*. Report No. UBC/EERC-87/01. Earthquake Engineering Research Center, University of California, Berkeley, CA.

Evolutionary Power Spectrum Estimation Using Harmonic Wavelets

Jale Tezcan

Graduate Student, Civil and Environmental Engineering Department, Rice University

Research Supervisor: Pol. D. Spanos, L.B. Ryon Chair in Engineering

Summary

The problem of estimating the power spectra of non-stationary stochastic processes by using the harmonic wavelet transform is addressed in this paper. Conventional spectral analysis provides spectral coefficients that are averaged over time and thus, does not represent the evolutionary behavior of power spectra of non-stationary processes. In this study, evolutionary power spectrum of a non-stationary process is expressed in terms of its wavelet coefficients. Harmonic wavelets are chosen due to the appealing properties of the harmonic basis functions; the non-overlapping frequency feature of harmonic wavelets belonging to adjacent scales facilitates the spectral estimation task. The performance of dyadic, generalized and filtered Harmonic wavelets are compared by calculating the instantaneous mean square values of signals compatible with a given spectrum. It has been found that the filtered wavelet spectrum gives the best estimate for the power spectrum. The usefulness of the proposed method is demonstrated by estimating the evolutionary ground spectra of the Kocaeli, Turkey earthquake (08/17/1999).

Introduction

Wavelet transform involves computation of the magnitudes of correlation between a signal and a wavelet at different scales and translations. It extracts time-varying features of a signal because of the short duration of the nonzero portion of the wavelet. The wavelets at a position in time determine only the features of the signal near that position. Thus, the changes in wavelets that correlate highly with the signal at different times indicate the changes in features of the signal as time progresses.

The wavelet transform introduces a useful representation of a function in the time-frequency domain (Mallat 1989). Recent applications of the wavelet transform to engineering problems can be found in several studies that refer to stochastic mechanics, dynamic analysis of structures, system identification, and damage detection. This study applies the wavelet transform to the problem of estimating the power spectrum of stochastic processes, which can be input to dynamic systems.

The notion of the spectrum of a function or stochastic process can be associated with a trigonometric representation, which involves a decomposition of the process in sines and cosines. In this way, it is easy to identify the contribution of parts of the process with a specific frequency content to the total energy (Priestley 1981). Other forms of oscillatory functions can be used to represent non-stationary processes, in order to capture the change in time of the probabilistic characteristics of the process. (Priestley 1988). In this context, the Wigner-Ville time-frequency analysis has been used (Martin and Flandrin, 1985). However, the Wigner-Ville representation of the

spectrum lacks physical meaning since it yields negative values for the spectrum in several cases. Wavelets, which are oscillatory functions of zero mean and of finite energy, can be used to obtain a time-frequency representation of a process. In several studies, the wavelet transform has been used to derive energy relationships of non-stationary signals. (Basu and Gupta, 1997; Iyama and Kuwamura, 1999).

This paper provides explicit relationships between the wavelet coefficients of non-stationary stochastic processes and their spectrum. These formulas are obtained by relating the evolutionary spectrum theory for a stochastic process to its wavelet representation involving the Harmonic wavelet family.

The procedure developed herein is applied to ground acceleration records associated with the Kocaeli, Turkey Earthquake (08/17/1999) and evolutionary seismic spectra are derived.

Harmonic Wavelet Transform

Harmonic wavelets are defined to have a box-like spectrum so that its Fourier Transform magnitude is zero except for an octave band of frequencies (Newland 1993). The mother wavelet for Harmonic Wavelet Transform is defined as $W(\omega)=1/2\pi$ for $2\pi \leq \omega \leq 4\pi$ and zero elsewhere. Inverse Fourier Transform of $W(\omega)$, gives the corresponding complex wavelet as $w(t)=(\exp(i.4\pi.t)-\exp(i.2\pi.t))/ (i.2\pi.t)$, whose real and imaginary parts are shown in Figure 1.

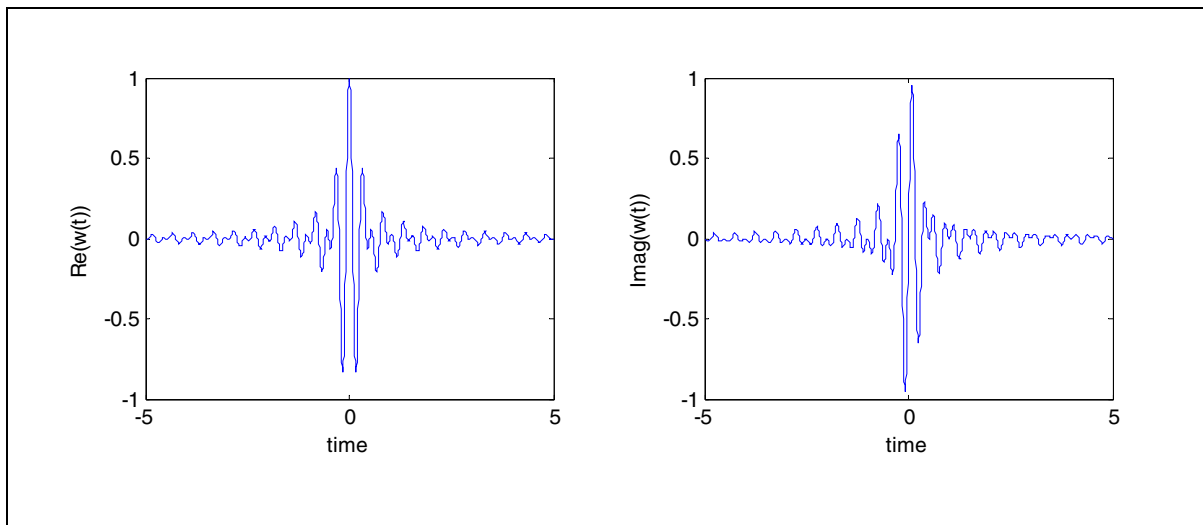


Figure 1. Real and imaginary parts of the harmonic mother wavelet

Evolutionary Power Spectrum Using Harmonic Wavelets

The local spectrum measures the contribution to the total energy coming from the vicinity of a point for a specific scale and translation, the size of the time-frequency window depending on the proper shape in physical and spectral space of the analyzing wavelet. The wavelet spectrum can be expressed as the average of the squared wavelet coefficients for a specific scale.

Three forms of the harmonic wavelets, namely, dyadic, generalized and filtered wavelets have been compared in terms of their performance in approximating the instantaneous mean square values.

Figure 2 compares the instantaneous mean square values using the three kinds of Harmonic Wavelet Transforms. The data used here consists of 500 time histories compatible with the Evolutionary Kanai Tajimi Spectrum, shown as the blue curve.

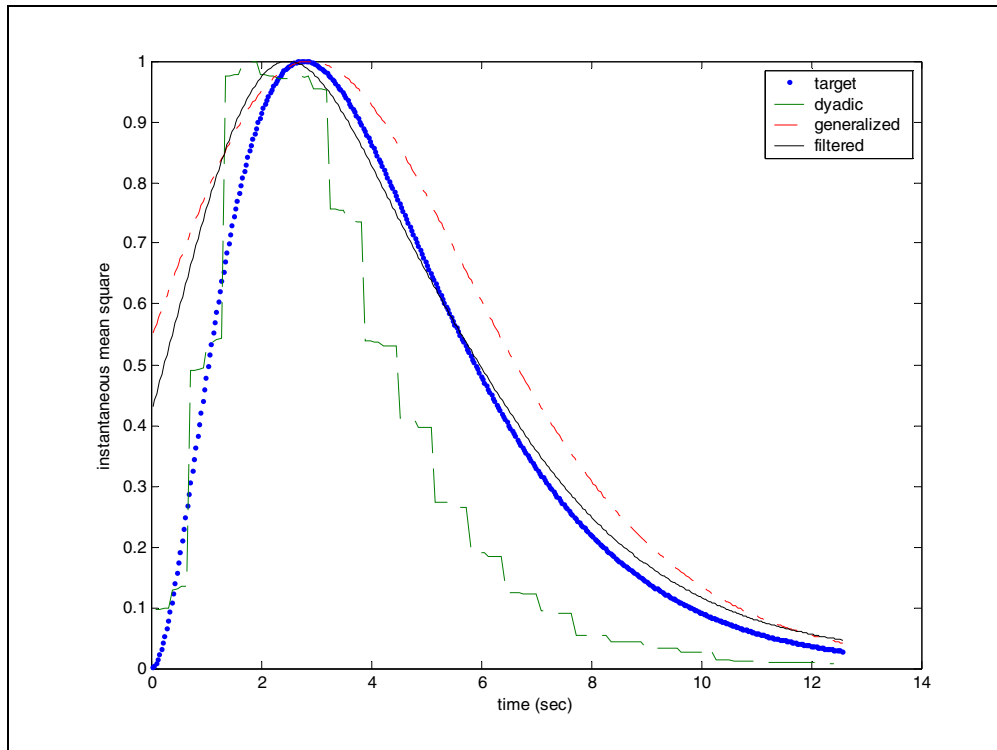


Figure 2. Instantaneous mean square from 500 time histories

Application to Kocaeli, Turkey Earthquake (1999)

The strong motion data used in this study are acceleration records of the Kocaeli earthquake which occurred in Turkey on 08/17/99. Records associated with this earthquake have been obtained from the PEER Strong Motion Database. The filtered Harmonic wavelet transform is employed in the analysis of these seismic records, since it has been found to be the best estimator of the Evolutionary Power Spectrum, as suggested by Figure 2. The sampling period for these records is equal to $T=0.02$ sec, while $N=4096$ sample points per record are used. In Figures 3 and 4, the evolutionary auto-spectra of the 0 and 90 degree ground accelerations, each calculated using 30 records from the Kocaeli earthquake, are shown.

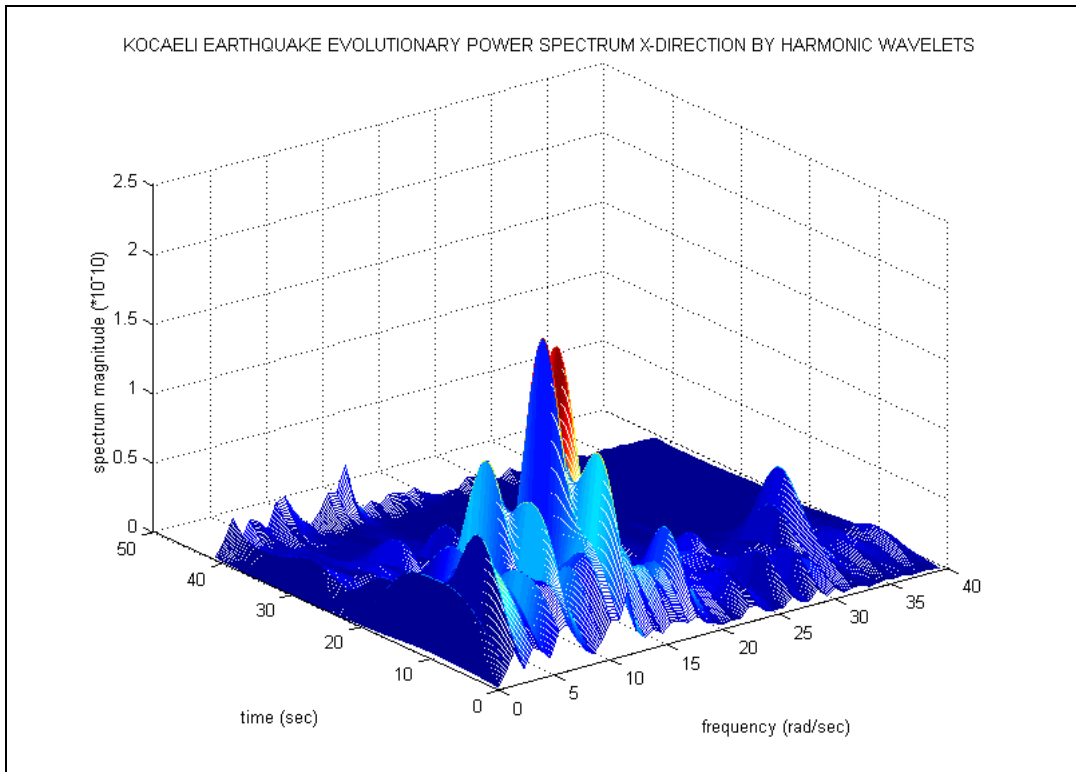


Figure 3. Kocaeli, Turkey earthquake (1999) power spectrum in x-direction

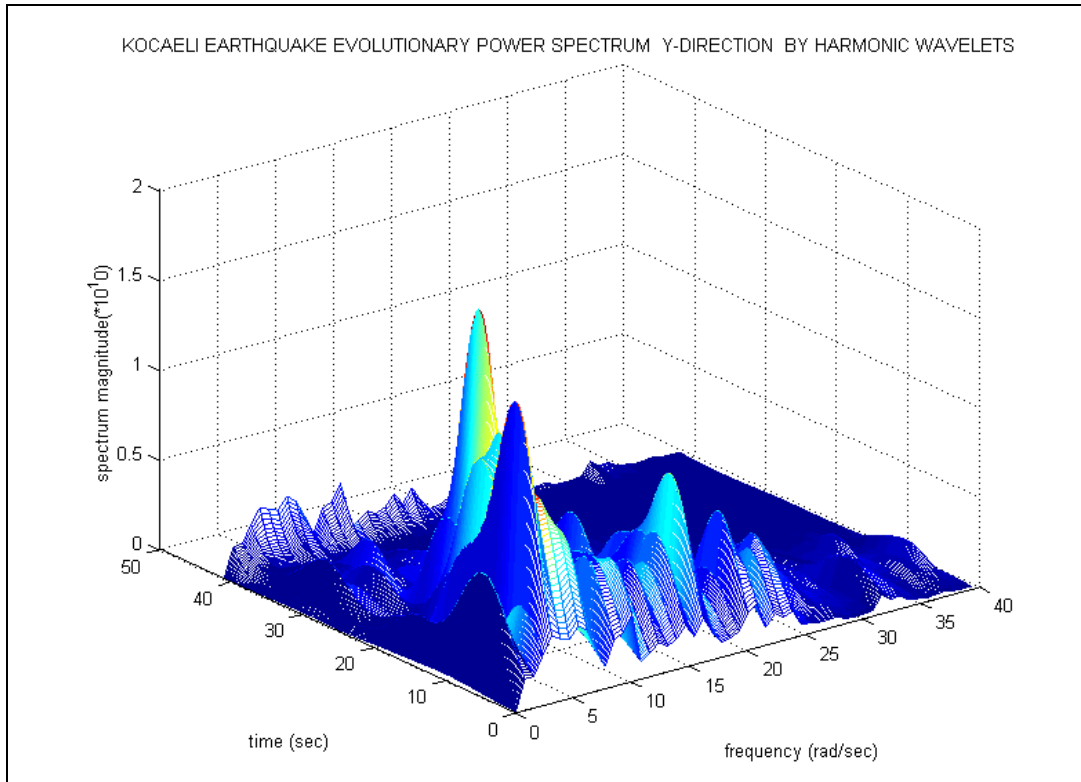


Figure 4. Kocaeli, Turkey earthquake (1999) power spectrum in y-direction

Concluding Remarks

The performance of the harmonic wavelet transform in estimating the power spectrum of stochastic processes has been investigated in this study. A theoretical basis has been developed in which the wavelet transform coefficients are related to the evolutionary spectrum of a stochastic process. The dyadic, the general, and the filtered harmonic wavelet schemes have been used towards assessing their appropriateness for estimating the spectrum of non-stationary processes. The filtered harmonic wavelet scheme has been found to be the most effective one in approximating evolutionary spectra of non-stationary processes.

The method has also been applied to the estimation of the evolutionary spectrum of seismic records. Specifically, ground acceleration records associated with the Kocaeli earthquake have been analyzed. It was shown that the wavelet-based evolutionary spectrum provides important information in the time-frequency domain that can lead to a better understanding of the nature of the seismic excitations and improve the analysis of structures subject to ground motions.

The next step in this study will be to investigate the effectiveness of the harmonic wavelets in nonlinear structural response and system identification problems.

Acknowledgements

This research was carried out under the supervision of Professor Pol D. Spanos, and was partially supported by the Earthquake Engineering Research Centers Program of the National Science Foundation, under award number EEC-9701471 to the Multidisciplinary Center for Earthquake Engineering Research.

References

- Basu B, Gupta VK (1997): Non-stationary seismic response of MDOF systems by wavelet transform, *Earthquake Engineering and Structural Dynamics*, **26**, 1243-1258.
- Iyama J, Kuwamura H (1999): Application of wavelets to analysis and simulation of earthquake motions, *Journal of Earthquake Engineering and Structural Dynamics*, **28**, 255-272.
- Mallat SG (1989): A theory of multiresolution signal decomposition: The wavelet representation, *IEEE Transactions on Pattern Analysis and Machine Intelligence*, **11**, 674-693.
- Martin W, Flandrin P (1985): Wigner-Ville spectral analysis of non-stationary processes, *IEEE Transactions on Acoustics, Speech and Signal-Processing*, **33**(6), 1461-1470.
- Newland DE (1993): *An introduction to random vibrations, spectral and wavelet analysis*, Longman Scientific & Technical.
- Priestley MB (1981): *Spectral analysis and time series*, Academic Press
- Priestley MB (1988): *Nonlinear and non-stationary time series analysis*, Academic Press.

Seismic Response of Single Degree of Freedom Systems with Structural Fuses

Ramiro E. Vargas

Graduate Student, Department of Civil, Structural & Environmental Engineering, University at Buffalo

Research Supervisor: Michel Bruneau, Professor and Director of MCEER

Summary

Passive energy dissipation (PED) devices have been implemented to enhance structural performance by reducing seismically induced structural damage. In this article, metallic dampers are defined to be structural fuses (SF) when they are designed such that all damage is concentrated on the PED devices, allowing the primary structure to remain elastic. Following a damaging earthquake, only the dampers would need to be replaced, making repair works easier and more expedient. Furthermore, SF introduce self-centering capabilities to the structure in that, once the ductile fuse devices have been removed, the elastic structure would return to its original position. A comprehensive parametric study is conducted, leading to the formulation of the SF concept, and allowing the identification of the possible combinations of key parameters essential to ensure adequate seismic performance for SF systems. Nonlinear time history analyses are conducted for several combinations of parameters, in order to cover the range of feasible designs.

Introduction

Typically, in seismic design, the loads resulting from an earthquake are reduced by a response modification factor, which allows the structure to undergo inelastic deformations, while most of the energy is dissipated through hysteretic behavior. Designs have always (implicitly or explicitly) relied on this reduction in the design forces. However, this methodology relies on the ability of the structural elements to accommodate inelastic deformations, without compromising the stability of the structure. Furthermore, inelastic behavior translates into some level of damage on these elements. This damage leads to permanent system deformations following an earthquake, leading to high cost for repair works, in the cases when repairs are possible. In fact, it is frequently the case following earthquakes that damage is so large that repairs are not viable, even though the structure has not collapsed, and the building must be demolished.

To achieve stringent seismic performance objective for buildings, an alternative design approach is desirable. In that perspective, it would be attractive to concentrate damage on disposable and easy to repair structural elements (i.e., “structural fuse”), while the main structure would be designed to remain elastic or with minor inelastic deformations.

The structural fuse concept is described in this study in a parametric formulation, considering the behavior of nonlinear single degree of freedom (SDOF) systems subjected to synthetic ground motions. Nonlinear dynamic response is presented in dimensionless charts normalized with respect

to key parameters. Allowable story drift is introduced as an upper bound limit to the charts, which produces ranges of admissible solutions, shown as shaded areas in the graphs.

Finally, a generic retrofit case study is presented to illustrate the benefits of adding metallic fuse elements to an existing frame. A comparative analysis is made between a bare frame (i.e., without metallic dampers), and the same frame retrofitted using metallic fuse elements, to improve the behavior of the existing structure.

Analytical Model of a SDOF System with Structural Fuses

A SDOF structure with metallic damper subjected to ground motion can be modeled as a lumped mass connected to the ground by elasto-plastic springs, and the inherent system viscous damping action represented by a linear dashpot. Figure 1 shows a general pushover curve for a SDOF system with two elasto-plastic springs in parallel. The total curve is tri-linear with the initial stiffness, K_1 , equal to the frame stiffness, K_f , plus the added structural fuse system stiffness, K_a .

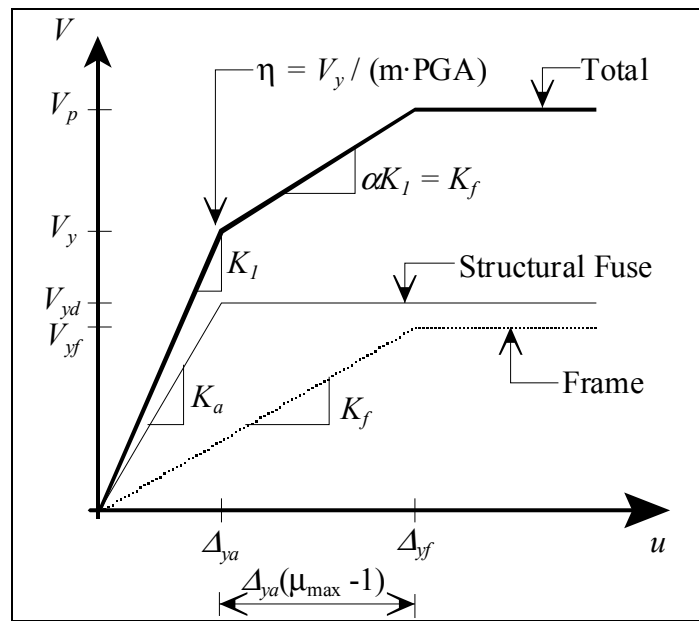


Figure 1. General pushover curve

The structural fuse concept requires that yield deformation of the damping system, Δ_{ya} , be less than the yield deformation corresponding to the bare frame, Δ_{yf} . Once the damping system reaches its yield deformation, Δ_{ya} , the increment on the lateral force is resisted only by the bare frame, being the second slope of the total curve equal to the frame stiffness, K_f . Three important parameters used in this study are obtained from Figure 1, namely, the strain-hardening ratio, α , the maximum displacement ductility, μ_{max} , and the strength-ratio, η . The strain-hardening ratio, α , is the relationship between the frame stiffness and the total initial stiffness. The maximum displacement ductility, μ_{max} , is the ratio of the frame yield displacement, Δ_{yf} , with respect to the yield displacement

of the damping system, Δ_{ya} . In other words, μ_{\max} is the maximum displacement ductility that the structure experiences before the frame undergoes inelastic deformations. The strength-ratio, η , is the relationship between the yield strength, V_y , and the maximum ground force applied during the motion, $m \cdot \text{PGA}$, where m is the system mass, and PGA is the peak ground acceleration.

In Figure 1, V_{yf} and V_{yd} are the shear capacity of the bare frame and the damping system, respectively; and V_y and V_p are the total system yield strength and shear capacity, respectively.

Parametric Formulation

In linear dynamic analysis of SDOF systems, the spring force is considered proportional to the mass relative displacement. However, for a nonlinear SDOF with hysteretic behavior, once the yield point is exceeded, the spring force is no longer proportional to the relative displacement. Mahin and Lin (1983) proposed a normalized version of the nonlinear dynamic equation of motion adapted by this study, and expressed it in terms of the above defined parameters (i.e., α , μ_{\max} , and η).

For a specific ground acceleration, $\ddot{u}_g(t)$, the equation of motion can be solved throughout nonlinear dynamic analyses, in terms of the selected parameters, assuming a damping ratio, ξ , of 5% in this study. The system response can be expressed in terms of the frame ductility, μ_f , which is the ratio of the maximum relative displacement, u_{\max} , with respect to the frame yielding, Δ_{yf} (i.e., $\mu_f = u_{\max} / \Delta_{yf}$).

Nonlinear Dynamic Response

A design response spectrum was constructed based on the National Earthquake Hazard Reduction Program Recommended Provisions (FEMA 2001) for Sherman Oaks, California, and site soil-type class B. This site was chosen because it corresponds to the location of the Demonstration Hospital used by the Multidisciplinary Center for Earthquake Engineering Research (MCEER) in some of its projects. Accordingly, the design spectral accelerations for this site are $S_{DS} = 1.3 \text{ g}$, and $S_{D1} = 0.58 \text{ g}$. Using the Target Acceleration Spectra Compatible Time Histories (TARSCETHS) code, by Halldorsson et al. (2002), a set of three spectra-compatible synthetic ground motions were generated to match the NEHRP 2000 target design spectrum.

Nonlinear time history analyses were conducted using the Structural Analysis Program, SAP 2000, (Computers and Structures, Inc. 2000). Analyses were performed for a range of systems using the following parameters: $\alpha = 0.05, 0.25, 0.50$; $\mu_{\max} = 10, 5, 2.5, 1.67$; $\eta = 0.2, 0.4, 0.6, 1.0$; and elastic period, $T = 0.1 \text{ s}, 0.25 \text{ s}, 0.50 \text{ s}, 1.0 \text{ s}, 1.5 \text{ s}, 2.0 \text{ s}$. The combination of these parameters resulted in 288 analyses for each ground motion generated (i.e., a total of 864 nonlinear time history analyses), where the response of the system is expressed in terms of the frame ductility, μ_f , as a function of the above system parameters.

Many alternatives for plotting results in either two or tri-dimensional charts were evaluated. However, for the purpose of parametric analysis, two dimensional charts were found to be more appropriate, since a matrix of plots can be formed for the whole set of parameters. Figure 2 shows the matrix of results corresponding to the nonlinear analyses conducted in terms of frame ductility, μ_f , as a function of the elastic period, T . Each plot corresponds to a fixed set of α and μ_{\max} values, while each curve represents a constant strength-ratio, η . All the points having $\mu_f < 1$ in Figure 2 represent elastic behavior of the frame (which is the objective of the structural fuse concept).

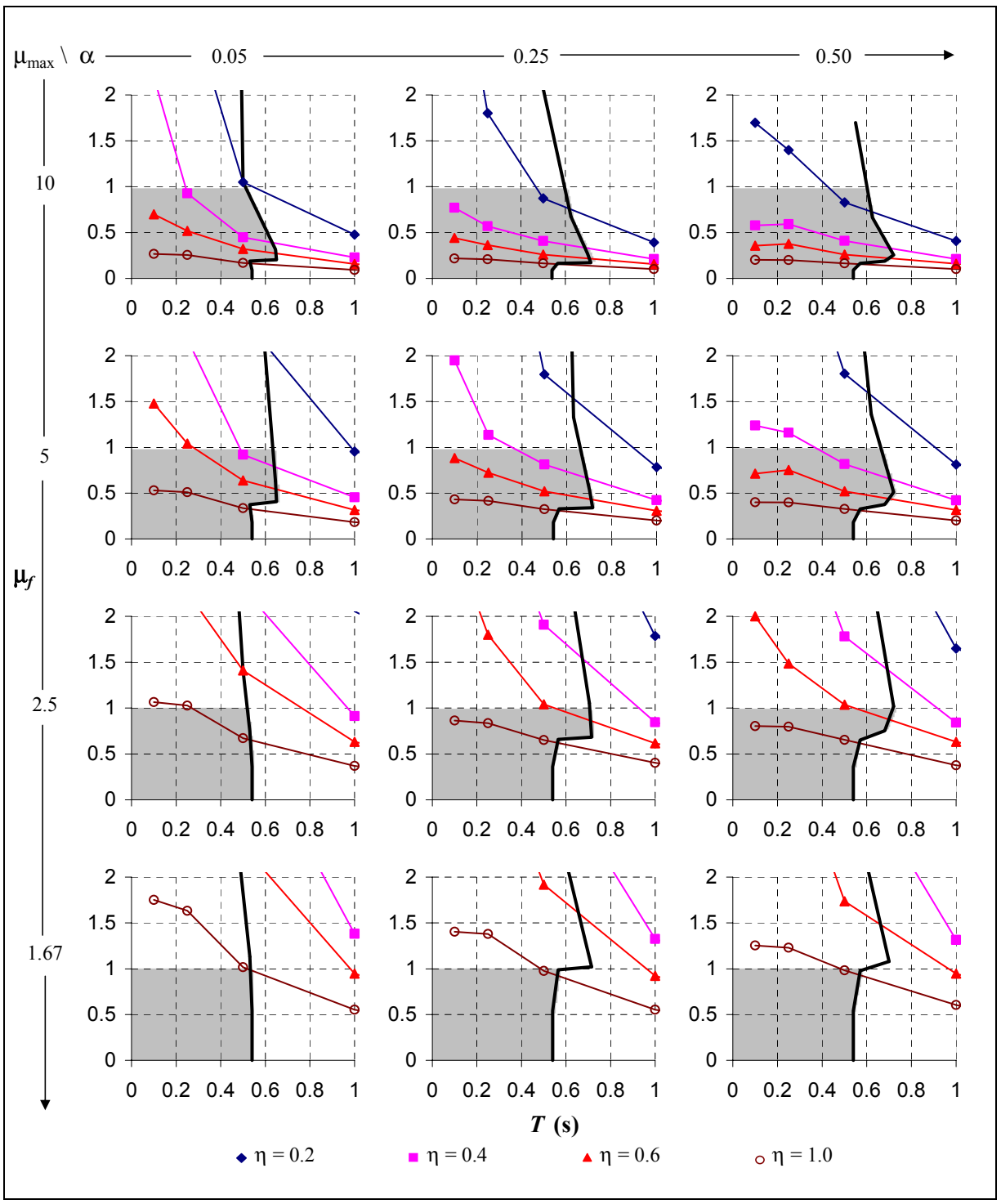


Figure 2. Regions of admissible solutions in terms of frame ductility, μ_f , and story drift of 2%

Allowable story drift has also been introduced in terms of period limit, in order to control relative displacements between consecutive floors. By maintaining the lateral displacement under tolerable levels, instability problems due to secondary effects (frequently called P- Δ effects), as well as damage to some nonstructural components, can be prevented.

For illustration purposes here, the NEHRP 2000 provisions recommended story drift limit of 2% is used, which translates into a limit period of about 0.5 s (solid line on Figure 2). This selected story drift limit, along with the maximum allowable ductility (i.e., $\mu_f \leq 1.0$), define the range of acceptable solutions that satisfy the structural fuse concept as shaded areas on figures such as Figure 2.

Note that for large strength-ratio and period values (i.e., $\eta > 0.6$ and $T > 1.0$ s), the structure tends to behave elastically, which means that metallic dampers only provide additional stiffness with no energy dissipation. Elastic behavior of the metallic dampers contradicts the objective of using PED devices, other than the benefit of reducing the lateral displacements to below certain limits (something that could be done just as well with conventional structural elements).

Generic Retrofit Case Study

In this section, a case study comparison is made between seismic response of a SDOF system without metallic dampers called the bare frame (BF) and the same SDOF system retrofitted with a structural fuse (SF). The same format used to present results for the SDOF system with structural fuses is used to show ductility demand of the BF system as a function of other characteristic parameters. The BF system is modeled as an elasto-plastic SDOF, i.e., with strain-hardening ratio and maximum displacement ductility taken as $\alpha = 1$, and $\mu_{\max} = \infty$, respectively.

For the purpose of this case study, a BF with $m = 0.044$ kN·s²/mm, $K_f = 1.75$ kN/mm, and $V_{yf} = 127.4$ kN (i.e., $T = 1.0$ s) is arbitrarily selected as a system that does not meet the drift requirements, and that would behave inelastically without seismic retrofit under an earthquake with peak ground acceleration of 0.58 g. That existing frame is then retrofitted by the addition of a structural fuse, with $K_a = 5.25$ kN/mm, and $V_{yd} = 76.4$ kN (i.e., $\alpha = 0.25$, $\mu_{\max} = 5$, $T = 0.5$ s, and $\eta = 0.4$).

Figure 3 shows the response of both systems. The arrow in this figure shows how the behavior of the retrofitted system has been “moved” into the area of admissible solutions. The period is reduced to one half of the original value ($T = 0.5$ s), and the frame ductility reduces from 1.9 to 0.8 (i.e., frame response remains elastic). Note the reduction of the strength-ratio of the systems (from 0.5 to 0.4). This is caused partly by the fact that for the chosen parameters for the case study, the SF has a yield strength lower than that of the corresponding BF (i.e., $V_y < V_{yf}$).

Note that a period reduction of one half translates into an increase in the lateral stiffness of four times, and the corresponding maximum base shear (related to peak acceleration) is also increased in this example (not shown here).

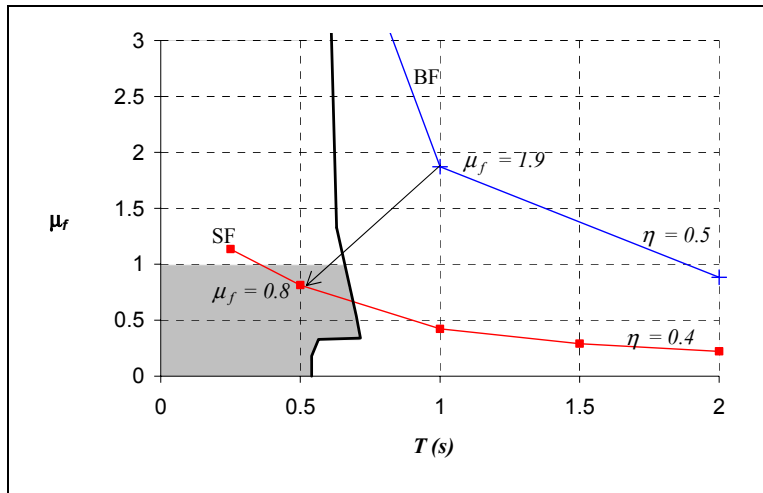


Figure 3. Bare frame (BF) and structural fuse (SF) response

Figure 4 shows the difference in energy dissipation between the BF and SF systems. Initially, in the BF, the energy is absorbed by viscous damping action while the frame is still elastic. Once the yield point is reached (at 4.7 s), the increment in input energy is dissipated mainly by hysteretic behavior of the frame. The inclusion of a structural fuse eliminates any frame hysteretic energy in the SF case (i.e., BF remains elastic), by introducing hysteretic action exclusively in the fuses, while the energy absorbed by viscous damping is not significantly affected. While in this example, the inclusion of a structural fuse causes an important increase in the input energy, this increase is totally absorbed by the fuse action, as shown in Figure 4.

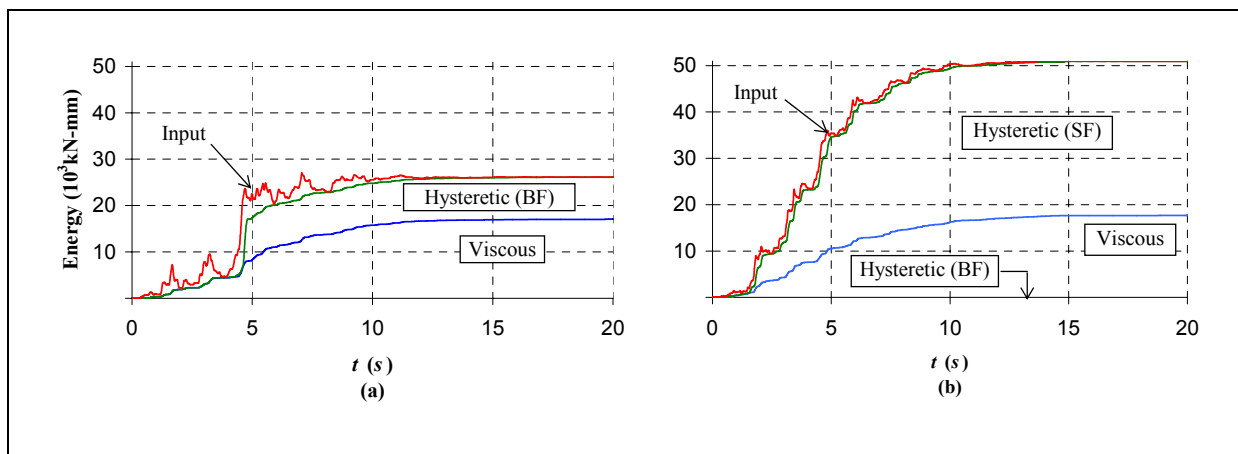


Figure 4. Energy dissipated; (a) bare frame (BF), (b) structural fuse (SF)

Conclusions

The structural fuse concept has been introduced in this paper and validated through a parametric study of the seismic response of SDOF systems. It has been found that the range of admissible solutions that satisfy the structural fuse concept can be parametrically defined, including (as an option) the story drift limit expressed as an elastic period limit. As shown in Figure 2, as a design tool, this can be represented graphically with shaded areas delimiting the range of admissible solutions. It was found that systems having $\mu_{\max} \geq 5$ offer a broader choice of acceptable designs over a greater range of η values.

Even though ductility demand, μ_f , does not vary significantly with α (except for small values, i.e., $\alpha = 0.05$), the hysteretic energy substantially increases with decreases in α values. In other words, substantially different amounts of hysteretic energy can be dissipated by a system having identical ductility demands.

Acknowledgements

This research was carried out under the supervision of Dr. Michel Bruneau, and primarily supported by the Earthquake Engineering Research Centers Program of the National Science Foundation, under award number EEC-9701471. This financial support is gratefully acknowledged.

References

- Computers and Structures Inc. (2000): *Structural analysis program, SAP-2000NL version 7.40: integrated finite element analysis and design of structures*. Computers and Structures Inc., Berkeley, California.
- Federal Emergency Management Agency (2001): *NEHRP recommended provisions for seismic regulations for new buildings and other structures*. Reports No. FEMA 368 and FEMA 369, Washington, D.C.
- Halldorsson B, Dong G, and Papageorgiou A.S. (2002): Earthquake motion input and its dissemination via the internet *Journal of Earthquake Engineering and Engineering Vibration*, **1** (1), 20-26. (<http://civil.eng.buffalo.edu/EngSeisLab/>)
- Mahin SA., Lin J (1983). *Construction of inelastic response spectra for single-degree-of-freedom systems*. Report No. UCB-83/17, Earthquake Engineering Center, University of California, Berkeley.

Seismic Retrofit of Bridge Steel Truss Pier Anchorage Connections

Michael Pollino

Graduate Student, Department of Civil, Structural & Environmental Engineering, University at Buffalo

Research Supervisor: Michel Bruneau, Professor and Director of MCEER

Summary

In assessments of the seismic adequacy of existing steel bridges, the anchorage of steel truss piers to their foundations often has insufficient strength to resist seismic demands. Many other non-ductile failure locations may also exist along the seismic load path that cannot provide adequate seismic performance. Although strengthening is an option, this approach may only transfer damage to another location. An alternative solution could be to release the anchorage connection, allowing development of a rocking bridge pier system. The retrofit solution proposed here allows this rocking mechanism to develop, but complements it by adding passive energy dissipation devices across the anchorage interface to control the rocking response. Specially detailed, hysteretic energy dissipating elements (unbonded braces) act as ductile structural “fuses” in this application. An inherent re-centering capability is also possible. This research investigates the dynamic characteristics of the above proposed controlled rocking/energy dissipation system with focus on design implications.

Introduction

Recent earthquakes, such as the 1989 Loma Prieta, 1994 Northridge, and 1995 Kobe earthquake in Japan have demonstrated the need for improved methods for the design and construction of highway bridges to withstand seismic force and displacement demands. While collapse is rare, undesirable damage can leave the bridge unusable until repairs can be made. Highway bridges deemed critical in the response and recovery efforts following a major earthquake need to remain operational after an earthquake, requiring the bridge to respond in a mostly elastic manner with little to no residual displacements.

Steel truss bridges are found in nearly every region of the U.S. Many existing steel truss bridge piers consist of riveted construction with built-up, lattice type members in an x- or v-braced configuration supporting a slab-on-girder bridge deck. These built-up lattice type members and their connections can be the weak link in the seismic load path. Recent experimental testing of these members revealed that they suffer global and local buckling, causing significant member strength and stiffness degradation resulting in loss of pier lateral strength and major structural damage during an earthquake (Lee and Bruneau, 2003). Existing, riveted connections and deck diaphragm bracing members typically possess little to no ductility (Ritchie et. al., 1999). Another possible non-ductile failure location is the anchorage connection at the pier-to-foundation interface. Analysis of “typical” steel-concrete connections suggests it may be unable to resist even moderate seismic demands.

While strengthening these existing, vulnerable elements to resist seismic demands elastically is an option, this method can be expensive and also gives no assurance of performance beyond the elastic limit. Therefore, it is desirable to have structures able to deform inelastically, limiting damage to easily replaceable, ductile structural “fuses” able to produce stable hysteretic behavior while protecting existing non-ductile elements and preventing residual deformations using a capacity-based design procedure.

Failure or release of the anchorage connection allows a steel truss pier to step back-and-forth or rock on its foundation, partially isolating the pier. Addition of passive energy dissipation devices at the uplifting location can control the rocking response while providing energy dissipation. This system also provides an inherent restoring force capability allowing for automatic re-centering of the tower, leaving the bridge with no residual displacements after an earthquake. The device used in this application is the unbonded brace. An unbonded brace consists of a steel core surrounded by a restraining part, allowing the brace to reach full yield in tension and compression. Experimental testing of the braces can be found in Iwata et al., 2000. Also, this strategy limits the retrofit effort by working at a fairly accessible location. A sketch of a retrofitted bridge pier is shown in Figure 1.

A controlled rocking approach to seismic resistance was implemented in the design of the South Rangitikei Rail Bridge, Mangaweka, New Zealand in the early 1970's (Priestley et. al., 1996) and was later used as a seismic retrofit technique in the Lions' Gate Bridge located in Vancouver, British Columbia (Dowdell and Hamersley, 2001), shown in Figure 2. Both bridges use steel yielding devices across the anchorage interface.

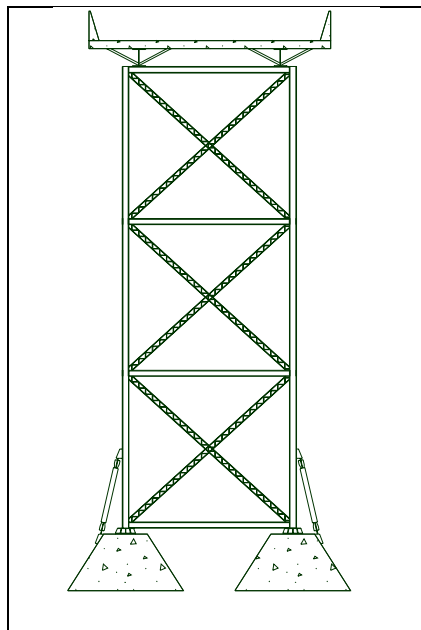


Figure 1. Sketch of retrofitted pier

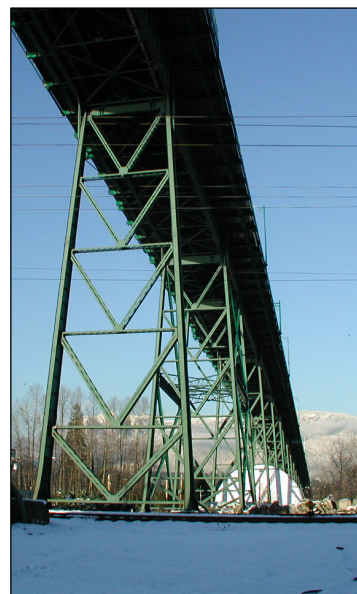


Figure 2. Lions' Gate bridge

This paper presents results from research on the dynamic characteristics of the above proposed rocking/energy dissipation system. Nonlinear time history analyses are used to assess the seismic behavior of the bridges retrofitted per this strategy. Observations on the resulting response, along with capacity design concepts and other constraints, needed to protect all other elements, are used to formulate a design procedure for the proposed controlled rocking retrofit strategy. This procedure is briefly outlined, including an overview of ongoing and future work to validate the concept.

Controlled Rocking System for Seismic Retrofit

The controlled rocking bridge pier system considered can be shown to develop a flag-shaped hysteresis. This is due to the combination of pure rocking response from the restoring moment provided by the bridge deck weight and energy dissipation provided by yielding of the unbonded braces. The key parameters for the hysteretic response of the rocking bridge pier system considered here include the fixed-base lateral stiffness of the existing steel truss pier (k_o), the aspect ratio of the pier (h / d) and the cross-sectional area (A_{ub}), effective length (L_{ub}) and yield stress of the unbonded brace (F_{yub}). Also, the weight excited by horizontally imposed accelerations (W_h) and the vertical gravity weight carried by a pier (W_v) are assumed equal here and expressed as W . A strength ratio, η_L , is defined here as the ratio of unbonded brace yield strength ($A_{ub}F_{yub}$) to half of the vertical weight ($W_v/2$). This is a measure of the hysteretic energy dissipation per cycle and $\eta_L < 1$ provides for pier re-centering. The various steps and physical behaviors that develop through a typical half-cycle are shown qualitatively in Figure 3a and the corresponding actions of the unbonded brace during the controlled rocking response are shown in Figure 3b.

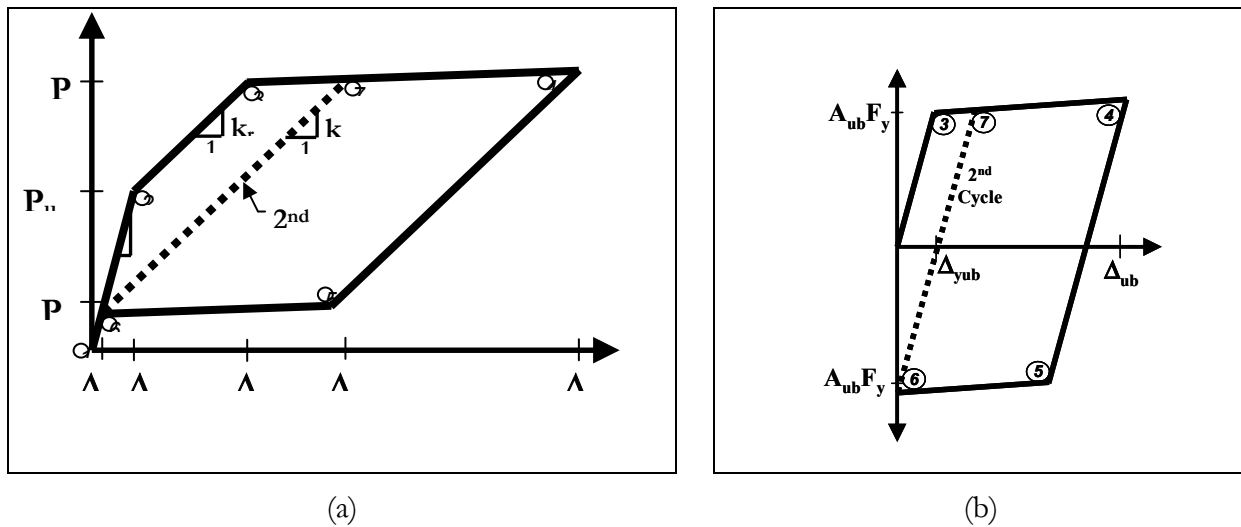


Figure 3. System hysteretic behavior (half-cycle)

By symmetry, the behavior repeats itself for movement in the other direction. Transition from first to second cycle response occurs when the unbonded braces yield in compression and the braces carry a portion of the weight after the system comes to rest upon completion of the cycle.

Parametric Study

In order to provide a preliminary understanding of system behavior, a parametric study was undertaken to observe the dynamic system response and to assess the accuracy of some approximate, simplified techniques in predicting seismic response. Therefore, a number of such procedures were considered. Two of the methods of analysis considered to characterize system response are similar to the nonlinear static procedure (NSP) in FEMA 356 (FEMA 2000) while another is similar to the nonlinear static procedure for passive energy dissipation systems found in FEMA 274 (FEMA 1997). An analysis procedure similar to the latter can be found in the NCHRP 12-49 document (ATC/MCEER 2003).

The NSP requires the development of the system pushover curve, incorporating the nonlinear load-deformation characteristics of individual elements. The second cycle properties are used for determining the displacement demand due to the system's increased flexibility after the first cycle, as was described previously. Using results from the pushover analysis, a rational expression for the effective stiffness can be taken as:

$$k_{\text{eff}} = k_o \left(\frac{\Delta_{\text{up}2}}{\Delta_{y2}} \right) + k_r \left(\frac{\Delta_{y2} - \Delta_{\text{up}2}}{\Delta_{y2}} \right) \quad (1)$$

which uses the pre- and post-uplift properties of the system. This is referred to as Method 1.

The capacity spectrum method for the design of passive energy dissipation (PED) systems uses spectral capacity and demand curves to represent the response in a graphical format. The added energy dissipation from the unbonded braces is converted to equivalent viscous damping thus reducing the seismic demand curve from the 2% damped spectrum. Each pier is assumed to have a single degree of freedom representing the dominant horizontal mode of vibration. This is referred to as Method 2.

Time history analysis is used to verify the adequacy of the simplified methods of analysis and to observe dynamic behavior. Analytical models were developed of representative piers subjected to a horizontal excitation applied in a primary orthogonal direction. Each pier is assumed to carry an equal mass both vertically and horizontally. The pier itself is modeled with its elastic properties and all nonlinear action occurs at the foundation interface. "Gap" and hysteretic elements are placed in parallel across the anchorage interface to model the rocking mechanism. The hysteretic element is based on the model proposed by Wen (1976). Braces are aligned vertically in the analytical model, however, they may be implemented inclined to the pier. Restraints are provided at the anchorage level that prevent movement in the horizontal direction but provide no resistance to vertical movements. Inherent structural damping is approximated by assigning 2% equivalent viscous damping to each mode. The Target Acceleration Spectra Compatible Time Histories (TARSCTHS) software developed by the Engineering Seismology Laboratory (ESL) at the University at Buffalo is

used to generate synthetic ground motions attempting to match elastic response spectra defined by the NCHRP 12-49 (ATC/MCEER 2003) spectrum. These motions are applied to the analytical model.

Sample results are shown in Figure 4, for an aspect ratio of 4 and strength ratios, η_L , of 0.25 and 0.5. The deck-level displacement from time history analysis (Δ_{TH}) is normalized by the displacement predicted from design methods 1 and 2 (Δ_{design}). The design methods were able to predict response with sufficient accuracy for design. With this type of system (flag-shaped hysteretic), it was shown (including results not presented here) that Method 2 will be more reliable for all possible designs. Method 1 uses a design philosophy that was initially established for elasto-plastic systems; however, it appears to work reasonably well for systems with $\eta_L > 0.6$.

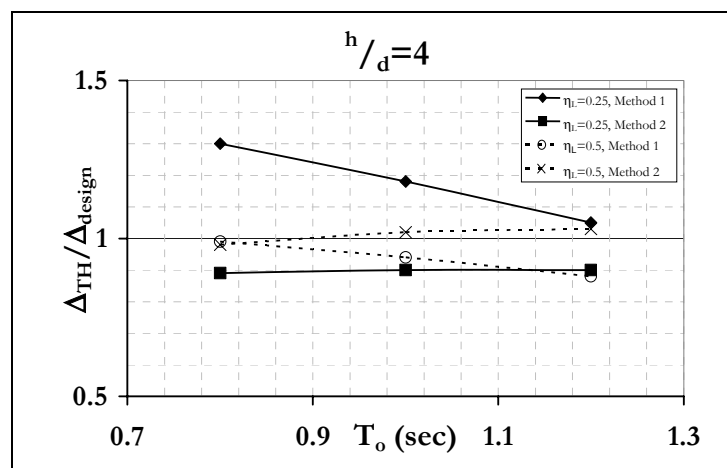


Figure 4. Sample results of parametric study

Proposed Capacity Based Design Procedure

In the perspective of seismic retrofit, a capacity based design procedure is proposed here to protect non-ductile elements while dissipating energy in specially detailed steel yielding devices. A large number of constraints exist and thus a systematic design procedure that attempts to obey all constraints is desirable. The proposed design procedure uses a graphical approach in which the boundaries of compliance and non-compliance of the design constraints are plotted with respect to two key design parameters. The two design parameters used are the length and cross-sectional area of the unbonded brace, L_{ub} and A_{ub} , respectively.

Deck-level Displacement

To the writer's knowledge, there exists no solidly established rule for determining maximum allowable displacements for bridges. Although there are no non-structural components in bridge structures that would warrant the specification of limited drifts to prevent damage, there likely exist structural elements for which deformations must be limited to prevent their damage or damage of their connections. Such deformation limits vary from bridge to bridge. Here, the deformation limits

considered are those that attempt to prevent P- Δ effects from affecting the seismic behavior and a limit based on overturning stability. The smaller of these two limits is used.

Ductility Demand on Unbonded Brace

Limits on the inelastic strain demands are set in order to ensure that the brace behaves in a stable, predictable manner. These limits should be based on engineering judgment and experimental test data. Experimental test data of the inelastic cyclic response of an unbonded brace, adapted from Iwata et al., 2000, is shown in Figure 5. A strain of 1.5% has been selected for a “maximum considered” type earthquake, as appropriate for unbonded braces based on many reported experimental results.

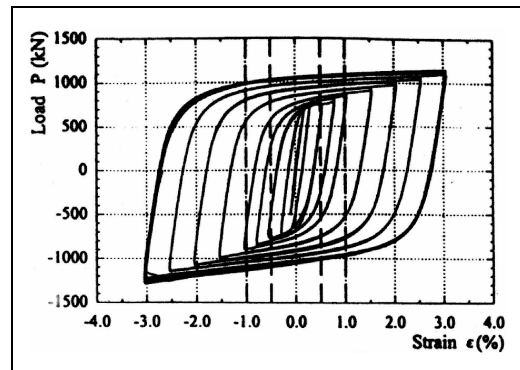


Figure 5. Experimental test results (adapted from Iwata et al., 2000)

Impact Velocity to Foundation

After a tower leg uplifts from the foundation, it eventually returns to the foundation with a velocity upon impact. Assuming the maximum velocity of the bridge deck to be equal to the inelastic pseudo spectral velocity (PS_{vi}) and the maximum to occur the moment before impact, the impact velocity can be taken for design purposes as:

$$v_{imp} = PS_{vi} \left(\frac{d}{h} \right) \quad (2)$$

Forces to Existing Members and Connections

Capacity design procedures are used to conservatively predict the maximum force demand such that the non-ductile elements can remain elastic, forcing all inelastic action to the specially detailed, ductile structural elements. The base shear demand is determined by the static system yield force amplified by a factor, R_{dup} , to account for dynamic effects resulting from uplift from the foundation. A conservative estimate of the maximum axial force developed within pier legs is essential due to the pier legs being the primary gravity load resisting system of the bridge. Energy principles are used to account for the impacting of the pier legs and impulsive loading applied during rocking.

Conclusions

A new retrofit strategy relying on controlled rocking has been proposed to achieve ductile seismic performance of steel truss bridge piers. Unbonded braces are used to provide energy dissipation to

the system while limiting the base overturning moment. This retrofit strategy allows the existing pier and superstructure to remain elastic, and provide self-recentering of the structure following earthquakes, providing a higher level of performance during earthquake motions and increasing the probability that the bridge will remain operational for response and recovery efforts following an earthquake. Results suggest that the proposed retrofit strategy using the capacity design procedure can predict response such that desired performance is achieved. Further analytical research is needed to investigate response of the rocking system subjected to bi-directional and vertical excitation, refine the existing design procedure and develop details for the implementation of the system. Dynamic experimental testing of rocking steel truss piers with passive energy dissipation devices implemented at the anchorage location is expected thereafter.

Acknowledgement

This research was carried out under the supervision of Professor Michel Bruneau, and was supported by the Federal Highway Administration under contract number DTFH61-98-C-00094 to the Multidisciplinary Center for Earthquake Engineering Research.

References

ATC/MCEER (2003): *NCHRP 12-49 Recommended LRFD guidelines for the seismic design of highway bridges, Part I: specifications*. ATC/MCEER Joint Venture.

Dowdell D, Hamersley B (2001): Lions gate bridge north approach: seismic retrofit. *Behaviour of Steel Structures in Seismic Areas. Proceedings of the Third International Conference. STESSA 2000*. Montreal, Canada, August 21-24, 2000, 319-326.

FEMA (1997): *FEMA 274 NEHRP recommended provisions for seismic regulations for new buildings and other structures. Part-2-commentary*. Building Seismic Safety Council for the Federal Emergency Management Agency, Washington, D.C.

FEMA (2000): *FEMA 356 NEHRP recommended provisions for seismic regulations for new buildings and other structures*. Building Seismic Safety Council for the Federal Emergency Management Agency, Washington, D.C.

Iwata M, Kato T, and Wada A (2000): Buckling-restrained braces as hysteretic dampers. *Behaviour of Steel Structures in Seismic Areas. STESSA 2000*, 33-38.

Lee K, Bruneau M (2003): *Review of energy dissipation of compression members in concentrically braced frames*. Technical Report MCEER-02-0005. Multidisciplinary Center for Earthquake Engineering Research. University at Buffalo, Buffalo, NY.

Priestley MJN, Seible F, and Calvi GM (1996): *Seismic design and retrofit of bridges*. John Wiley & Sons, New York.

Ritchie P, Kahl N, and Kulicki J (1999): *Critical seismic issues for existing steel bridges*. Technical Report MCEER-99-0013. Multidisciplinary Center for Earthquake Engineering Research, University at Buffalo, Buffalo, NY.

Wen YK (1976): Method for random vibration of hysteretic systems. *Journal of the Engineering Mechanics Division*. ASCE, **102** (EM2).

Performance Estimates in Seismically Isolated Bridge Structures

Gordon P. Wam

Graduate Student, Department of Civil, Structural, & Environmental Engineering, University at Buffalo

Research Supervisor: Andrew S. Whittaker, Associate Professor

Summary

An analytical study investigating the performance of seismically isolated bridge structures subjected to earthquake excitation is summarized. Here, performance is assessed using the following descriptors: maximum isolator displacement and energy demand imposed on individual seismic isolators. Nonlinear response-history analysis is employed considering twenty different isolation systems and three bins of earthquake ground motions. Results of these analyses are used to: (1) review the accuracy of the current AASHTO equation for the calculation of displacements in seismically isolated bridge structures, (2) determine the increase in maximum horizontal displacement of a seismic isolator due to bidirectional seismic excitation, and (3) review the current AASHTO prototype testing requirements for seismic isolators under seismic loading conditions. The current AASHTO equation for calculating maximum isolator displacements is shown to underestimate median maximum horizontal displacements determined from bidirectional nonlinear response-history analysis. Maximum isolator displacements determined from bidirectional seismic excitation are shown to be significantly larger than those considering unidirectional seismic excitation. Two factors contributing to the increase in maximum isolator displacement are identified; additional displacement demand from a second (orthogonal) component, and the coupled response of seismic isolators. The current prototype testing requirements for seismic loading specified by AASHTO are shown to result in energy demands that are inconsistent with those determined from numerical simulation of maximum earthquake shaking. An improved prototype testing protocol for seismic isolators subjected to seismic loading is proposed.

Introduction

The key design variable for seismic isolation systems is displacement over the isolation interface. Isolator displacement dictates (a) the space around the isolated superstructure to facilitate unrestricted movement of the superstructure, (b) the shear strain in elastomeric isolators and isolator stability, (c) the plan geometry of sliding isolators, and (d) forces transmitted to the bridge substructure for given isolator stiffness. Mechanical properties of the isolator assumed in the design and analysis of the isolation system are checked prior to fabrication of production seismic isolators and installation in the bridge structure through prototype testing.

The current design procedure for seismic isolation systems for bridge structures is set forth in the American Association of State Highway and Transportation Officials (AASHTO) Guide Specifications for Seismic Isolation Design (AASHTO 1999). An estimate of the maximum displacement is calculated using a static-isolator (benchmark) calculation, Equation 3 of the Uniform Load Method of the Guide Specifications. Equation 3 (in SI units of millimeters) is presented here

$$d = \frac{250AS_iT_{eff}}{B} \quad (1)$$

where $250AS_i$ is the 5-percent damped spectral displacement corresponding to a 1-second period; T_{eff} is the effective period of the isolated structure at the design displacement in seconds; and B is a coefficient that modifies the spectrum for equivalent viscous damping other than 5-percent. The 1-second spectral displacement is a function of the acceleration coefficient, A , and the site coefficient S_i . Values of A and S_i are given in Division 1-A: Seismic Design of the AASHTO Standard Specifications for Highway Bridges (AASHTO 1996). Equation 1 assumes the effective period of the isolation system falls in the constant velocity portion of the design spectrum in which displacements are assumed to increase linearly with period.

Section 13.2 of the Guide Specifications include requirements for prototype testing of seismic isolators subjected to seismic loading, which include multiple cycles to the maximum design displacement, d . A combination of three tests result in 22 cycles to a displacement equal to or greater than the design displacement and 31 cycles of displacement to various amplitudes typically conducted at low maximum speed (frequency). Accordingly, it is of significant import to bridge (and building) isolation construction that an estimate of maximum isolator displacement established using the procedures set forth in the AASHTO Guide Specifications be sufficiently accurate and that a prototype testing protocol be representative of the demand imposed on seismic isolators during maximum earthquake.

Previous research has demonstrated that Friction (F), Friction-Pendulum (FP) and Lead-Rubber (LR) isolation bearings exhibit a coupling between the response in each orthogonal direction (Mokha et al., 1993, Huang et al., 2000 and Mosqueda et al., 2003). Ignoring this coupling results in an underestimation of maximum isolator displacement by as much as 20-percent (Mokha et al., 1993). To capture the behavior of these seismic isolators under dynamic loading the coupled behavior must be considered (Mokha et al., 1993). This research (Mokha et al., 1993, Huang et al., 2000 and Mosqueda et al., 2003) also demonstrated that Coupled-Plasticity, Bouc-Wen, and similar formulations are capable of predicting the response of seismic isolation systems composed of F, FP and LR isolators with reasonable accuracy.

Objectives and Technical Approach

The objectives of this research study are (1) to review the accuracy of the current AASHTO equation for calculating displacements in seismically isolated bridge structures, (2) to determine the increase in maximum isolator displacement due to bidirectional seismic excitation and to quantify the contribution due to the coupled behavior of the seismic isolators and (3) to determine energy-related demands imposed on seismic isolators subjected to earthquake excitation and to translate these demands into a prototype testing protocol for seismic isolators subjected to seismic loading.

For this study, response-history analysis is employed. A simple seismically isolated bridge structure is considered and subjected to unidirectional and bidirectional earthquake excitation. The simplicity of the assumed bridge structure enables a clear understanding of the behavior of seismic isolation systems subjected to bidirectional earthquake excitation. Physical properties of the single-span superstructure are based on the middle span of a three-span example bridge structure set forth in a report by the Applied Technology Council (ATC 1986). The seismic isolators are idealized using a bilinear representation and modeled using a rate-independent coupled plasticity formulation (Huang

et al., 2000 and Mosqueda et al., 2003). Properties of the bilinear isolators, namely, Q_d the zero-displacement force-intercept and K_d the second-slope stiffness are varied widely to ensure the results of this research are broadly applicable to seismically isolated bridge structures in the United States. This bilinear characterization and defining parameters is shown in Figure 1. This presentation is similar to one used in the AASHTO Specifications (1999).

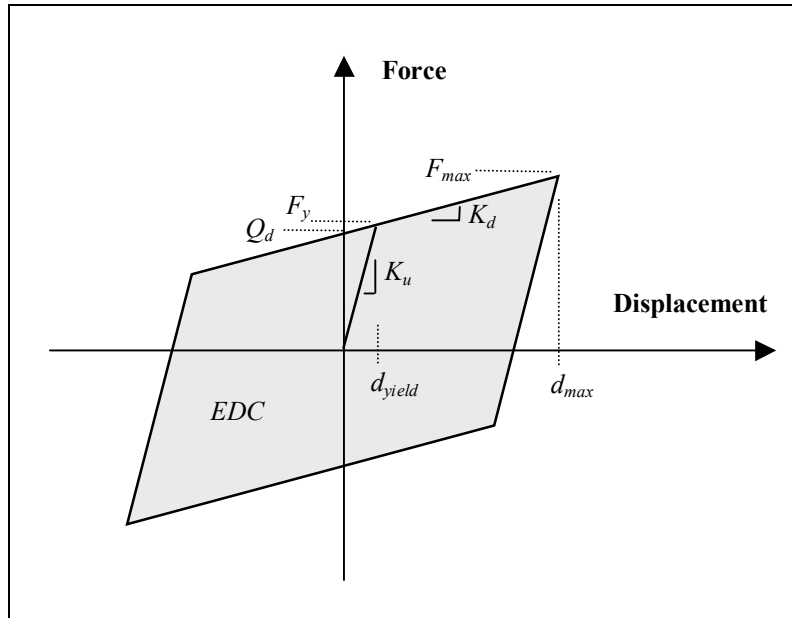


Figure 1. Idealized bilinear force-displacement relationship for seismic isolators

Results of the response-history analyses are mined to determine maximum isolator displacements (displacement across the isolation interface). Maximum isolator displacement data is statistically sorted for each isolation system considered and used to review the accuracy of the current equation (Equation 1) for calculating displacements at the center of rigidity of an isolation system. Response data is further utilized to provide new knowledge related to the energy demands on seismic isolators and seismic isolation systems during maximum earthquake shaking. Energy demands are determined by numerically integrating the force-displacement response of individual seismic isolators obtained from response-history analysis. This information is used to review the current AASHTO prototype testing requirements for seismic isolators subjected to seismic loading (AASHTO 1999) and to propose an improved prototype testing protocol for seismic isolators subjected to seismic loading.

Earthquake Ground Motions

Organization

A total of 72 pairs of earthquake ground motions were collected and organized into seven bins: an approach for organizing ground motions proposed by Krawinkler (2001). Information on all seven bins is provided in Warn (2003). Three of these bins (32 pairs) and corresponding results are presented in this paper. Ground motions contained in these three bins represent levels of seismic

hazard for which seismic isolation is typically employed. All but six pairs of the acceleration histories were extracted from two sources: the Pacific Earthquake Engineering Research (PEER) database (PEER 2000) and the SAC Steel Project database (SAC 1997). Six ground motion pairs were obtained from Miranda (2002).

Presented in Table 1 is information related to the ground motion bins such as the Number of Components, Moment Magnitude, Distance to Fault, Site Class and Classification. The ground motion bins are denoted: (1) Near-Field, (2M) Large-Magnitude, Small-Distance, and (7) Large-Magnitude, Soft-Soil.

Table 1. Earthquake ground motion bins

| Bin | Number of Components | Description | Moment Magnitude | Distance to Fault (km) | Site Class | Classification |
|-----|----------------------|-------------|------------------|------------------------|------------|----------------|
| 1 | 24 | NF | 6.7 – 7.6 | < 10 | D | NEHRP |
| 2M | 20 | LMSD | 6.5 – 7.3 | 10 – 30 | A,B,C | USGS |
| 7 | 20 | LM – SS | 6.9 – 8.1 | 2.6 - 385 | E,F | NEHRP |

Eight of the twelve ground motion pairs contained in Bin 1 exhibited strong directivity effects, i.e., response from one component (fault normal) is significantly greater than the response from the orthogonal component (fault parallel) for periods greater than 1.0 second. Ground motions contained in Bins 2M and 7 exhibit no clear directivity effects. Due to the limited number of large magnitude, soft soil records available, distance-to-fault criteria was relaxed.

Spectral Demand

Response spectra were generated for each ground motion component used in this study. All spectra were generated for 5-percent critical damping. A goodness-of-fit test was conducted on several samples of spectral acceleration data for various periods considering two continuous probability distribution functions, the normal (or Gaussian) and the lognormal distributions. From this investigation it was determined that a lognormal distribution better characterized the distribution of spectral acceleration data (Warn 2003). Therefore, the seismic hazard for each bin is characterized using the median of all spectra. Median spectra were determined using the sample mean and sample standard deviation of the logarithm of the spectral acceleration data. Median 1-second spectral accelerations were determined to be 0.83 g, 0.36 g and 0.30 g for Bins 1, 2M, and 7, respectively. The median 1-second spectral accelerations were used to calculate the design displacements for the simple isolated bridge using the AASHTO Uniform Load Method (AASHTO 1999).

Displacement Estimates

The results of unidirectional and bidirectional nonlinear response-history analysis were mined to determine maximum isolator displacements. Only the results of bidirectional response-history analysis are presented here. Maximum horizontal isolator displacements were determined from the square-root-sum-of-squares (SRSS) displacement response calculated at each time step during the analysis. Median maximum horizontal isolator displacements, denoted $d_{y,}$, were computed for each

isolation system and ground motion bin and compared with isolator displacements determined from the AASHTO calculation.

Figure 2 shows the AASHTO calculated displacement for Bin 2M underestimates the median maximum horizontal isolator displacement for twelve of the twenty isolation systems with the maximum difference (d_{xy}/d) of 1.8.

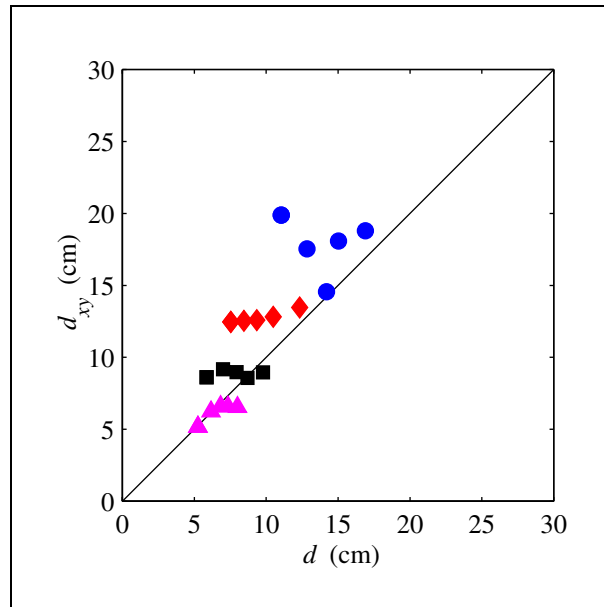


Figure 2. Comparison of median maximum isolator displacements from bidirectional response-history analysis and maximum isolator displacements per AASHTO for Bin 2M

Energy Demands on Seismic Isolators

Normalized Energy Dissipated

Force-displacement response data determined from the results of unidirectional and bidirectional response-history analysis conducted in support of the maximum isolator displacement study were mined to determine energy related demands imposed on seismic isolators during maximum earthquake shaking. For this study, the energy dissipation capacity of the isolators is assumed to be equal to the energy demands imposed on the seismic isolators. The cumulative energy demand imposed on individual seismic isolators was determined by numerically integrating the force-displacement response. For bidirectional excitation the total cumulative energy demand is calculated as the sum of the total energy in the x- and y-directions. For this study, the total cumulative energy has been normalized by the energy dissipated from one fully reversed cycle to the maximum displacement, determined from response-history analysis. Normalized energy dissipated (*NED*) is defined as

$$NED = \frac{\int F du}{EDC} \quad (2)$$

where F is the restoring force of the seismic isolator; du is an incremental displacement; and EDC is the energy dissipated from one fully reversed cycle to the maximum displacement, where the maximum isolator displacement is determined from response-history analysis. The EDC by a bilinear isolator (see Figure 1) is calculated using Equation 3 and was adopted from the AASHTO Guide Specifications (AASHTO 1999)

$$EDC = 4 Q_d (d_{max} - d_{yield}) \quad (3)$$

where d_{max} is the maximum isolator displacement and d_{yield} is the yield displacement assumed herein to be negligible. Normalizing the total energy dissipated by the EDC allows the results of this study to be generally applicable to isolators and isolation systems idealized using a bilinear force-displacement relationship and represents the number of harmonic cycles to the maximum displacement to dissipate an amount of energy equivalent to the total energy demand due to a severe earthquake.

Sample energy demand data determined from the results of bidirectional analysis is presented herein. Shown in Figure 3 are mean and mean plus one standard deviation ($\text{mean} + 1\sigma$) NED data for Bins 1, 2M and 7 for all isolation systems with $T_d = 2.0$ seconds. From Figure 3a it is observed that $NED = 4.0$ (4 fully reversed cycles to the maximum displacement) conservatively estimates mean total energy demands for isolation systems with $Q_d/W \geq 0.06$ (typical of bridge applications). Considering the same isolation systems, $NED = 5.0$ is observed to reasonably estimate the $\text{mean} + 1\sigma$ energy demands for each ground motion bin shown in Figure 3b.

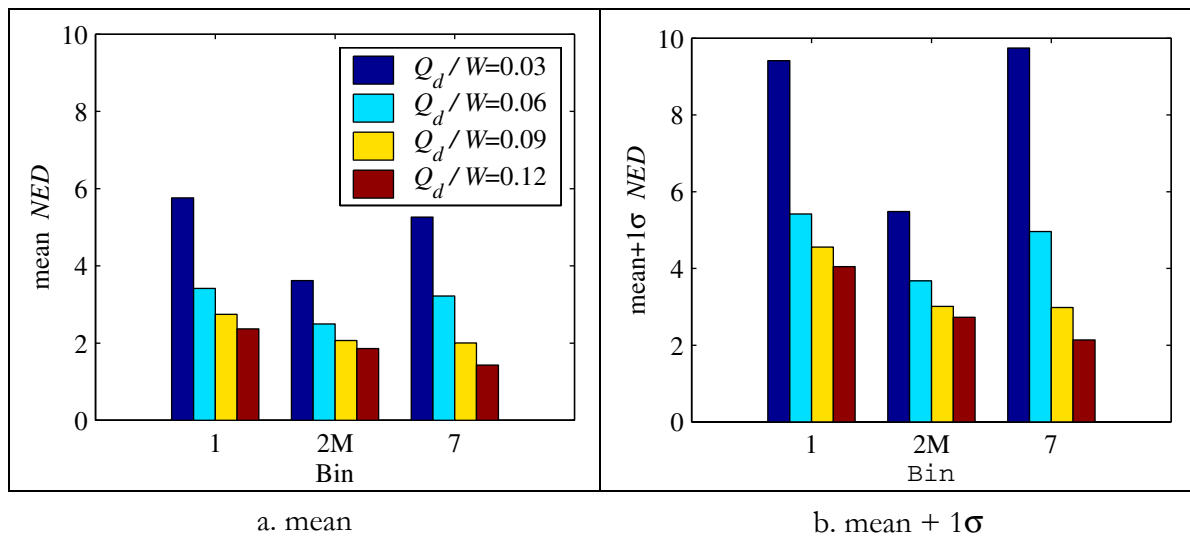


Figure 3. Normalized energy dissipated statistics for ground motion bins 1, 2M, and 7 and isolation systems with $T_d = 2.0$ seconds

Concluding Remarks

The results of this study show the current AASHTO equation underestimates median maximum horizontal isolator displacements, despite the use of conservative (small) values of the damping

coefficient and assumed linearly increasing displacements for periods greater than 1-second. Both the second component of excitation and the coupled behavior contribute significantly to maximum horizontal isolator displacements with the exception of Bin 1 where the second component was observed to contribute little (results presented in Warn et al., 2003). Results of the investigation of energy demands imposed on seismic isolators suggest the current AASHTO prototype testing protocol for seismic loading is inconsistent with the energy demands observed from numerical simulation of maximum earthquake shaking. Recommendations for the prototype testing protocol for seismic isolators subjected to seismic loading include: four fully reversed cycles to the total design displacement at a frequency equal to $1/T$, where the total design displacement includes the maximum isolator displacement, plus a provision for an increase due to torsion where T is the effective period of the isolated structure. Justification for the use of T to determine the testing frequency is presented in Warn et al., (2003).

Acknowledgements

This research was carried out under the supervision of Professor Andrew Whittaker, and supported by the Federal Highway Administration, under contract number DTFH61-98-C-00094 to the Multidisciplinary Center for Earthquake Engineering Research. This support is gratefully acknowledged. The author also wishes to thank Professor Eduardo Miranda of Stanford University for contributing ground motion records for use in this study and Dr. Gilberto Mosqueda of the University of California at Berkeley for providing the Matlab code for the coupled plasticity model. The opinions expressed in this paper are those of the writer and do not reflect the opinions of the Multidisciplinary Center for Earthquake Engineering Research or the Federal Highway Administration. No guarantee regarding the results, findings, and recommendations are offered by either the Multidisciplinary Center of Earthquake Engineering Research or the Federal Highway Administration.

References

- AASHTO (1999): *Guide specifications for seismic isolation design*. American Association of State Highway Officials, Washington, D.C.
- AASHTO (1996): *Standard specifications for highway bridges*. (16th Edition). American Association of State Highway Officials, Washington, D.C.
- ATC (1986): *Seismic design guidelines for highway bridges*. Report 6. Applied Technology Council, Redwood City, CA.
- Huang WH, Fenves GL, Whittaker AS, Mahin SA (2000): Characterization of seismic isolation bearings for bridges from bi-directional testing. *Proceedings of the 12th World Conference on Earthquake Engineering*, Auckland, New Zealand, p. 2047-2048.
- Krawinkler H (2001): Private communication.
- Miranda E (2002): Private communication.
- Mokha AS, Constantinou MC, Reinhorn AM (1993): Verification of friction model of teflon bearings under triaxial load. *Journal of Structural Engineering*, ASCE, **119** (1), 240-261.
- Mosqueda G, Whittaker AS, Fenves GL (2003): Characterization and modeling of friction pendulum bearings subjected to multiple components of excitation. *Journal of Structural Engineering*, ASCE, accepted for publication.

PEER (2000): *Strong motion database*. Pacific Earthquake Research Center, <http://peer.berkeley.edu/smcat/>.

SAC (1997): *Suites of earthquake ground motions for analysis of steel moment frame structures*. SAC Steel Project, http://nisee.berkeley.edu/data/strong_motion/sacsteel/ground_motions.html/.

Warn GP (2003): *Performance estimates in seismically isolated bridge structures*. MS Thesis, University at Buffalo, Buffalo, NY.

Warn GP, Whittaker AS (2003): Performance estimates in seismically isolated bridge structures. *Engineering Structures*, Wiley, submitted for review and possible publication.

Seismic Fragility Testing of Suspended Ceiling Systems

Hiram Badillo-Almaraz

Graduate Student, Department of Civil, Structural & Environmental Engineering, University at Buffalo

Research Supervisor: Andrew S. Whittaker, Associate Professor

Summary

The failure of suspended ceiling systems (SCS) has been one of the most widely reported types of nonstructural damage in past earthquakes. In this research, fragility methods were used to characterize the vulnerability of SCS. Since SCS are not amenable to traditional structural analysis, full-scale experimental testing on an earthquake simulator was performed to obtain the fragility data. Four limit states of response were defined using physical definitions of damage. Based on the fragility data obtained, it was found that (a) the use of retainer clips improved the performance of SCS in terms of loss of tiles, (b) including recycled cross-tees in the assemblage of the suspended grid increased the vulnerability of the SCS, (c) undersized (poorly fitting) tiles are substantially more vulnerable than properly fitted tiles, and (d) including compression posts improves the seismic performance in SCS; however, the effectiveness remains questionable when it is compared with the required installation efforts.

Introduction

The response of nonstructural components can significantly affect the functionality of a building after an earthquake, even when the structural components are undamaged. Poor performance of nonstructural components in past earthquakes has led to the evacuation of buildings, to substantial economic losses due to business interruption and, in extreme cases, to the loss of life. Reconnaissance following past earthquakes has shown that failures of ceiling systems during earthquakes have caused significant economic losses and disruption in important or critical facilities.

The development of fragility curves generally involves the use of both mathematical modeling and physical observations. In the case of SCS, mathematical analysis is difficult to accomplish due to uncertainties in the physical behavior of elements and components of the system once they are installed in the ceiling system. Further, the complexity of the mathematical model and the highly nonlinear behavior of the components once tiles are dislodged make robust structural analysis of SCS unrealistic. Since analytical methods are generally not applicable to the study of SCS and data collected following past earthquakes are not suitable for fragility characterization, experimental methods represent the best and most reliable technique to obtain fragility curves for SCS.

Although several studies have indicated that some improvement in the seismic capacity of SCS has been achieved in recent years (Rihal and Granneman, 1984 and Yao 2000), there exists no robust fragility data and no proven strategies to increase the seismic strength of SCS. The main goal of this study was to develop fragility curves of SCS subjected to earthquake shaking. Fragility curves were

obtained by experimental testing of SCS on an earthquake simulator. The specific objectives of the research program were: (1) to study the performance of a SCS that is commonly installed in the United States, (2) to evaluate improvements in response offered by the use of retainer clips that secure the ceiling panels (tiles) to a suspension system, (3) to investigate the effectiveness of including a vertical strut (or compression post) as seismic reinforcement in ceiling systems, and (4) to evaluate the effect of different boundary conditions on the response of a SCS.

Experimental Facilities for Seismic Testing and Test Specimens

The earthquake simulator in the Structural Engineering and Earthquake Simulation Laboratory of the University at Buffalo was used to evaluate the SCS. A 16 x 16 ft square frame of ASTM Grade 50 steel was constructed to test the SCS. The frame was attached to the simulator platform. Figure 1 is a photograph of the test frame mounted on the earthquake simulator at the University at Buffalo.



Figure 1. Test frame mounted on the simulator at the University at Buffalo

Each ceiling system consisted of two key components: a suspension system and tiles. The ceiling systems were installed in a grid that was hung with suspension wires from the top of the test frame. A compression post was placed 5 ft from the south and east sides of the frame. Since the actual sizes of tiles may differ from the nominal size, two types of tiles were used for fragility testing in this study: normal sized if their plan dimensions are not smaller than the nominal dimensions by more than 1/4 in and undersized otherwise. One of the tiles tested was the Armstrong Fine Fissured tile (undersized). The other tile used in this study was the Armstrong Dune tile (normal sized). Table 1 presents summary information on each of the two tiles used in this study. Figure 2a is a photograph of the Dune tile. Clips similar to those shown in Figure 2b were installed to investigate possible improvements in the seismic performance of SCS.

Table 1. Summary information on the tiles used in this study

| Tile name | Description | Panel dimensions [in.] | | Weight (lb/tile) |
|---------------|------------------------------|------------------------|-------------------------|------------------|
| | | Nominal size | Actual size | |
| Fine Fissured | HumiGuard Plus mineral fiber | [24 x 24 x 5/8] | [23-1/2 x 23-1/2 x 5/8] | 2.8 |
| Dune | HumiGuard Plus mineral fiber | [24 x 24 x 5/8] | [23-3/4 x 23-3/4 x 5/8] | 3.8 |

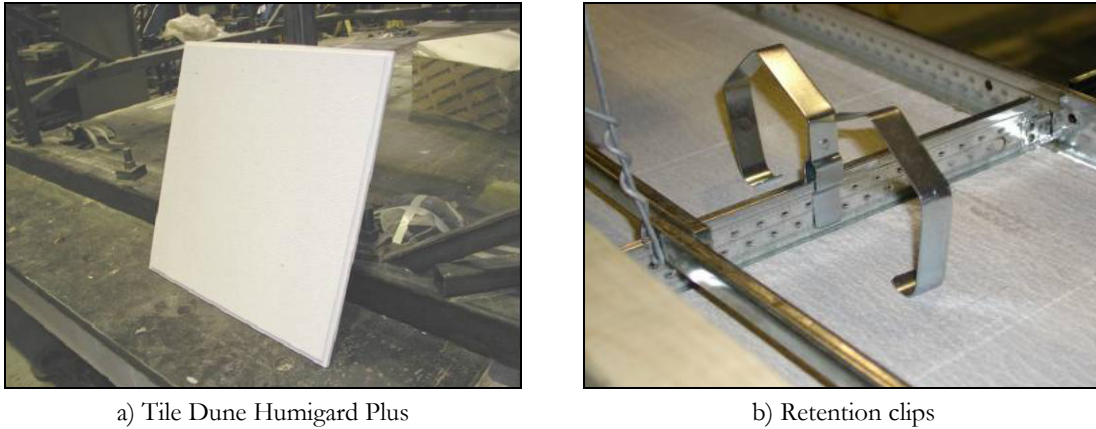


Figure 2. Tile and clips used in the fragility study

Seismic Qualification and Fragility Testing Protocol

The protocol for fragility testing followed the procedures set forth in the ICBO-AC156 “Acceptance Criteria for Seismic Qualification Testing of Nonstructural Components” (ICBO 2000). The first step to develop earthquake histories was to define a required response spectrum (RRS) as a function of the mapped spectral acceleration at short period S_s . For details, refer to ICBO (2000). The testing protocol for fragility testing consisted of sets of horizontal and vertical dynamic excitations. Each set included unidirectional and bi-directional resonance search tests using white noise excitation along the North-South and vertical directions. Each set of excitations also included a series of unidirectional and bi-directional spectrum-compatible earthquake motions that were established for different multiples of RRS. The parameter selected to characterize the ground motion for input to the simulator was the mapped spectral acceleration at short periods, S_s . The target of shaking levels ranged from a $S_s = 0.25$ g through $S_s = 2.5$ g. For details, refer to Badillo (2003). Figure 3 presents the horizontal and vertical response spectra (target and calculated) for a level of shaking corresponding to $S_s = 1.0$ g.

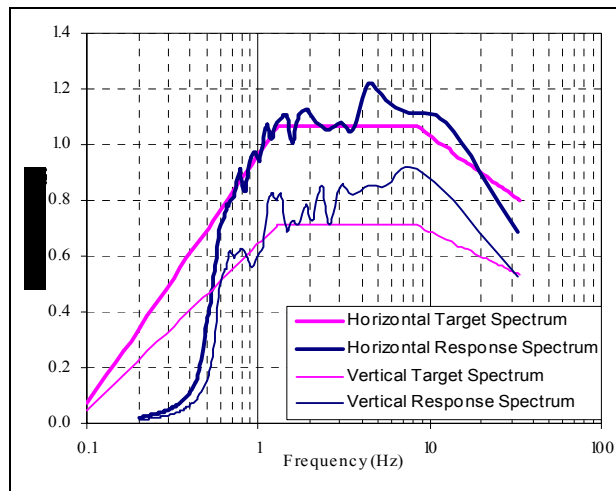


Figure 3. Response spectra (target and calculated) for a level of shaking corresponding to $S_s = 1.0$ g

Fragility Analysis and Data Evaluation

Four variables that affect the seismic performance of SCS were investigated in this study: (1) the size and weight of tiles, (2) the use of retainer clips, (3) the use of compression posts, and (4) the physical condition of grid components. A total of six set-ups were configured using different combinations of these variables: (1) undersized tiles (series A-D), (2) undersized tiles with retainer clips (series E-G), (3) undersized tiles with recycled grid components (series H-J), (4) normal sized tiles (series L-O, Q, R and BB), (5) normal sized tiles with retainer clips (series P and S-U) and (6) normal sized tiles without the compression post (series: V-Z and AA).

A fragility curve describes the probability of reaching or exceeding a damage (or limit) state at a specified level of excitation. Thus, a fragility curve for a particular limit state is obtained by computing the conditional probabilities of reaching or exceeding that limit state at various levels of excitation. A limit state is useful in describing the expected performance of a component or system when it is subjected to specific earthquake demands by characterizing the physical post-earthquake state of the component or structure. Limit states express qualitatively or quantitatively permissible levels of damage. Four limit states were defined in this study to characterize the seismic response of SCS. Limit states 1 through 3 account for the number (or percentage) of tiles that fell from the suspension grid. The fourth limit state is associated with structural damage to the suspension grid. The four limit states were: (1) minor damage (loss of 1% of the tiles from the grid), (2) moderate damage (loss of 10% of the tiles from the grid), (3) major damage (loss of 33% of the tiles from the grid), and (4) grid failure. Detailed descriptions of limit states are provided in Badillo (2003) and Badillo et al. (2003).

Several intensity parameters have been used in previous studies to create fragility curves, namely peak ground acceleration, peak ground velocity, spectral acceleration at specific periods, and spectral acceleration over a frequency range that would bracket the in-service dynamic properties of a specific system. In this study, two excitation parameters were used to construct the fragility curves presented below and in Badillo (2003) and Badillo et al. (2003): (1) peak ground acceleration, and (2) average horizontal spectral accelerations at selected periods. The selected periods represent a broad range that should include most in-service conditions for SCS in buildings: 0.2, 0.5, 1.0, 1.5 and 2.0 seconds. The spectral acceleration ordinates were obtained by calculating the mean spectral acceleration for each ceiling system configuration tested.

The procedure to develop the fragility curves for each configuration is as follows: (1) obtain the mean spectral acceleration response for each shaking level with the accelerometer mounted on the simulator platform, (2) compute the spectral accelerations at selected periods from the mean spectral accelerations, (3) count the number of tiles that fell from the grid for each system at each shaking level as a percentage of the total number of tiles in the ceiling system, (4) compare the percent tile failure with each limit state for each system, and (5) calculate the probability of reaching or exceeding the limit state.

Figures 4 and 5 present sample fragility curves developed using data from the earthquake simulator testing program. Figure 4a presents the fragility curve for peak ground acceleration, and Figure 4b presents the fragility curve for the spectral period of 1.5 seconds, for configuration 1 for each limit state defined earlier. Similar figures were obtained in this study for each of the spectral acceleration periods selected and for each of the six configurations. Figure 5 presents the same information as Figure 4, for each of the six configurations for the case 7 minor damage. Similar figures were

obtained in this study for each of the spectral acceleration periods selected and for each limit state defined. Some of the fragility curves were incomplete because the maximum acceleration, velocity, and displacement of the simulator are limited to 1.5 g, 94 cm/sec (37 in/sec) and 14 cm (5.5 in.), respectively. Different scales were used in plotting the fragility curves because the magnitude of the spectral acceleration changed substantially as a function of period.

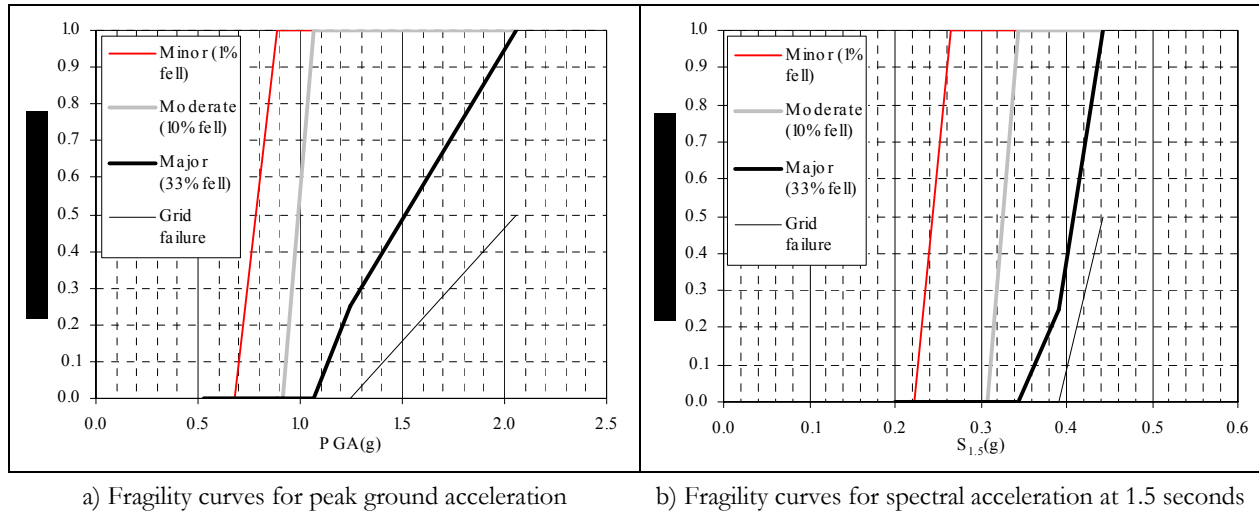


Figure 4. Fragility curves for configuration 1: undersized tiles

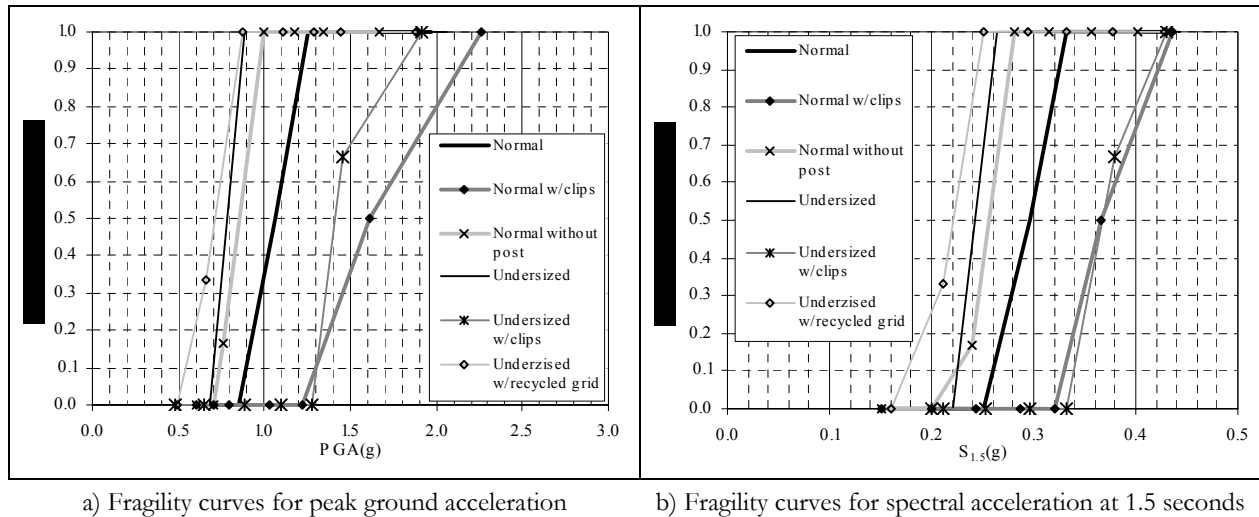


Figure 5. Fragility curves for limit state 1: minor damage

Concluding Remarks

The use of retainer clips substantially improved the behavior of the SCS in terms of loss of tiles. The loss of tiles in systems with retention clips was due primarily to the failure of grid components. Including recycled cross-tees in the assemblage of the suspended grid substantially increased the number of tiles that fell during the earthquake tests. The number of tiles that fell during the shaking

tests of ceiling systems with undersized tiles was substantially larger in comparison to the systems equipped with normal sized tiles. Damage in the ceiling systems in terms of loss of tiles was much larger when a rivet failed than when all of the rivets were undamaged and the cross tees remained firmly attached to the wall molding. The region beyond the intersection of the fragility curves for limit state 3 (major tile failure) and limit state 4 (grid failure) should be avoided because failure of large sections of tiles and grid could cause a life-safety hazard. The usefulness of fragility curves was demonstrated when it was not clear from field observations whether including compression posts improved the seismic performance of the SCS. Using the fragility curves, it was clear that including the compression post in SCS improves the seismic performance of the systems in terms of reduced damage to the tiles and grid. However the effectiveness remains questionable when it is compared with the installation efforts that the compression post field assemblage requires. A more extensive testing program using different SCS configurations with and without seismic compression posts is recommended to give definitive conclusions.

Acknowledgements

This research was carried out under the supervision of Andrew S. Whittaker. Partial support for the work described here was provided by supported by the Earthquake Engineering Research Centers Program of the National Science Foundation, under award number EEC-9701471 to the Multidisciplinary Center for Earthquake Engineering Research.

Armstrong World Industries Inc. provided all of the ceiling system components for the fragility-testing program. This support is gratefully acknowledged. Special thanks are due to Messrs Paul Hough and Thomas Fritz of Armstrong World Industries and Messrs Mark Pitman, Scot Weinreber and Dwayne Kowalski of the Department of Civil, Structural and Environmental Engineering at the University at Buffalo for their technical guidance and support at different times over the course of this study.

References

AISC (1998): *Manual of steel construction – Load and resistance factor design*. American Institute of Steel Construction, Chicago, IL.

Badillo H (2003): *Seismic fragility testing of suspended ceiling systems*. M.S. Thesis, Department of Civil, Structural, and Environmental Engineering, University at Buffalo.

Badillo H, Whittaker AS, and Reinhorn AM (2003): Seismic fragility of suspended ceiling systems. Paper submitted for review. *Earthquake Spectra*, November.

ICBO and ICBO AC156 (2000): *Acceptance criteria for the seismic qualification of nonstructural components*. ICBO Evaluation Service, Inc. International Conference of Building Officials. Whittier, California 90601-2298.

Rihal S, Granneman G (1984): *Experimental investigation of the dynamic behavior of building partitions and suspended ceilings during earthquakes*. Rep. No. ARCE R84-1. California Polytechnic State University, Pomona, California.

Yao GC (2000): Seismic performance of direct hung suspended ceiling systems. *Journal of Architectural Engineering*, **6** (1).

Seismic Behavior of Welded Hospital Piping Systems

Elliott Goodwin

Graduate Student, Civil Engineering Department, University of Nevada, Reno

Research Supervisors: Emmanuel Maragakis, Professor and Chair, and Ahmad Itani, Associate Professor

Summary

This paper presents findings from shake table experiments on cable-braced and unbraced welded hospital piping systems. The research identifies the capacity characteristics of a hospital piping system with and without bracings as well as the system's weak points. The system was tested to the ICBO AC156 acceptance criteria for nonstructural components. The input motion of 1g was amplified to almost 2.6g at the top of the braced and unbraced piping systems. There was no significant damage to the piping system due to the high displacements and accelerations. Two of the eleven braces failed at the highest input excitation, the 2 1/2" diameter vertical hanger rods failed during the unbraced tests, and a flanged connection began to leak during a pushover test. Preliminary results show that the braces limited the displacements, but they did not significantly reduce the accelerations of the system.

Background

The functioning of an essential facility, such as a hospital, after an earthquake relies heavily on proper functioning of its nonstructural components such as fire suppression and water distribution systems, elevators and medical equipment. In recent earthquakes, nonstructural components in hospitals and medical buildings have suffered a large amount of damage, which resulted in a significant reduction of the functionality of the facilities. The 1971 San Fernando Earthquake caused severe damage to many hospitals and medical facilities. As a result of that damage, four of the 11 damaged medical facilities in the area had to be evacuated (Wasilewski 1998). Due to this unacceptable performance, the State of California passed the Hospital Seismic Safety Act, which required that medical facilities be designed and built to remain operational after an earthquake event (Ayres and Phillips, 1998). The California Office of Statewide Health Planning and Development (OSHPD) was charged with certifying that bracing components installed in California hospitals met a certain level of strength.

Test Specimen

In consultation with OSHPD engineers, the experimental hospital piping system was modeled after a system in the University of California, Davis hospital. The system was modified slightly to accommodate the dimensions and geometry restrictions of the testing facility. The system is made up of approximately 100' of 3" and 4" diameter schedule 40 ASTM grade A-53 black steel pipe. The system includes two water heaters, one simulated heat exchanger, one y-strainer, two check valves and one gate valve. The water heaters and the heat exchanger were anchored to the shake table,

while the pipes were braced and hung from a stationary frame, which rested on the lab floor. The fixed frame permitted direct measurement of relative displacements.

Figures 1 and 2 illustrate the plan and elevation views of the system. The water heaters were braced on the table to avoid premature failure of the piping system due to excessive rigid body motion of the water heaters. The water heaters were connected to the system through a four bolt flanged connection. The heat exchanger and all of the valves were connected to the pipes through an eight bolt flanged connection. All of the elbow to pipe connections were welded using a shielded metal arc welding process.

The bracings used were cable style braces. There were seven brace points and four hanger points in which there were vertical supports only. The cables were made of $\frac{1}{8}$ " diameter prestretched galvanized 7x19 aircraft grade steel. The vertical hanger rods were of two sizes: $\frac{5}{8}$ " diameter all-thread rod for supporting the 4" diameter pipe and $\frac{1}{2}$ " diameter all-thread rod for supporting the 3" diameter pipe. The vertical hanger rods were braced continuously along their length with $1\frac{5}{8}$ " square, 12 gauge strut. The system was white washed so that any leaks would be noticeable.

Two systems, one braced and one unbraced, were tested in the experimental program. The unbraced system was the same piping system as the braced one, except that the cable braces, the strut bracing the all-thread vertical rod and the clevis cross braces were removed, reflecting actual field unbraced conditions.

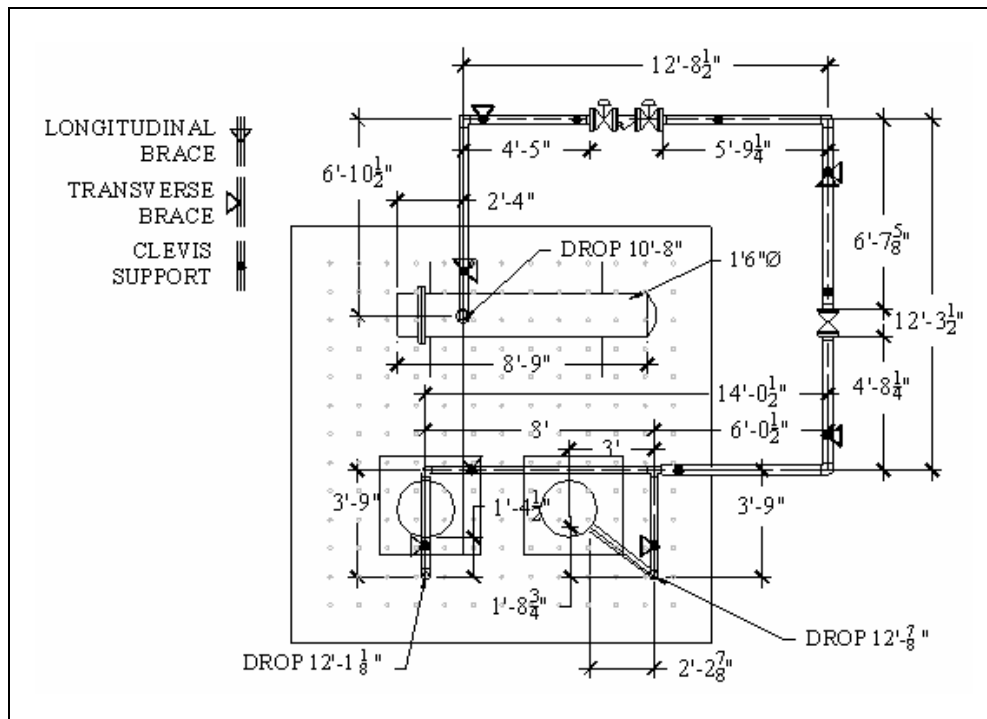


Figure 1. Plan view of experimental setup

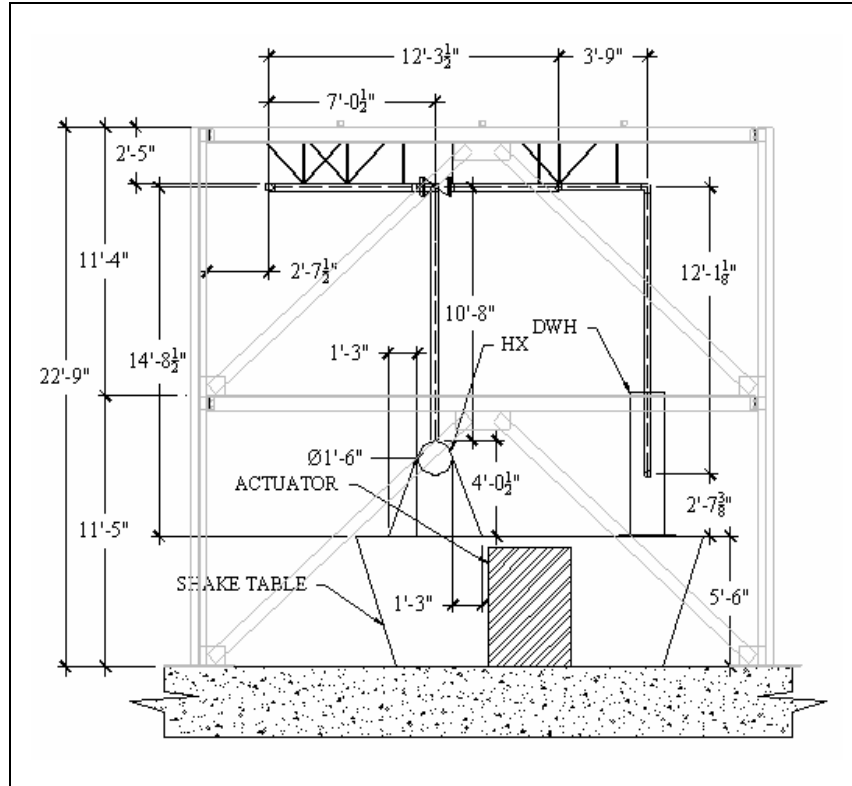


Figure 2. Elevation view of experimental setup

Testing Criteria

The piping system was tested to meet the ICBO AC156 Acceptance Criteria for Seismic Qualification Testing of Nonstructural Components (ICBO Evaluation Service, Inc., 2000). AC156 requires that the nonstructural component be subjected to a synthetic input motion that meets a response spectra where the maximum spectral acceleration is determined according to the formula:

$$A = 2.5C_a \left(1 + 3 \frac{h_x}{h_r} \right) < 4C_a \quad (1)$$

where:

C_a = seismic coefficient (UBC Table 16-Q)

h_x = element or component attachment elevation with respect to grade

h_r = structure roof elevation with respect to grade

For this research, the following assumptions were made:

$C_a = 0.44N_a$

$Z = 0.4$, seismic zone factor (UBC Figure 16-2)

S_D soil type

N_a = near source factor (UBC Table 16-S)

$C_a = 0.66$

$h_x = h_r$

Formula (1) is derived from Equation 16-32-2 of the 1997 UBC, Formula (2) in this paper. By using Formula (1), the maximum spectral acceleration was found to be 2.64g. Figure 3 shows the required response spectra (RRS), the envelope that the AC156 requires the synthetic motion response spectra fall between (bold lines), and the response spectra of the generated motions. The AC156 requires that the input motion have a build, hold and decay curve of 5, 15 and 10 seconds, respectively.

The program SIMQKE (Gasparini and Vanmarcke, 1976) was used to generate a synthetic input motion that conforms to the AC156, as shown in Figure 4. The program required the following items to generate a motion:

- Points describing the required response spectra
- Build, hold and decay envelope
- A maximum input acceleration

A maximum acceleration of 1 g was chosen as the SIMQKE input. An additional synthetic motion using the program RSC TH (Halldorsson et al., 2002) was also generated. The RSC TH motion met the response spectra as seen in Figure 6, but did not meet AC156 due to the fact that it could not produce a motion that had a build, hold and decay envelope. Using the maximum displacement input of the SIMQKE motion of 8.32” and considering 16.5’ as a story height, the story drift ratio that was achieved with the SIMQKE motion was 4.18%.

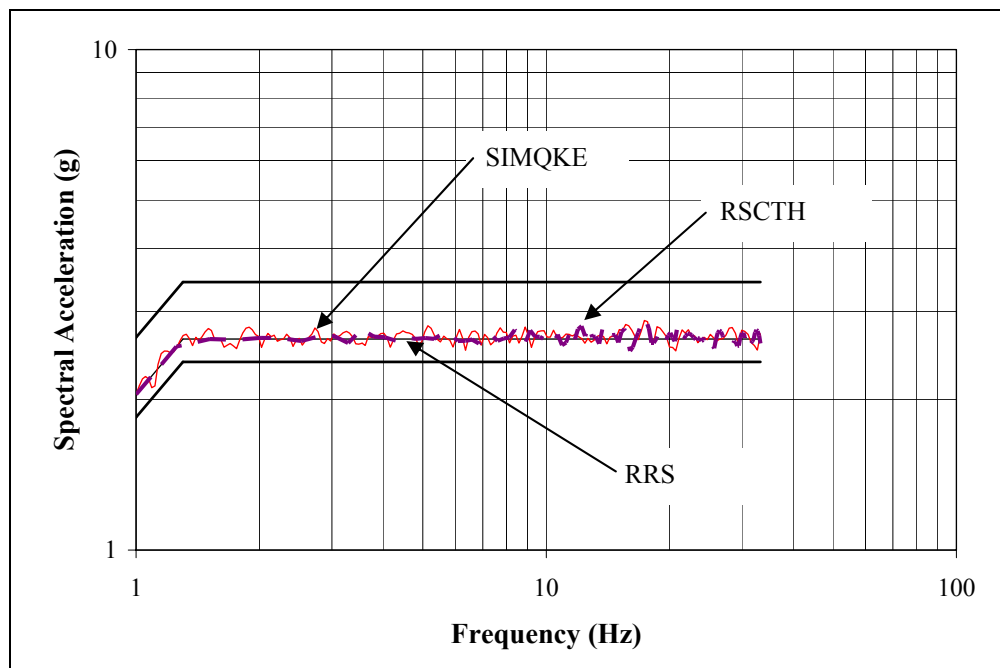


Figure 3. Required and generated response spectra

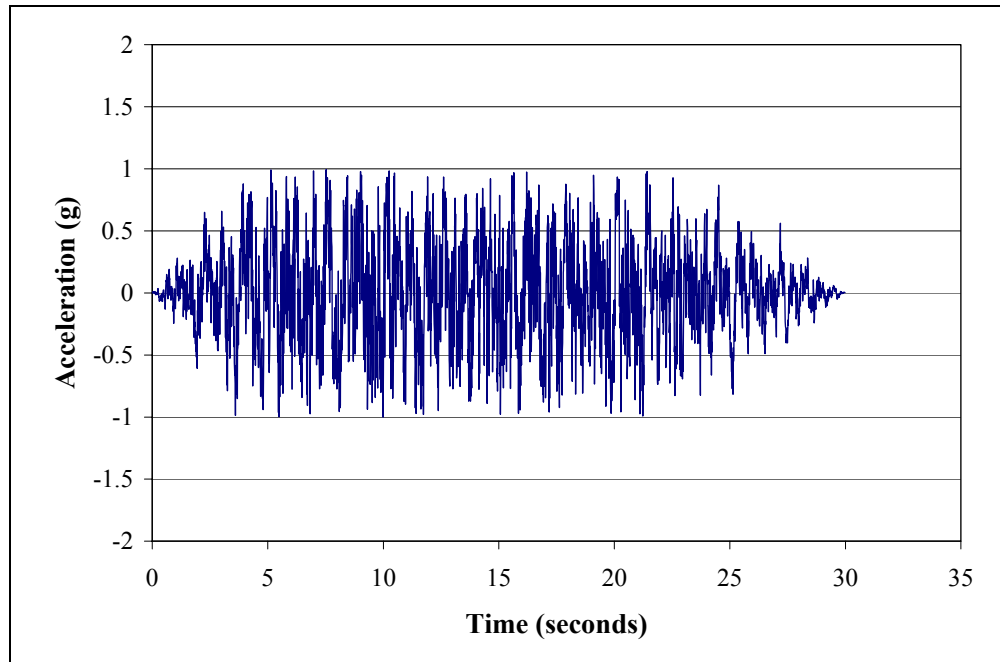


Figure 4. SIMQKE generated input motion

Test Protocol

A test protocol was developed that subjected the braced and unbraced systems to varying intensities of the SIMQKE and RSCTH motions in both principle axes as well as a biaxial excitation at 45° with respect to the principle axes. Both systems were subjected to a varying frequency sinusoidal sweep with a constant amplitude of 0.8.” The braced system was also subjected to a dynamic pushover. Overall, each system was subject to 61 runs.

Experimental Results

During the braced E-W 100% SIMQKE input motion, two of the braces bracing the 4” pipe failed. The flanged connection joining the heat exchanger to the pipe began to leak during the braced 10” dynamic pushover. White washing the surface of the pipes not only aided in identifying leaks, but also illustrated the permanent relative displacement of the braces to the piping system. The clevis hangers scraped off the whitewash in the places it had touched the pipe during the excitation. Every brace point had at least 1” of permanent displacement after the testing of the braced system and one brace moved permanently 4.” During the unbraced biaxial input motions, the only 2½” diameter rods failed. None of the 5/8” diameter rods failed.

Figure 5 shows a comparison of the braced and unbraced displacement response of instrument nv26. Figure 6 shows the braced and unbraced acceleration response of instrument nv17. As seen in these graphs, the braces significantly reduced the displacement response but did not have a major effect on the acceleration response of the system. The maximum acceleration responses for the braced and the unbraced cases were 2.62 g and 2.58 g, respectively. Similar behavior was observed with the response of other instruments.

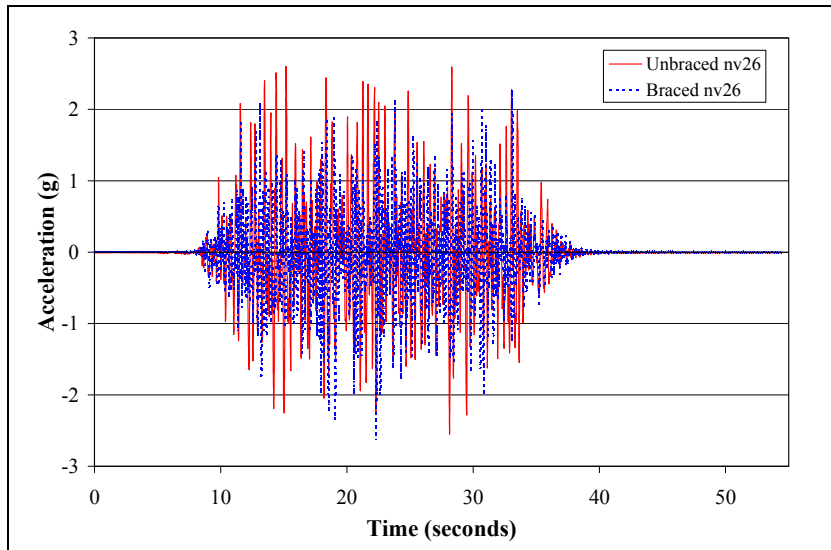


Figure 5. Acceleration response of instrument nv26

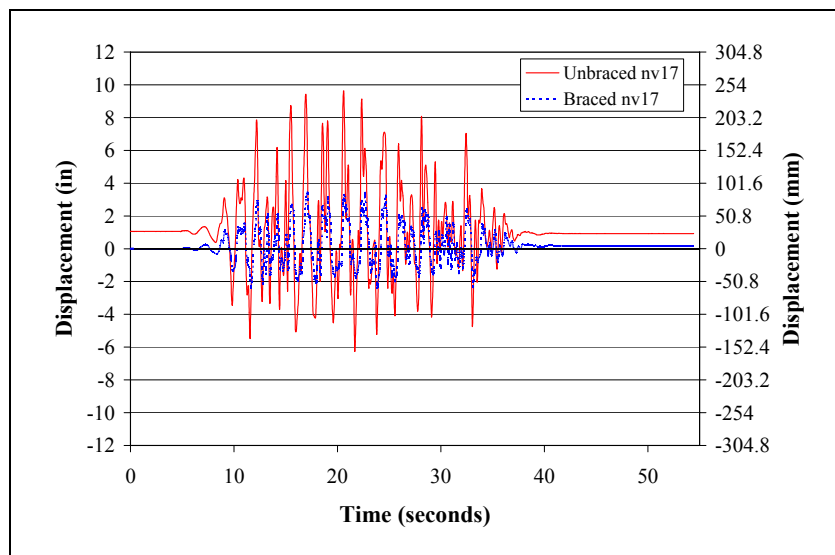
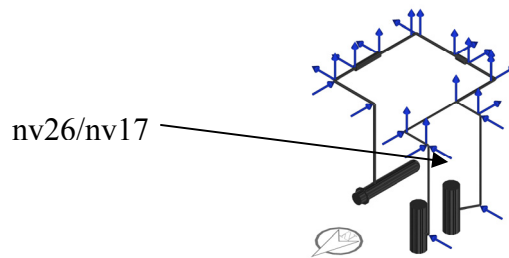


Figure 6. Displacement response of instrument nv17

Concluding Remarks

The system did not have any failure level damage during either the braced or unbraced experiments. The long vertical pipe run into the heat exchanger began to leak during the pushover test, and there were two braces that failed in the cables during the highest SIMQKE input excitation. For the unbraced test, the only damage to the system was the failure of 2½” diameter rods at the highest SIMQKE input excitation. The displacements were significantly reduced by the addition of the braces. However, the accelerations were not significantly affected by the presence of the braces.

Another system will be tested in early winter of 2003/2004. The system will have the same geometry and same brace layout; however, the connections will be threaded instead of welded. In the past, threaded connections have been the source of multiple failures in hospital piping systems, and it is expected that there will be more damage to the threaded system than there was in the welded system.

Acknowledgements

This research was carried out under the supervision of Drs. Emmanuel Maragakis and Ahmad Itani, and primarily supported by the Earthquake Engineering Research Centers Program of the National Science Foundation, under award number EEC-9701471 to the Multidisciplinary Center for Earthquake Engineering Research. Special thanks to William Staehlin and Chris Tokas of the California Office of State Wide Health Planning and Development, David Ainsworth of Stecher-Ainsworth-Miner, Mechanical Engineers, Rich Lloyd of Mason Industries and Pete Rezac from Cooper B-Line.

References

- Ayres JM, Phillips RJ (1998): Water damage in hospitals resulting from the Northridge earthquake, *ASHRAE Trans.* 1998, **104** (Part 1), American Society of Heating, Refrigerating and Air-Conditioning Engineers, Atlanta, Georgia.
- Gasparini DA, Vanmarcke EH (1976): *Simulated earthquake motions compatible with prescribed response spectra*, Massachusetts Institute of Technology, Cambridge, Massachusetts.
- Halldorsson B, Dong G, and Papageorgiou AS (2002): Earthquake motion input and its dissemination via the internet, *Journal of Earthquake Engineering and Engineering Vibration*, **1** (1), 20-26. (<http://civil.eng.buffalo.edu/EngSeisLab/>)
- ICBO Evaluation Service, Inc. (2000): *Acceptance criteria for seismic qualification testing of nonstructural components*, AC156, International Conference of Building Officials, Whittier, California.
- International Conference of Building Officials (1997): *Uniform building code, structural engineering design requirements*, **2** (1997 Edition), 2-24 to 2-35, Whittier, California.
- Wasilweski RJ (1998): Seismic restraints for piping systems, *ASHRAE Trans.* 1998, **104**, (Part 1), American Society of Heating, Refrigerating and Air-Conditioning Engineers, Atlanta, Georgia.

Advanced Composite Multi-infill Panels for Seismic Retrofitting

Wooyoung Jung

Graduate Student, Department of Civil, Structural & Environmental Engineering, University at Buffalo

Research Supervisor: Amjad J Aref, Associate Professor

Summary

In this paper, a conceptual design, fabrication, and testing of the advanced Polymer Matrix Composite (PMC) infill system are presented as a seismic retrofit strategy. Such a system is designed to have multi-infill PMC panels with a passive energy mechanism. This system has two separate components – an inner PMC sandwich panel and outer damping panels. The interaction of these two components may produce considerable stiffness and enhanced damping properties in the structure at different drift levels. As part of this research, analytical and experimental studies were performed to investigate the effectiveness of the proposed multi-infill panel concept. The prefabricated multi-panel PMC infill holds great promise for enhanced damping performance, simplification of the construction process, faster implementation and reduced cost when used for seismic retrofitting applications.

Introduction/Motivation

In the United States, many older structures located in seismic zones lack strength and damping. One approach for correcting these deficiencies was the construction of infill walls to strengthen and stiffen the structure. As such, large numbers of buildings throughout the U.S. have structural frames infilled with unreinforced clay brick, concrete masonry, or structural clay tile. This infill construction has been prevalent since the late 1800's, and is still popular in moderate seismic regions of the central and eastern United States. However, sometimes cost, time constraints, or the need to limit disruptions to building operations may dictate that solutions other than cast-in-place construction be used. A new rehabilitation scheme is needed that will simplify the construction process; reduce time, cost and inconvenience of construction; and reduce the loss of functional use of a structure both during and after construction. Disadvantages associated with many of the traditional strengthening techniques have led researchers to develop innovative methods using advanced composite materials. The use of advanced composites for a variety of rehabilitating applications has been rapidly increasing in recent years. The main reasons for using composites are their superior strength-to-weight ratio, stiffness-to-weight ratio, and durability in corrosive environments as compared with conventional materials. Such benefits have the potential to conveniently and effectively aid in the mitigation of earthquake damage.

In this paper, the conceptual design of the multi-panel PMC infill system, composed of an inner PMC sandwich infill and outer FRP damping panels with passively combined interface damping layers, is proposed and tested to investigate its effectiveness as one approach to seismic retrofitting. The main scope of this research is focused on the shear deformation of both combined interface

damping layers and the structural response of a steel frame infilled by the multi-infill PMC panels subjected to monotonic and cyclic loads.

Background of this Research

In the 1980's, the National Science Foundation (NSF) began to fund research on seismic rehabilitation. The objectives of the program were to provide information for evaluation of the vulnerability of existing structures at various levels of seismicity, and to develop advanced strategies for repair and retrofitting. Nonstructural rehabilitation was accomplished through replacement, strengthening, repair, bracing, or attachment. Recently, new rehabilitation approaches for critical facilities have been identified. Hospitals are classified as among the most important public facilities and are an important part in hazard emergency management. Hospitals are expected to provide uninterrupted and efficient medical services during and after an earthquake, or any natural hazard. As part of MCEER's research initiatives in the area of advanced analyses and protective technologies for seismic retrofit of critical facilities, FRP composite materials have been investigated as a new seismic strategy. The proposed methods may provide the solution to creating cost-effective and stakeholder-acceptable retrofitting strategies for maintaining functionality of critical facilities and their contents during earthquakes. As an innovative alternative, the lightweight FRP composite has the potential to emerge as an alternative material for non-structural elements, such as infill walls, that can be used as a seismic retrofitting strategy in regions of moderate to high seismicity.

Conceptual Design and Construction

The basic design philosophy and structural technique considered herein focuses on increasing the efficiency of retrofitting a structure before and after earthquake damage. The properties of the prefabricated PMC infill systems can be easily modified to suit their functional purposes. Fiber orientations and stacking sequence of the PMC materials can be adjusted to enhance structural behavior without any limitations imposed by existing configurations. Also, the ductile behavior of PMC infill systems can prevent catastrophic failure of the overall structure. From a construction point of view, PMC infill systems can be easily installed during the strengthening and retrofitting process of existing structures. A full-scale multi-panel PMC infill system was planned to test these parameters.

The proposed multi-panel PMC infill system is composed of two separate, basic structural components: an inner PMC panel and outer FRP damping panels. Figure 1 shows the geometric configuration of these basic structural components. The primary design concept of the proposed multi-panel PMC infill system emphasized two aspects; (1) enhancement of damping properties from the passive interface damping layers, and (2) providing considerable lateral stiffness by the PMC infill at high drift level to resist severe earthquake excitation, and avoid excessive relative floor displacements that cause both structural and non-structural damage. These two separate components, along with the steel frame, are intended to provide the desired stiffness or/and damping following different drift values.

For the inner PMC component, a sandwich type was considered to reduce the weight, sound, and vibration as well as to improve the structural rigidity of the composite wall. The PMC sandwich infill consisted of two fiber-reinforced polymer (FRP) laminates with an infill of Divinycell H-100 sheet foam in between. The Divinycell foam is a semi-rigid PVC used as a core material in conjunction with high-strength skins to produce strong, stiff, lightweight composite structures. As observed in previous research (Jung and Aref, 2003), the dominant failure of the PMC sandwich infill panel was

elastic buckling under racking load. By considering the observed failure mode, an iterative process by numerous finite element simulations was carried out. The maximization of buckling loads with respect to laminate configuration was the objective function of the inner PMC panel design. Since the structural behavior of sandwich constructions is strongly affected not only by the types of fiber reinforced composite materials used, but also by the fiber orientations and stacking sequences of individual plies constituting the sandwich faces, the determination of optimum stacking sequence is a significant key parameter in the design process. By considering several stacking sequences, Figure 2 shows the maximum buckling force obtained from finite element analysis (ABAQUS 2000).

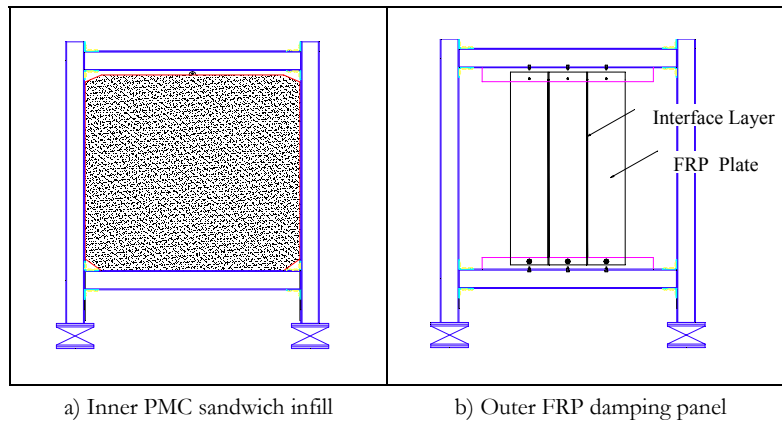


Figure 1. Configuration of a multi-panel PMC infill system

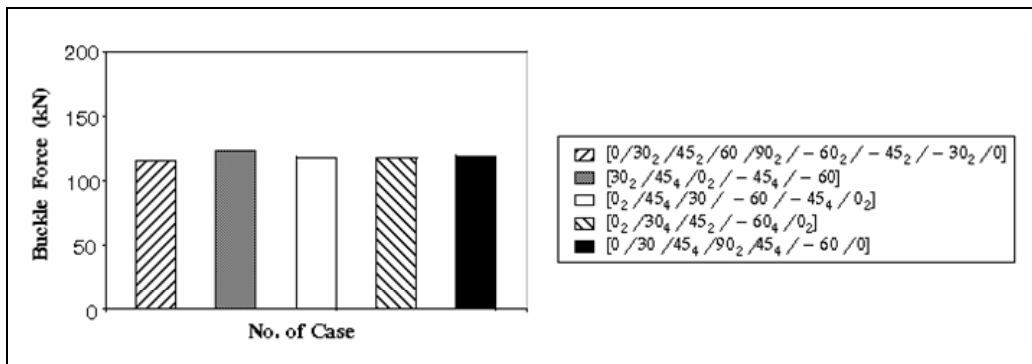
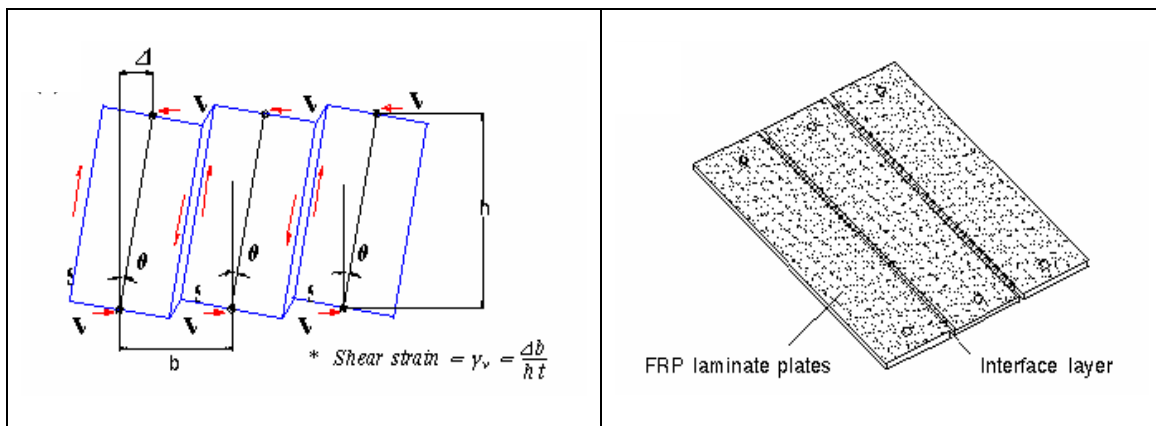


Figure 2. Results for maximum buckling force of applied fiber stacking sequences

For the steel frame with infills, the presence of gaps between the columns and the infill wall, and/or between the top beam and the infill wall, may be unavoidable. These gaps may negate some or all of the stiffness provided by the infill (Riddington 1984). In the design of the PMC sandwich infill, these unavoidable gaps between the infill and the opening of the steel frame can be used as the other design parameter to achieve the increased lateral resistance at specific drift. The post-action of the infill after allowing some amount of horizontal deflection would be expected to prevent excessive relative floor displacements. However, large gaps are not practically tolerable for pure infilled frame structures, because they are normally subjected to alternating loads. On the basis of previous results

(Dawe and Seah, 1989), it is assumed arbitrarily that the maximum designed side gap was allowed to have less than 0.4% of the infill dimensions, even if there is little decrease in the stiffness and/or strength of the infill action. By using finite element simulations to represent the PMC infilled frame with different side gap distances at the interface, the force–displacement response was evaluated. Finally, the contact target was designed in the range of 2% to 2.5% for lateral drifts to allow enough shear straining of the combined interface layers.

For the outer damping panel design, the passive damping panel concept of Gasparini et al., 1981 was adopted, with shear deformation of the interface layers between FRP plates along the relative motion of the top and bottom beams. These outer FRP panels were designed to achieve initial static stiffness and an acceptable maximum strain at the interface layers. The selected FRP laminate was made of the same materials used in the fabrication of the inner PMC sandwich infill, and the proposed interface damping layers consisted of two composite damping materials, such as 3M viscoelastic solid and polymer honeycomb materials. The basic concept of these combined composite damping materials was proposed by Jung and Aref (2003), and the enhanced damping property was observed by experimental and analytical studies. Practically, the proposed damping system could be used in as many panels as necessary to achieve different levels of damping and stiffness. In this study, by considering an optimum case relative to high material costs, the geometric configuration of the outer damping panels was determined to have three FRP laminate plates and combined interface damping materials at the interface between them as shown in Figure 3.



(a) Geometry of the deformed panels during inter-story drift (Gasparini et al., 1981)

(b) Fabrication

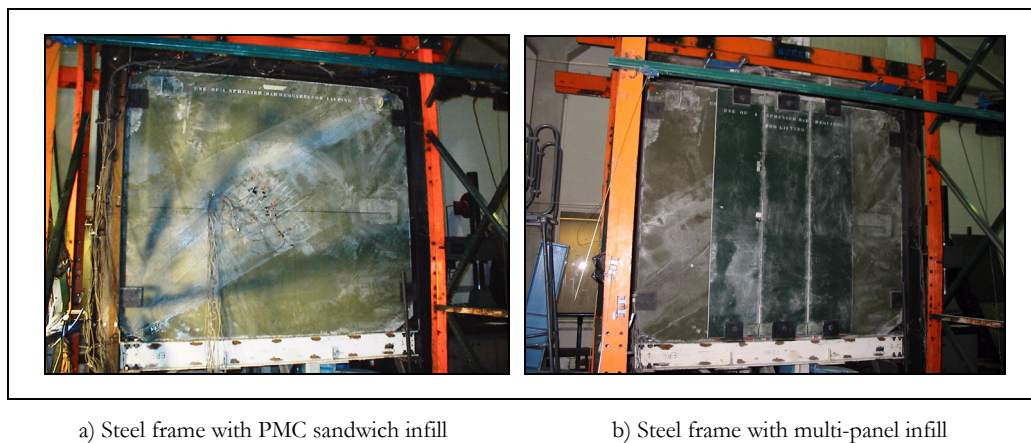
Figure 3. Design and construction of the outer damping panels

As a key design parameter of the combined interface damping layers, the design can be carried out for the required damping ratio of the structure. According to the required design damping ratio, the geometric size of the FRP plates, and the interface viscoelastic layer dimensions and properties can be determined by simple calculation. As shown in Figure 3a, an idealized symmetric motion was assumed; accordingly, the thickness of the FRP laminates was designed to have rigid body motion to make idealized shear deformation in the combined interface damping layers. That is, the laminate thickness could be determined from the maximum allowable interface deformation to insure the maximum shear strain in the viscoelastic materials. For the bonding effect of the interface layers, a

perfect bonding was assumed. Therefore, the geometric size of the outer damping panels can be adjusted to the configuration of the combined interface damping layers. In this study, considering the natural frequency of the undamped structure, 5-10% increased damping was considered as a design target due to expensive viscoelastic material and limited experimental results. The selected mixing ratio of viscoelastic material was designed to have about 60% of total damper area, while the honeycomb material was used as the remaining portion of the combined damping layer.

Experimental Investigation and Results

In the experimental phase, testing of a steel frame with and without a composite infill wall was planned. In the experimental setup procedure, a steel frame with a PMC sandwich infill was tested first. Figure 4a shows a steel frame in which a PMC sandwich infill has been placed. The objective of this test was to investigate the in-plane response of the PMC infill when top and side gaps were allowed between the infill and the opening perimeter of the steel frame. Consequently, the outer damping panels were set up as shown in Figure 4b, and tested to evaluate the overall response of the multi-panel PMC infilled frame structure. Monotonic and cyclic loading was applied in the tests.



a) Steel frame with PMC sandwich infill

b) Steel frame with multi-panel infill

Figure 4. Experimental specimen setup

Testing of a Steel Frame with PMC Sandwich Infill

The purpose of this test was to investigate in-plane behaviors of the PMC sandwich infill along with preset initial top and side gaps. Figure 5a presents the numerical and experimental responses of the PMC sandwich infill panel with allowed initial gaps under push-over load. The force-displacement relationship obtained from the test clearly indicated that the contact point of the PMC infill with a 7.6 mm initial side gap was approximately 5.0 cm. Beyond that point, there is a progressive increase in lateral load resistance as the contact area increases. From the stress and strain outputs of the testing of the steel frame infilled with a PMC sandwich panel, the compressive strut angle for the infill was evaluated and compared with the numerical results (depicted in Figure 5b).

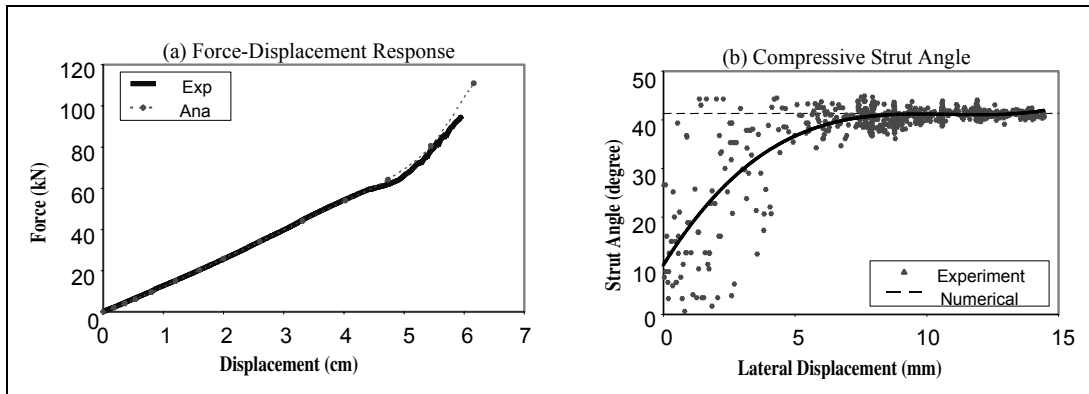


Figure 5. Results of steel frame with PMC sandwich infill (1.0% drift, push-over load test)

Testing of a Steel Frame with Multi-panel PMC Infill

Monotonic tests were conducted at 0.5%, 1.0%, and 1.5% drift. Important information about in-plane stiffness and the effect of the interface layer can be obtained from such experiments. As shown in Figure 6a, the measured overall stiffness of the multi-panel PMC infilled frame was larger than that of the steel frame. It is evident that the interface layer increased the lateral resistance by the contribution of the viscoelastic materials. However, the stiffness of the multi-panel PMC infilled frame was found to vary from 0.96 kN/mm to 1.35 kN/mm after allowing 0.8 cm of lateral displacement during the test. In the fabrication, bolt holes of each connector between the outer FRP panels and the steel beams were made 0.125 inches larger than the bolt shaft diameter. As such, there was a slippage between the bolt shank-to-bolt holes until the pin or slot connector is locked in place. Once a desirable locking configuration is achieved, the interface layer will be subjected to shear force. Figure 6b presents the shear deformation of the interface layer after locking the connectors.

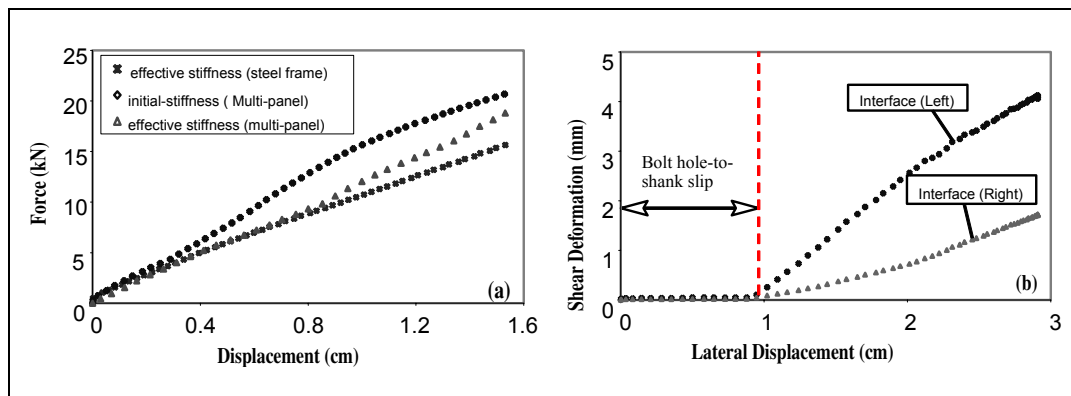


Figure 6. Results of steel frame with PMC sandwich infill (1.0% drift, push-over load test)

Finally, the energy dissipation that existed in the multi-panel PMC infilled frame was investigated. Generally, the overall damping exhibited by a structure arises from many sources, such as cyclic straining of structural and nonstructural elements, friction at interfaces, and nonlinear behavior. In

the multi-panel PMC infill system, primary damping arises from cyclic straining of the damping materials at the interface between the FRP laminates. As such, of concern herein is the availability of increasing the damping that arises from the cyclic straining of the materials in the composite frame, and the feasibility of the design concept. Frictional and nonstructural sources are not considered herein. Therefore, the exact overall damping of a structure is not quantified. The experimental results are evaluated by considering force–displacement curves, the stiffness degradation under successively applied cycles, and the dissipated energy. The experimental hysteretic responses are shown in Figure 7. Figure 7a presents the hysteretic responses before or after the PMC sandwich infill contacted the steel frame. It is observed that the outer FRP damping panels produced the damping without significant lateral resistance, while the increased lateral resistance of the structure was provided by the PMC infill beyond the point where the contact took place. The hysteretic energy observed during the applied cycles of the tests is compared for the steel frame and the multi-panel PMC infilled frame. By comparing the hysteretic energy of both cases in Figure 7b, one can observe the effect of the application of the combined interface damping layers at 0.16% drift. It is evident that the enhanced energy dissipation produced by the interface damping layers will be effective in attenuating the seismic response of the structure and will be competitive with other similar seismic strategies, such as concrete shear walls and masonry infill walls, which currently dominate the market for mid-rise structures.

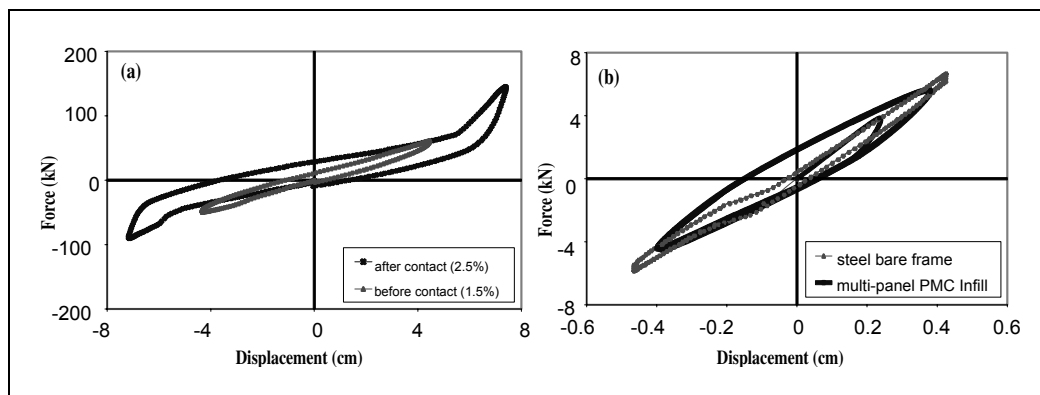


Figure 7. Hysteretic behavior of the multi-panel PMC infilled frame tests

Concluding Remarks

The multi-panel PMC infill system was designed to provide considerable stiffness as well as enhanced damping properties. According to the numerical and experimental studies, using the passive concept of combined interface damping layers provided enhanced damping characteristics through the outer damping panels. Also, as lateral drift increases, the contribution of the PMC sandwich infill panel can increase the stiffness when it wedges within the steel frame; thus, the additional contact and enhanced stiffness provide a mechanism to avoid excessively large relative floor displacements. Moreover, the influence of this stiffening by the PMC sandwich infill panel minimizes damage to the steel column.

Acknowledgements

This research was carried out under the supervision of Dr. Amjad J Aref, and primarily supported by the Earthquake Engineering Research Centers Program of the National Science Foundation, under award number EEC-9701471 to the Multidisciplinary Center for Earthquake Engineering Research.

References

ABAQUS/STANDARD (2000): *User's manual. Version 6.1*, Hibbit, Karlsson & Sorensen, Inc., Pawtucket, RI.

Dawe JL, Seah CK (1989): Behavior of masonry infill steel frames. *Canadian Journal of Civil Engineering*, **16**, 865-876.

Jung WY, Aref AJ (2003): A combined honeycomb and solid viscoelastic material for structural damping applications. *Mechanics of Materials*, **35** (8), 831-844.

Gasparini DA, Curry LW, and Debchaudhury A (1981): Damping of frames with viscoelastic infill panels. *Journal of the Structural Division*, **107** (5), ASCE, 889-905

Riddington JR (1984): Influence of initial gaps on infilled frame behavior. *Proceedings of the Institution of Civil Engineers*, Institution of Civil Engineers (Great Britain), **77**, 295-310, London, UK.

Seismic Performance Assessment by Fragility and Loss Estimation

Cagdas Kafali

Graduate Student, School of Civil and Environmental Engineering, Cornell University

Research Supervisor: Mircea Grigoriu, Professor

Summary

A methodology for assessing the seismic performance of a system with structural and nonstructural components is developed using fragility analysis and loss estimation. System properties, seismic hazard characterization and performance criteria are required to calculate system fragility, and estimate losses and recovery times. A structural/nonstructural system located in New York City is used to demonstrate the methodology. Fragility surfaces for different limit states and cost histograms are obtained.

Introduction

Several methods are available for calculating component fragility information. In HAZUS (1999), lognormal distributions are used for structural and nonstructural component fragility. Fragility of components may also be obtained through testing. In Badillo-Almaraz (2003), experimental fragility curves are obtained for suspended ceiling systems using short period spectral acceleration as the intensity of the ground motion. System fragility information can also be obtained by Monte Carlo simulation and system reliability analysis. A methodology for calculating the reliability of nonstructural systems from the fragility of their components is presented in Grigoriu and Waisman (1998), in which components are assumed to have random independent properties and behave statically. Once the fragility of the system is obtained and the lifetime is selected, the seismic performance can be evaluated using a seismic hazard model and a financial model. A methodology is presented in this paper for assessing the seismic performance of a system by its fragility analysis and loss estimation.

Methods

Figure 1 illustrates the framework of the methodology presented. System definition (structural, nonstructural, geotechnical), characterization of the seismic hazard (a seismic activity model, a seismic ground acceleration model, lifetime) and performance criteria (limit states, a financial model) are used to evaluate the seismic performance of the system through fragility analysis and loss estimation. System performance and available resources can be further used to calculate the restoration time. The overall objective is to enhance the seismic resiliency which is characterized by reduced probability of system failure, reduced consequences due to failure and reduced time to system restoration.

Seismic performance assessment by fragility and loss estimation consists of two main steps. First, system fragility information is obtained. Then, the loss is estimated through a cost-benefit analysis

consisting of (1) a time horizon, (2) seismic hazard at the site of interest and (3) cost functions including, for example, retrofit and repair costs, loss of use, and loss of life, as well as some potential monetary benefits of retrofit, such as rent increase.

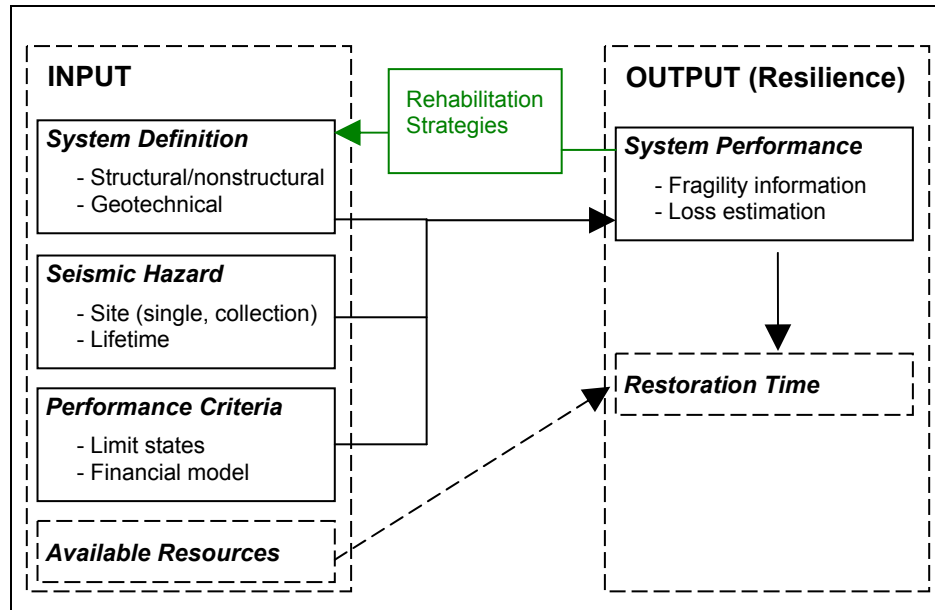


Figure 1. Framework of the methodology

Suppose that a system experiences an earthquake with magnitude m , occurring at a seismic source at distance r from the system site. Following the earthquake, the system enters a damage state, $d_s(m;r)$, with a probability, $p_s(m;r)$, given by the system fragility surfaces. Suppose also that the system is repaired so that it is brought to its initial state immediately following this earthquake. Denote by c_s the cost of bringing the system from damage state, $d_s(m;r)$, to its initial state. This elementary cost structure presented here for illustration can be augmented to include the components mentioned above. Consider now a sample of the seismic hazard at the system site. Let $(m_i;r_i)$ denote the values of $(m;r)$ corresponding to earthquake i in a sample of the seismic hazard. The corresponding damage states, $d_s(m_i;r_i)$, and their probabilities, $p_s(m_i;r_i)$, result from the system fragility surfaces. Denote by c_s the repair cost associated with the damage state, $d_s(m_i;r_i)$. Since damage state s has the probability, $p_s(m_i;r_i)$, the repair cost for the seismic event i is $C_i = \sum_s c_s p_s(m_i;r_i)$. The total cost for this sample of the seismic hazard is $C = \sum_i C_i$. The cost C is a random variable, whose properties can be estimated from a collection of seismic hazard samples.

Numerical Example

Denote by S the structural system and NS the nonstructural system (e.g., water distribution system) consisting of two components, C_1 and C_2 (such as a water tank and piping system) of a health care facility located in New York City (see Figure 2). The assumptions for the system are as follows, (i) soil-structure interaction is not considered, (ii) all systems are linear, (iii) cascade analysis applies and (iv) S is highly reliable compared to NS . The specific barrier model (Papageorgiou and Aki, 1983a and b) is used to characterize seismic ground accelerations at the site. Linear random vibration theory, Monte Carlo simulation and crossing theory for stochastic vector processes (Veneziano et al., 1977) are used for the analysis.

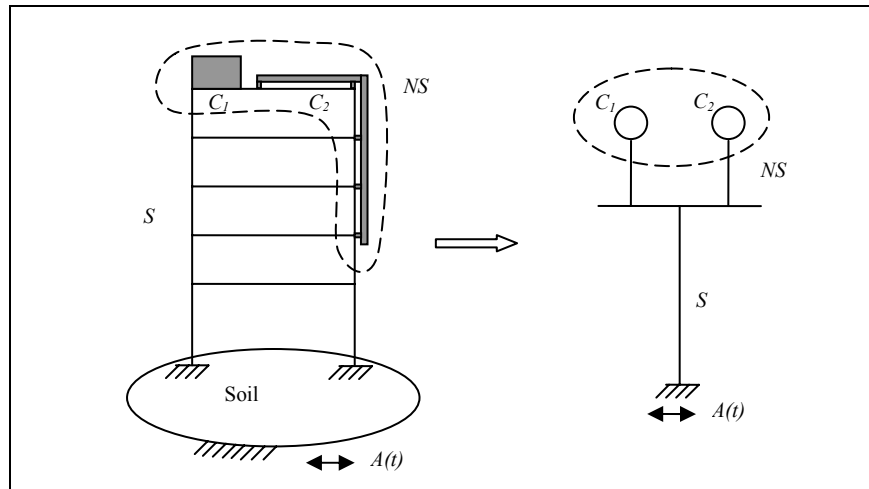


Figure 2. Structural and nonstructural systems

Two rehabilitation strategies are considered, system with *no rehabilitation* and system with *rehabilitation*. Properties of the two systems are given in Table 1.

Table 1. System definition

| | <i>S</i> | <i>C</i> ₁ (no rehab) | <i>C</i> ₂ (no rehab) | <i>C</i> ₁ (rehab) | <i>C</i> ₂ (rehab) |
|--------------------------|----------|----------------------------------|----------------------------------|-------------------------------|-------------------------------|
| Natural frequency | 5 | 11 | 12 | 18 | 17 |
| Damping ratio | 0.050 | 0.015 | 0.020 | 0.020 | 0.025 |

Figure 3 shows the seismic activity matrix and a sample of the seismic hazard in NYC assuming that the lifetime of the hospital is 50 years.

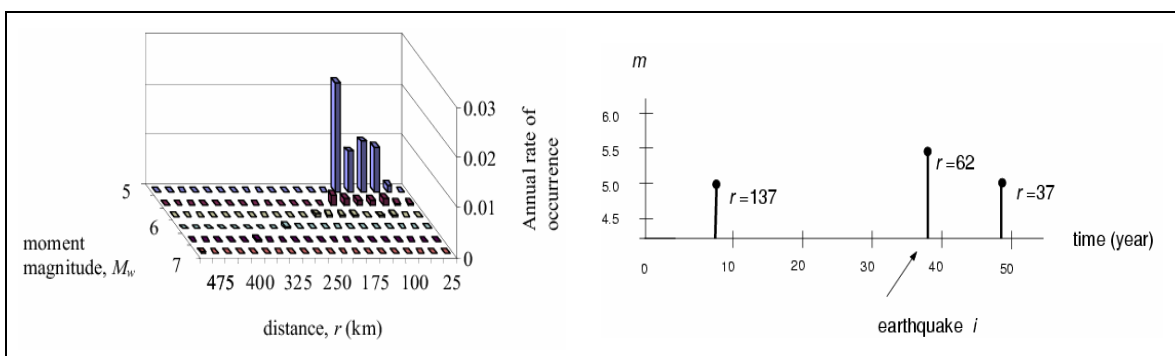


Figure 3. Seismic hazard for NYC

Two limit states, representing moderate and extensive damage, for the responses of components C_1 and C_2 , are given in Table 2.

Table 2. Performance criteria

| Damage state | Displacement response of C_1 | Velocity response of C_2 |
|--------------|--------------------------------|----------------------------|
| Moderate | 0.5 | 0.4 |
| Extensive | 1.0 | 0.8 |

The parameters of the financial model are shown in Table 3.

Table 3. Financial model

| Interest rate (%) | Discount rate (%) | Percent financed | Repair costs (\$) | | Rehabilitation costs (\$) |
|-------------------|-------------------|------------------|-------------------|-----------|---------------------------|
| | | | Moderate | Extensive | |
| 0.12 | 0.15 | 0.60 | 25,000 | 75,000 | 50,000 |

Results

The fragility surfaces for the components C_1 and C_2 and for the nonstructural system NS are obtained for the two rehabilitation alternatives for each damage state. Fragility surfaces for the *no rehabilitation* case and for *extensive* damage state are shown in Figure 5. Cost histograms for the two rehabilitation strategies are given in Figure 6.

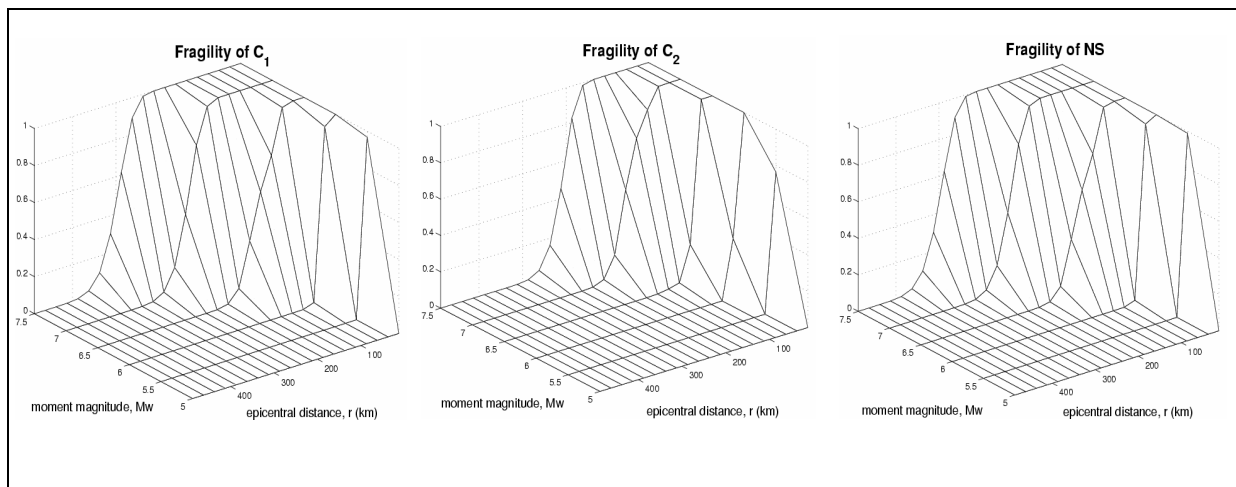


Figure 5. Fragility surfaces

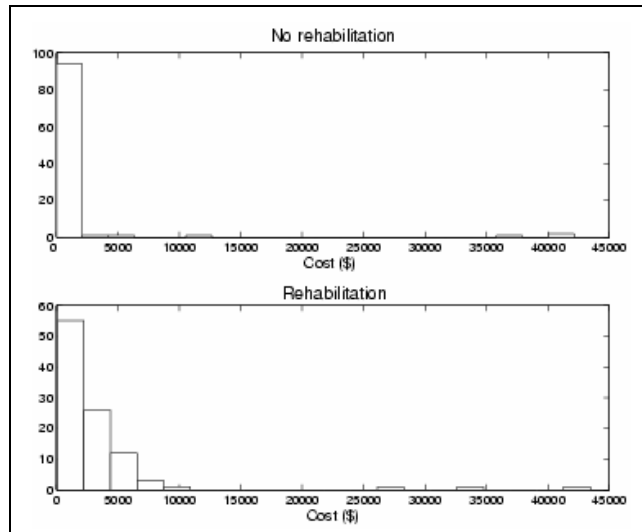


Figure 6. Cost histograms

Conclusions

A methodology for assessing the seismic performance of a system with structural and nonstructural components is presented. The methodology uses system properties, characterization of the seismic hazard, and performance criteria to assess the system performance through fragility analysis and loss estimation. A numerical example is presented. Two retrofitting strategies for the nonstructural system, representing a water distribution system, are considered: *no rehabilitation* and *rehabilitation*.

The optimal strategy for the water distribution system is *no rehabilitation*.

Acknowledgements

This research was carried out under the supervision of Dr. M. Grigoriu, and primarily supported by the Earthquake Engineering Research Centers Program of the National Science Foundation, under award number EEC-9701471 to the Multidisciplinary Center for Earthquake Engineering Research.

References

- HAZUS (1999): *HAZUS 99-Estimated annualized earthquake losses for the United States*. Federal Emergency Management Agency.
- Badillo-Almaraz H (2003): *Seismic fragility testing of suspended ceiling systems*. Master's Thesis, Department of Civil, Structural and Environmental Engineering, University at Buffalo.
- Grigoriu M, Waisman F (1998): Seismic reliability and performance of nonstructural components. *ATC-29-1, Seminar Technical Papers*, 337-348.

Papageorgiou AS, Aki K (1983a): A specific barrier model for the quantitative description of the inhomogeneous faulting and the prediction of strong ground motion. Part I. Description of the model. *Bulletin of the Seismological Society of America*, **73**, 693-722.

Papageorgiou AS, Aki K (1983b): A specific barrier model for the quantitative description of the inhomogeneous faulting and the prediction of strong ground motion. Part II. Applications of the model. *Bulletin of the Seismological Society of America*, **73**, 953-978.

Veneziano D, Grigoriu M, and Cornell A (1977): Vector process models for system reliability. *Journal of the Engineering Mechanics Division*, 441-460.

Issues of Seismic Response and Retrofit for Critical Substation Equipment

Ali Ashrafi

Graduate Student, Department of Civil and Environmental Engineering, New Jersey Institute of Technology

Research Supervisor: M. Ala Saadeghvaziri, Professor

Summary

This study focuses on a means to reduce the seismic hazard for transformer-bushing systems and different issues of the response and rehabilitation of transformers. The primary means of seismic mitigation investigated is the use of Friction Pendulum System (FPS) bearings to seismically isolate transformers. This is done by developing a finite element model representing the behavior of FPS bearings and implementing this model in an ADINA finite element package for further use in analytical studies. This model is used to study the behavior of isolated primary-secondary systems and the effects of parameters like different FPS radii or vertical excitations. Also studied are the effects of isolation on forces applied to the foundations and the corresponding design of foundations compared to the commonly used fixed-base forces. Further, the interaction of transformer-bushings with interconnecting equipment in the substation is studied and corresponding graphs indicating the amount of required slack in connecting cables are presented. Finally, the behavior of internal components of transformers under seismic excitation has been studied. Possible failure and damage modes are identified and a model is developed and analyzed to assess damage risk.

Introduction

Electric substations are among the most important parts of any electric power network. In societies deeply dependent on electric energy, any damage to these substations, or anything interrupting their functioning, has immense adverse effects on the society. Such effects include economic damage, disruption of life, interruption in provision of services, and safety problems. Especially in case of earthquakes, the uninterrupted functioning of electric power systems is an integral condition for all activities aimed at recovery, restoration, and reconstruction of the seismically damaged environment.

The objective of this research is to develop the tools and a framework to evaluate and assess the seismic performance of various substation components and the influence of their interaction on the response of the system as a whole. This research is also intended to evaluate the application of technologies to improve the seismic resiliency of substations and to perform research addressing structural and functional problems that are unique to a substation facility.

This research deals with different issues of behavior and improvement of electric substations under earthquake conditions (Ashrafi 2003). Transformers and bushings are diagnosed as the most important components of an electric substation. Hence, the study is focused on a means to reduce the seismic hazard to transformer-bushing systems and different issues concerning the response and rehabilitation of transformers. The primary means of seismic mitigation chosen here is the use of the Friction Pendulum System to seismically isolate transformers. This job is done by developing a finite



Figure 1. Typical substation

element model representing the behavior of FPS bearings and implementing it in the ADINA finite element package for further use in analytical studies. This element is used to study the behavior of the isolation system on primary-secondary system responses for a wide range of frequencies with emphasis on frequencies close to those of real transformers and bushings. The effects of parameters such as FPS radii, and vertical excitation on different responses are studied. Also studied are the effects of isolation on forces applied to the foundation and the corresponding design of the foundation, compared to the commonly used fixed-base forces. Comparisons are made in terms of foundation cost and size and economic benefits of use of FPS. Furthermore, the interaction of transformer-bushing with interconnecting equipment in the substation is studied and interaction effects on various elements are evaluated. Corresponding graphs are provided showing the amount of slack required for different levels of peak ground acceleration and FPS radius. The seismic behavior of internal components of transformers is also investigated. Possible modes of damage and failure are identified for the internal components and seismic analyses are performed to assess the risk.

Details and Results

Studying the behavior of a complex structure isolated through the use of an FPS requires an analytic model that can take into account complex behavior on a curved low-friction surface including the effects of changes in normal force, interaction of friction behavior in different directions, changes in friction behavior due to change in sliding velocity and normal force, and large displacement effects. This model should be accompanied by a structural modeling tool that permits modeling of nonlinear structures with all their details. Hence, the behavior of the FPS is modeled through a finite element model using the user-supplied element subroutine CUSERG in ADINA.

The response of a wide range of fixed and isolated primary-secondary systems is analyzed. The system characteristics were chosen based on previous studies (Ersoy 2002, Gilani et al., 1999) in such a way to represent the actual transformer and bushing characteristic range. The primary systems are also flexible in the vertical direction to include the effects of vertical excitation in different response parameters as well. The results show the effectiveness of FPS in reducing bushing response for all frequencies. Isolation is effective, even for high system frequencies, and prevents bushing response resonance when its frequency is close to that of the transformer. The base shear

force and response of the transformer are also reduced considerably by use of FPS. Figure 2 shows the bushing response for bushings mounted on a transformer with a horizontal frequency of 8 Hz.

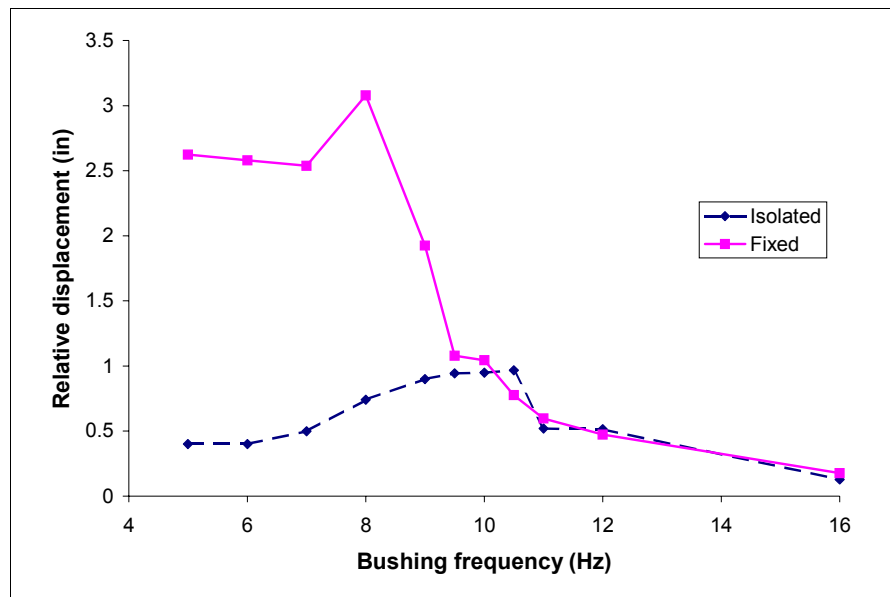


Figure 2. Response of a bushing mounted on a transformer

The foundation design is performed for fixed and isolated cases and it is observed that isolation can make the footing size much smaller and remove the need for big piles that can cost \$50,000 to \$100,000. This might make the use of FPS economical, even on initial cost basis.

To study the interaction between transformer-bushing and other interconnecting equipment, a simplified model is used. The cable connection to the interconnecting equipment can be taut or have different amounts of slack. The interaction between transformer-bushing and interconnecting equipment is observed to have an adverse effect on different responses, particularly bushing response. This effect exists independent of the relative value of the FPS frequency to that of the interconnecting equipment. This phenomenon is even observed when these frequencies are equal. The FPS response is the predominant factor determining the behavior of the various interacting components. Figure 3 shows the significant effects on bushing and interconnecting equipment, caused when the FPS slides away from the interconnecting equipment, causing tension loads in the connecting cable. Even the slightest interaction has significant adverse effects. Therefore, interaction of the transformer-bushing with the interconnecting equipment must be prevented at any cost. One way to insure this is to provide a slack equal to the sum of the maximum absolute values of FPS and the interconnecting displacements in the connecting cable. To help choose the appropriate FPS radius and slack amount, numerous analyses were performed for several earthquake records and different soil conditions, FPS radii, and ground accelerations. Graphs are developed showing the FPS displacement and the inertia reduction for different situations and suggestions are made, based on these graphs, on how to choose the proper FPS radius. Figure 4 shows such a graph, providing the average inertia reduction versus ground acceleration for records on soil.

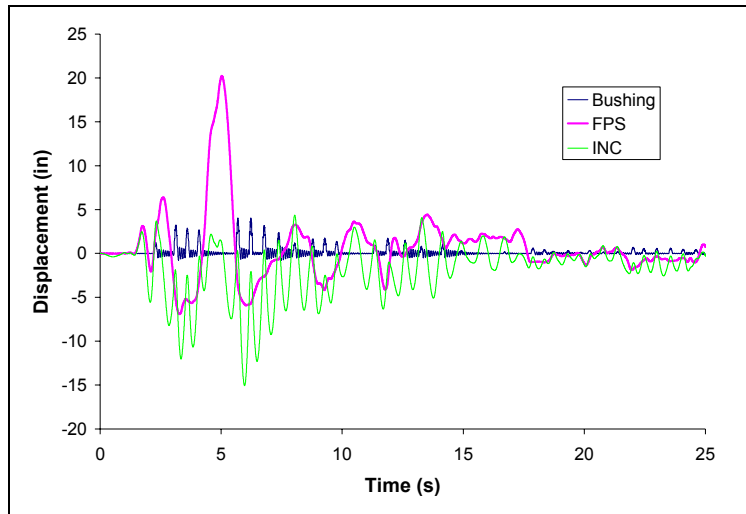


Figure 3. Time history responses in the interaction of transformer-bushing and interconnecting equipment

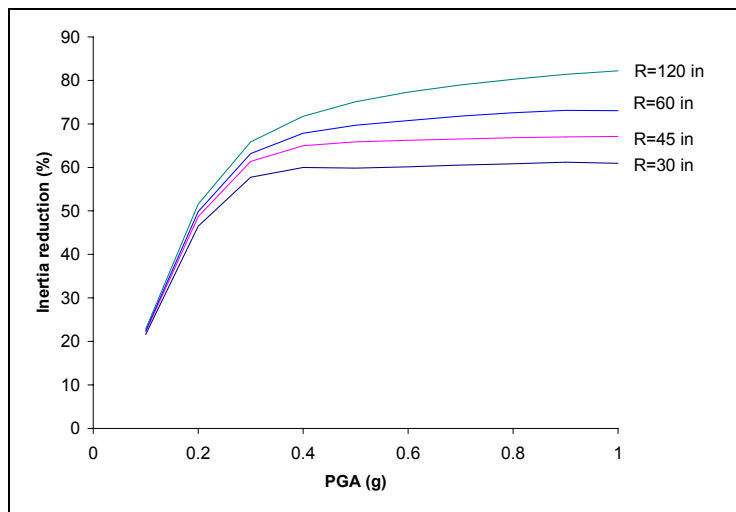


Figure 4. Average inertia reduction versus peak ground acceleration for soil

The seismic behavior of internal components of a transformer is studied to ensure that they are not structurally damaged and can continue their electrical function after an earthquake. Four modes of damage and failure are identified for the internal components, of which the sliding of key spacers and loss of close fitting tolerances between limbs and yokes are investigated as the most critical cases. Both of these damage modes can be attributed to loss of prestressing. The tensile forces in windings and core caused by vertical excitation are modest, and are easily offset by the typical prestressing forces. Therefore, it seems that failures of internal components in earthquakes for structural reasons is very unlikely, unless the prestressing is lost before the earthquake occurs. This also suggests that more focus should be put on other reasons to explain the occasional internal damage observed in past earthquakes in the form of slipping of key spacers. This subject is still under study and further analyses are being conducted. Figure 5 shows the internal components of a transformer.



Figure 5. Internal components of a transformer

Concluding Remarks

Proper functioning of transformers and bushings during and after an earthquake is crucial to the electric power network. The Friction Pendulum System is shown to be a good seismic improvement and retrofit tool for transformers. Its use considerably reduces the response of a bushing and transformer and the forces transferred to the foundation. This reduction will also result in large reductions in footing size and economic savings. Use of the FPS should be accompanied by provision of sufficient slack in the connecting cable to prevent any interaction with interconnecting equipment. The initial studies on the behavior of the internal components of transformers show no damage, except when the prestressing is lost in the core before the earthquake. The behavior of the internal components still requires further study, which is in progress.

Acknowledgements

This research was carried out under the supervision of Professor M. Ala Saadeghvaziri, and primarily supported by the Earthquake Engineering Research Centers Program of the National Science Foundation, under award number EEC-9701471 to the Multidisciplinary Center for Earthquake Engineering Research.

References

Ashrafi A (2003): *Issues of seismic response and retrofit for critical substation equipment*, Masters Thesis, New Jersey Institute of Technology.

Ersoy S (2002): *Seismic response of transformer bushing systems and their rehabilitation using friction pendulum system*, Doctoral Dissertation, New Jersey Institute of Technology.

Gilani AS, Whittaker AS, Fenves GL, Fujisaki E (1999): *Seismic evaluation of 550-kV porcelain transformer bushings*. Report PEER 1999/05, Pacific Earthquake Engineering Research Center, University of California, Berkeley.

Post-Earthquake Lifeline Service Restoration Modeling

Zehra Cagnan

Graduate Student, School of Civil and Environmental Engineering, Cornell University

Research Supervisor: Rachel Davidson, Assistant Professor

Summary

In this study, a simulation-based methodology is being developed to model post-earthquake restoration processes of lifelines as part of the MCEER research on Los Angeles Department of Water and Power's (LADWP's) electric and water supply systems. Post-earthquake restoration models play an important role in estimating the economic impact of earthquake damage to lifeline systems. This paper begins with a discussion of the available restoration modeling approaches, listing advantages and disadvantages of each. The new simulation-based methodology is described, and key innovations that distinguish it from previous approaches are explained. Finally, plans for possible future extensions are discussed.

Introduction

Following an earthquake, loss of infrastructure function can significantly disturb normal economic activity. The duration of functional loss is a critical determinant of the magnitude of economic disruption. Because of this, models of post-earthquake restoration processes are important in evaluating economic losses.

This study is part of the MCEER research that aims to develop and demonstrate an advanced, integrated earthquake loss estimation methodology for urban lifeline systems. The MCEER earthquake loss estimation methodology was first developed as part of the Memphis Light, Gas and Water Division (MLGW) demonstration project (Chang et al., 1996, 1999 and 2002). The current study is part of the LADWP demonstration project which is a continuation of MLGW project. The MCEER loss estimation methodology consists of three main models: (1) damage estimation model, (2) restoration model, and (3) direct-indirect economic loss estimation model. For each scenario earthquake, the loss estimation process from damage to direct economic loss is simulated multiple times within a Monte Carlo framework. Initial damage and outage patterns obtained using a Monte Carlo simulation approach (Shinozuka 1994) are the input to the restoration model. Updated damage patterns are the output of the restoration model. For updated damage patterns, flow and connectivity analyses are carried out to produce the corresponding updated outage patterns. These results are then input into the direct economic loss model of business interruption. Using average outage and direct economic loss data, indirect economic loss is evaluated. Finally, by combining these estimates with probabilistic hazard data, expected annual loss is obtained (Chang et. al., 1999).

The objective of this study is to develop improved models of the post-earthquake restoration processes of the electric and water supply systems. Each model uses estimates of physical damage to

the system under consideration, and an understanding of the repair and recovery operations, to estimate expected restoration time, as well as the uncertainty surrounding this estimate. In these models, restoration processes are disaggregated both spatially and temporally, which enables incorporation of the temporal and spatial dimension of economic loss. Decision variables, such as repair prioritization plans and mutual aid agreements, are considered explicitly.

Successful completion of this study will help to improve the accuracy of estimates of economic loss due to earthquake damage, and will help guide improvement of the post-earthquake restoration processes for electric and water supply systems. Studying the effects of the decision variables on restoration time will help the LADWP to improve its post-earthquake restoration plans.

This study includes four main phases: (1) background research on available post-earthquake lifeline restoration modeling approaches and on other parts of the MCEER LADWP project with which this study directly interfaces, (2) information collection on how restoration takes place in reality, (3) development of restoration models, and (4) comparison of results with documented system performance in the 1994 Northridge and 1971 San Fernando earthquakes. Phases 1 and 2 of this study have been completed, and phase 3 is currently under development. The work that has been completed so far, and the future possible extensions of this study, are discussed in the following sections.

Previous Restoration Modeling Approaches

Four different approaches have been used previously in modeling post-earthquake lifeline restoration. The first method is based on statistical restoration curves. The other empirical approach is based on resource constraints. There also exist more theoretical approaches, such as, the Markov process approach and the network approach. The latter is mainly used for developing optimum restoration strategies. Each of these approaches is explained in more detail below.

In the statistical restoration curves approach, data obtained from previous earthquakes and/or from expert opinion are employed to fit restoration curves. This approach has been used in previous studies, such as, ATC-25-1 (1992), Chang et al. (1996) and Nojima et al. (2001). In ATC-25, restoration curves are constructed by using data sources excerpted from ATC-13 (1985) that are based on regression analysis of expert-opinion data obtained through an iterative questionnaire process. In Nojima et al. (2001), Gamma distributions are used as restoration curves, and parameters of the distributions are estimated as a function of damage level using data from previous earthquakes. Nojima et al. (2001) enables breaking down the single “system restoration curve” into many restoration curves depending on seismic intensity, and hence, spatially disaggregates the restoration process. In the statistical restoration curves approach, the primary determinant of system restoration time is ground shaking intensity. Issues such as personnel constraints and opportunities to reduce losses by speeding up or optimizing restoration are not considered (Chang et al., 1999).

In the deterministic resource constraint approach, the evolution of the restoration is modeled in a simplified way. The number of repairs that can be made in any time period is specified according to the number of repair personnel available. This approach allows depiction of restoration progress across both time and space, and enables exploring earthquake loss reduction in a variety of new directions, such as, speeding up total restoration times, prioritizing spatial sequencing of restoration, and developing mutual aid agreements (Chang et al., 1999). This approach has been employed in Isumi and Shibuya (1985), Ballantyne (1990), HAZUS – water distribution system section (NIBS 1997), and in Chang et al. (2002). In these studies, restoration processes are modeled

deterministically, so the uncertainty associated with expected restoration time is not estimated. It has also been assumed that restoration processes involve only the repair phase. However, restoration processes are more complex than that in reality; they include phases such as damage assessment, and initial inspection as well.

Hoshiya (1981) and Isoyama et al. (1985) model an individual lifeline's functional performance in the post-earthquake period using discrete-state, discrete-transition Markov processes. In later studies, such as Kozin and Zhou (1990) and Zhang (1992), a discrete-state, discrete-transition Markov process is employed to model evolutionary restoration process of various lifelines together as a system. Zhang (1992) takes into account the effects of interactions between various lifelines as well, by considering the transition probability of each subsystem not only as function of allocated resource but also as a function of the states of other subsystems. The Markov processes approach requires that the model parameters and probability values are estimated accurately. Even if adequate databases are established for this purpose, converting available data into the model parameters and probability values can be a real challenge.

In the network approach, a system consists of a supply node and a number of demand nodes. These are connected to each other via links that can be damaged or fully functional. In Nojima and Kameda (1992), graph theory (Minimum Spanning Tree and Shortest Path Tree) and optimization theory (Horn's Algorithm (Horn 1972)) are combined to develop an optimal restoration plan. In Okumura (1994), the proposed optimal repair sequencing method is based on the connectivity of a tree-shaped network and involves simplified flow analysis of the network as an approximate global optimization strategy. The network approach enables both spatial and temporal disaggregation of restoration processes and consideration of the effects of resource constraints. The main disadvantage is that the system (as source node, demand nodes, and links in between) and restoration process (only link repairs considered, other phases ignored) have to be simplified to be able to model the evolution of restoration with this approach.

Proposed Restoration Modeling Methodology

In this study, the post-earthquake restoration processes are modeled for electric and water supply systems by discrete event simulation (DES). DES is a dynamic simulation approach which can be either deterministic or stochastic. This simulation technique bases simulations on the events that take place in the simulated system and then recognizes the effects that these events have on the state of the system (Law and Kelton, 1991). In DES, system state changes occur instantaneously at specific points in time. The proposed methodological approach for modeling post-earthquake restoration processes of lifelines includes a number of improvements and expansions to the previously developed approaches.

In the proposed modeling approach, the restoration process does not only depend on the damage state but also on the available repair resources. Hence, the effects of resource constraints are considered. It allows spatial and time wise depiction of the restoration process, as well as explicit consideration of the effects of decision variables, such as repair prioritization plans and mutual aid agreements.

The proposed methodology is not deterministic. Statistical variability and uncertainties associated with key parameters, such as, post-earthquake damage inspection durations, start and finish time for repair of each damaged component, time needed for replacement of components that cannot be

repaired, and resource allocations are taken into account by defining these parameters as probability distributions. This enables quantification of uncertainty in the final restoration time estimates.

The key elements in a discrete event simulation are *variables* and *events*. Variables (e.g., damage state of various system components) define the system state and simulations are based on keeping track of changes in certain variables as time proceeds. Whenever an event (e.g., repair of a component) occurs, the values of variables are changed or updated. Objects of interest in the real system exist as *entities* in the simulation model (e.g., substations, pumping stations). *Resources* (e.g., repair teams) are a special type of entity: they provide service (e.g., damage assessment) to other objects of the system. Variables can be of two kinds, global variables that apply to the whole system, and attributes that are variables attached to entities. The one-to-one mapping between objects in the complex system being modeled and their abstractions in the simulation enables modeling the system under consideration quite accurately without the need to make considerable simplifications.

Table 1 lists the main restoration model components for electric power and water supply systems. Each entity obtains resources based on its priority level, which is a function of its attributes. Once an entity gets a resource, the resource becomes unavailable to other entities for the duration of the restoration phase it is in charge of. These durations are defined as random variables in the simulation, as mentioned above. When the resource completes its duty, the attributes related to the corresponding restoration phase are updated, and the resource moves to the next entity. Each simulation continues until the restoration process is complete. For each initial damage pattern, the restoration simulation is repeated many times; hence, uncertainty associated with restoration time estimates is quantified.

Table 1. List of electric and water supply system model components

| | Electric Power System | Water Supply System |
|-------------------|---|---|
| Entity | Substations Power Generation Stations | Pipes Pumping Stations Tanks Reservoirs Regulator Stations |
| Attributes | Damage Level Status (on/off) after the Earthquake Status (on/off) before the Earthquake Distance to Earthquake Epicenter | Damage Level Distance to Earthquake Epicenter Distance to Source Status after the Earthquake |
| Resource | On-duty Substation Operators On-duty Generation Station Operators Off-duty Substation Operators Damage Assessment Teams Repair Teams Repair Material | On-duty Personnel at Reservoirs Reservoir Inspection Teams Damage Assessment Teams Transmission Operators Repair Teams Repair Material |
| Event | Inspection Damage Assessment Repair Re-energizing | Inspection Valve Shut Down Damage Assessment Repair |

The model development phase of this study is still in progress, so no simulation outputs are presented here. The expected output of each simulation is a time history of the restoration process. This includes information about both the system components and the repair crews, for example at which instant of the repair process, repair of each system component is completed, what is the utility level of each repair crew, etc. Using this information, spatially disaggregated restoration curves will be developed, from which estimates of overall system restoration time and uncertainty associated with these estimates will be obtained.

Two possible directions in which the current study can be expanded in the future are: (1) by extending the proposed methodology to develop a multi-lifeline restoration model that takes into account interactions between lifeline systems, and (2) by developing and implementing optimization methods to examine both optimal post-earthquake restoration of lifelines systems and optimal pre-earthquake policies. Simulation models are usually built by specifying the entities in a system and the processes they follow as they go through the system. This implementation strategy is known as a process-interaction world view, and it will enable development of a multi-lifeline restoration model that very easily takes into account interaction effects. The second possible future expansion involves the development of an enhanced approach for discrete, simulation-based optimization. Application of this methodology would be beneficial to LADWP by enabling them to improve their post-earthquake restoration capabilities. It would also improve the earthquake resiliency of the community, by reducing the economic losses associated with earthquakes.

Concluding Remarks

A simulation-based methodology being developed for modeling post-earthquake restoration processes of electric power and water supply systems is described. Key innovations that distinguish this methodology from previously developed methodologies are: (1) temporal and spatial disaggregation of the restoration process, which enables incorporation of the temporal and spatial dimension of loss, (2) explicit consideration of the decision variables, which enables exploration of how post-event mitigation strategies, such as, mutual aid agreements and spatially prioritized restoration can reduce total economic loss, and (3) incorporation of statistical variations and uncertainties associated with key factors, which enables quantification of uncertainty associated with restoration time estimates.

Acknowledgements

This research was carried out under the supervision of Prof. Rachel Davidson of Cornell University, and primarily supported by the Earthquake Engineering Research Centers Program of the National Science Foundation, under award number EEC-9701471 to the Multidisciplinary Center for Earthquake Engineering Research.

References

Applied Technology Council (ATC) (1985): *Earthquake damage evaluation data for California*. Report No: ATC-13, Redwood City, CA.

ATC (1992): *A model methodology for assessment of seismic vulnerability and impact distribution of water supply systems*. Report No: ATC-25-1, Redwood City, CA.

Ballantyne DB (1990): *Earthquake loss estimation modeling of the Seattle water system*. Report to the U.S. Geological Survey, Federal Way, WA.

Chang SE, Svelka WD, Shinozuka M (2002): Linking infrastructure and urban economy: simulation of water-disruption impacts in earthquakes. *Environment and Planning B: Planning and Design* 2002, **29**, 281-301.

Chang SE, Seligson HA, Eguchi RT (1996): *Estimation of the economic impact of multiple lifeline disruption: Memphis Light, Gas and Water division case study*. Technical Report NCEER-96-0011, National Center for Earthquake Engineering Research, University at Buffalo.

Chang SE, Shinozuka M, Svekla W (1999): Modeling post – disaster urban lifeline restoration. in W.M. Elliott and P. McDonough, eds. *Optimizing Post Earthquake Lifeline System Reliability: Proceedings of the 5th U.S. Conference on Lifeline Earthquake Engineering*. ASCE Technical Council on Lifeline Earthquake Engineering Monograph (16), 602-611.

Horn WA (1972): Single-machine job sequencing with treelike precedence ordering and linear delay penalties. *SIAM, Journal of Applied Mathematics*, **23** (2) 189-202.

Hoshiya M (1981): Seismic damage restoration of underground water pipeline. *Proceedings of US-Japan Cooperation Res. Seismic Risk Analysis and Its Application to Lifeline System*, 229-244, Honolulu.

Isoyama R, Iwata T, Watanabe T (1985): Optimization of post-earthquake restoration of city gas systems. *Proceeding of the Trilateral Seminar Workshop on Lifeline Earthquake Engineering*, 43-57, Taipei, Taiwan.

Isumi M, Shibuya T (1985): Simulation of post earthquake restoration for lifeline systems. *International Journal of Mass Emergencies and Disasters*, 87-105.

Kozin F, Zhou H (1990): System study of urban response and reconstruction due to earthquake. *Journal of Engineering Mechanics*, ASCE, **116** 1959-1972.

Law A, Kelton WD (1991): *Simulation modeling and analysis*. McGraw-Hill, N.Y., USA.

National Institute of Building Sciences (NIBS) (1997): *HAZUS technical manual*. Washington, DC: NIBS.

Nojima N, Kameda H (1992): Optimal strategy by use of tree structure for post-earthquake restoration of lifeline network systems. *Proceedings of the 10th World Conference on Earthquake Engineering*, 5541-5546, Balkema, Rotterdam.

Nojima N, Ishikawa Y, Okumura T, Sugito M (2001): Empirical estimation of lifeline outage time in seismic disaster. *Proceedings of U.S.-Japan Joint Workshop and Third Grantee Meeting*, U.S.-Japan Cooperative Research on Urban Earthquake Disaster Mitigation, 516-517, Seattle, WA.

Okumura T (1994): Importance index of damaged lifeline-network components. *Structural Safety and Reliability: Proceedings of the 6th International Conference on Structural Safety and Reliability*, 2187-2194, Innsbruck, Austria.

Shinozuka M (1994): GIS applications in lifeline earthquake engineering, *Proceedings of the Second China - Japan - US Trilateral Symposium on Lifeline Earthquake Engineering*, Xi'an, China, 223-230.

Zhang RH (1992): Lifeline interaction and post earthquake urban system reconstruction. *Proceedings of 10th World Conference on Earthquake Engineering*, 5475-5480, Balkema, Rotterdam.

Fragility Analysis of a Water Supply System

Anita Jacobson

Graduate Student, Department of Civil and Environmental Engineering, Cornell University

Research Supervisor: Mircea Grigoriu, Professor

Summary

The seismic performance of a water supply system depends on the individual performance of its components and on system configuration. Components of a water supply system include pipes, tanks, tunnels, reservoirs, and other components. Complete fragility analysis is performed on pipes, including analysis of pipes under seismic wave hazard and fault displacement hazard, two commonly occurring types of hazard following a seismic event. The influence of seismic wave hazard is assumed to be more prominent for pipes located far away from seismic source, while fault displacement hazard is assumed to affect only pipes located on seismic sources, i.e., faults. Fragility information for other components is taken from the literature. Ongoing work focuses on performing Monte Carlo simulation and hydraulic analysis to generate fragility information on a damaged water supply system.

Introduction

The seismic performance of a water supply system depends on the individual seismic performance of its components (e.g., pipes, tanks, reservoirs, and other components). A methodology is developed for assessing the seismic performance of water supply systems by using fragility surface; providing the failure probability of the system as a function of seismic moment magnitude m and site-to-source distance r . Seismic performance of pipelines is analyzed under the influence of seismic wave and fault displacement to develop the fragility surfaces for pipes. Fragility data for other components of the water supply system are taken from the literature.

Combining flow analysis and Monte Carlo simulation, a damaged water supply system can be analyzed in order to produce a fragility surface for the system. Life cycle seismic hazard analysis and cost benefit analysis can be incorporated to optimize a retrofitting scheme appropriate for the damaged system.

Motivation for Using Fragility Surface

The seismic performance of components of a water supply system usually involves only one seismic parameter, such as peak ground acceleration (PGA). This type of characterization can be misleading; for example, the same PGA can lead to varying degrees of damage states. Fragility surface, which provides the failure probability of a system as a function of two or more seismic parameters, can yield a better representation of the seismic performance of a water supply system.

Methodology

Seismic wave and fault displacement are two types of seismic hazards considered herein to assess the seismic performance of a water supply system. Two types of ground motion excitation are generated: (1) far-fault ground motion for site-to-source distance more than 15 km (Papageorgiou and Aki, 1983a and b), and (2) near-fault ground motion for site-to-source distance less than or equal to 15 km (Mavroeidis and Papageorgiou, 2003).

Generation of fragility information for a pipe involves the calculation of the probability that some specified limit states are violated (O'Rourke, Grigoriu, and Khater, 1985). The typical limiting parameter for a pipe is the pipe limit strain ϵ_{limit} . The limit strain is used to calculate the limiting force F_{limit} for seismic wave analysis, and the limiting fault displacement D_{limit} for fault displacement analysis. Fragility analysis is performed by using Monte Carlo simulation to generate ground motion time history, and to calculate maximum force F_{max} for seismic wave analysis and maximum fault displacement D_{max} for fault displacement analysis. Failure is defined when response of the pipe is greater than the limit state. Figure 1 is a flowchart of pipe fragility analysis.

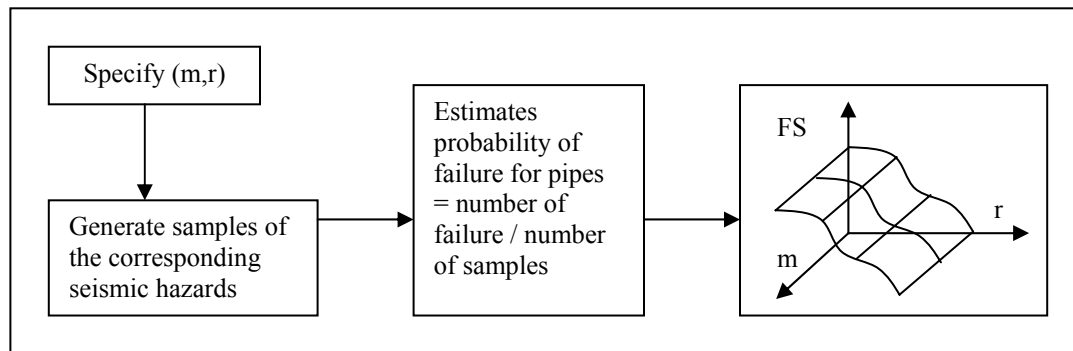


Figure 1. Flowchart of fragility analysis of pipes

An example of a fragility surface generated for a pipe under seismic wave analysis is shown in Figure 2. The limiting strain ϵ_{limit} of the pipe is assumed to be 0.025%. The pipe is made of steel with a modulus of elasticity $E = 29000$ ksi, 12 inch diameter and a thickness of $\frac{1}{2}$ inch. The center of the pipe is located 4 ft below the soil surface. The soil is categorized as stiff soil with a unit weight of 120 pcf, a coefficient of lateral earth pressure at rest of $K_0 = 1$, an angle of friction of 30 degrees, an apparent wave propagation of 2500 ft/s, and an angle between wave propagation and pipe of 0 degrees.

Fragility data for two other components of water supply system, tunnels and tanks, are provided by the American Lifelines Alliance (ALA 2001). Table 1 gives the complete tank database per ALA 2001. Table 2 gives the complete bored tunnels database per ALA 2001. Damage state one (DS1) indicates no damage, DS2 slight damage, DS3 moderate damage, DS4 extensive damage, and DS5 indicates total failure or collapse of the component.

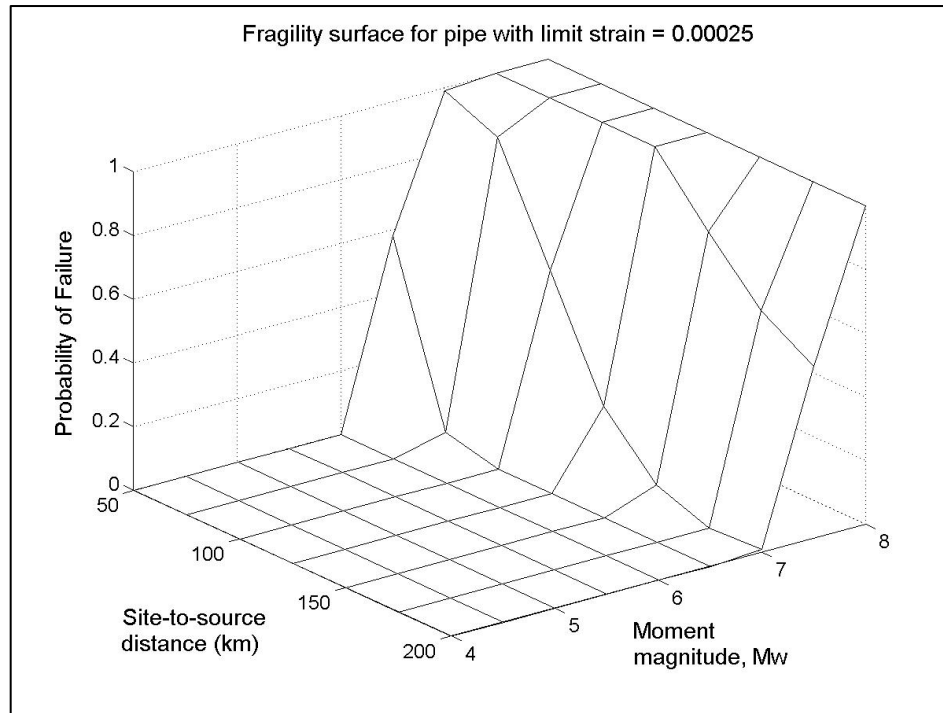


Figure 2. An example of fragility surface for pipe under seismic wave analysis

Table 1. Complete tank database

| PGA (g) | All Tanks | DS = 1 | DS = 2 | DS = 3 | DS = 4 | DS = 5 |
|---------|-----------|--------|--------|--------|--------|--------|
| 0.10 | 4 | 4 | 0 | 0 | 0 | 0 |
| 0.16 | 263 | 196 | 42 | 13 | 8 | 4 |
| 0.26 | 62 | 31 | 17 | 10 | 4 | 0 |
| 0.36 | 53 | 22 | 19 | 8 | 3 | 1 |
| 0.47 | 47 | 32 | 11 | 3 | 1 | 0 |
| 0.56 | 53 | 26 | 15 | 7 | 3 | 2 |
| 0.67 | 25 | 9 | 5 | 5 | 3 | 3 |
| 0.87 | 14 | 10 | 0 | 1 | 3 | 0 |
| 1.18 | 10 | 1 | 3 | 0 | 0 | 6 |
| Total | 531 | 331 | 112 | 47 | 25 | 16 |

Table 2. Complete bored tunnels database

| PGA (g) | All Tunnels | DS = 1 | DS = 2 | DS = 3 | DS = 4 |
|---------|-------------|--------|--------|--------|--------|
| 0.07 | 30 | 30 | 0 | 0 | 0 |
| 0.14 | 19 | 18 | 1 | 0 | 0 |
| 0.25 | 22 | 19 | 2 | 0 | 1 |
| 0.37 | 15 | 14 | 0 | 0 | 1 |
| 0.45 | 44 | 36 | 6 | 2 | 0 |
| 0.57 | 66 | 44 | 12 | 9 | 1 |
| 0.67 | 19 | 3 | 7 | 8 | 1 |
| 0.73 | 2 | 0 | 0 | 2 | 0 |
| Total | 217 | 164 | 28 | 21 | 4 |

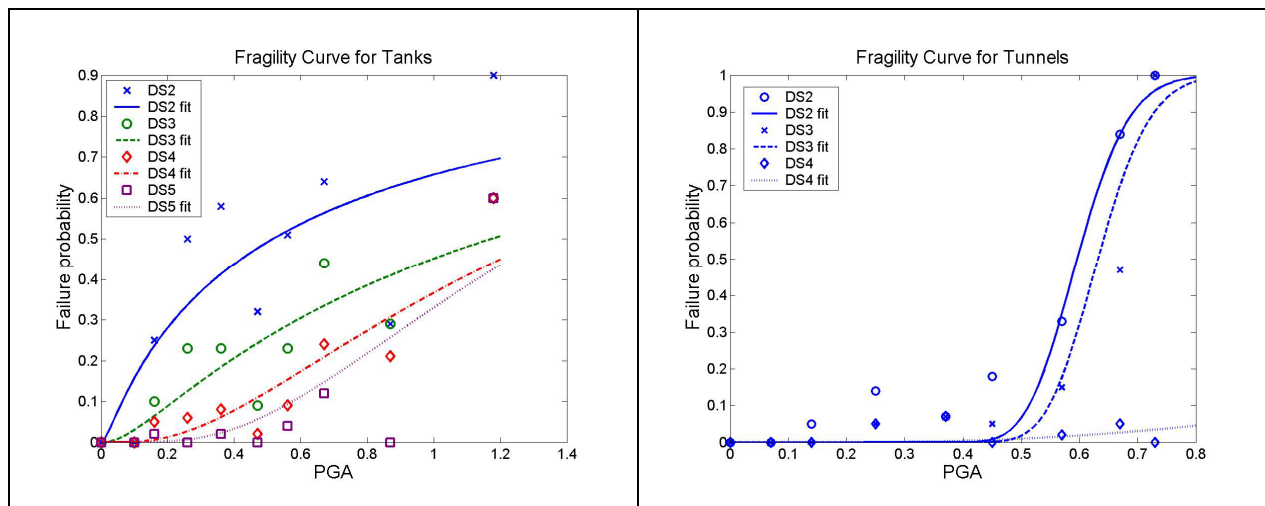


Figure 3. Fragility curves for tanks and bored tunnels

Based on the data given in Table 1 and Table 2, fragility curves for tanks and tunnels can be generated for the different damage states. Fragility curves provide the failure probability of a system (in this case tunnels and tanks) as a function of PGA. The fragility curves seen in Figure 3 are generated by curve fitting through the data by lognormal functions.

Future Works

The fragility of a water supply system will be generated based on the fragility information of its components. The methodology for the process is as follows:

1. Generate n damage states of a water supply system under a specified seismic magnitude m and site-to-source distance r and its corresponding components fragility information.
2. Perform hydraulic analysis on the damaged water supply system.
3. Check the satisfaction of system performance under some specified requirements.
4. Produce fragility surface for the overall system.

Figure 4 provides the flowchart of fragility analysis for water supply system.

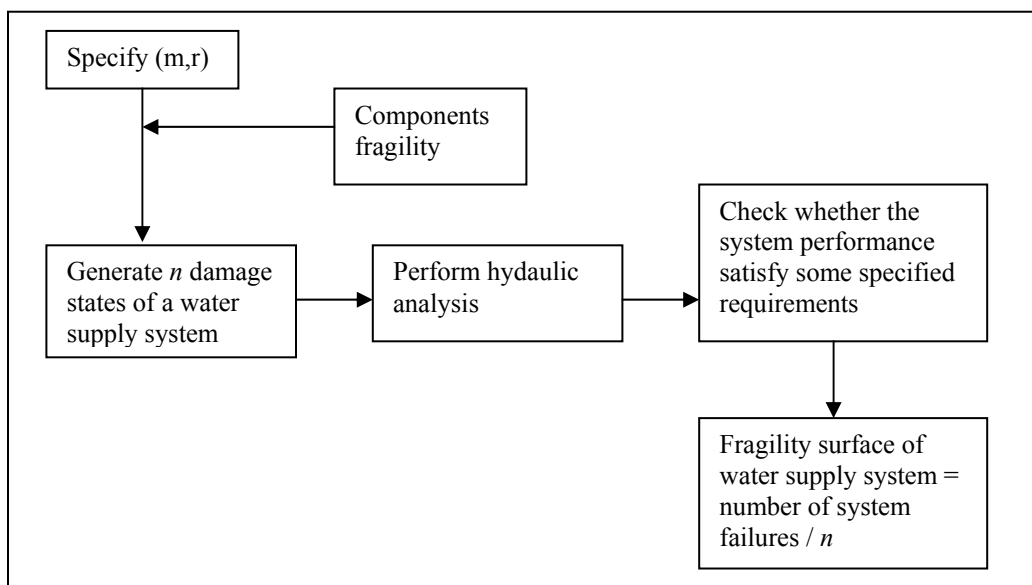


Figure 4. Flowchart of fragility analysis of water supply systems

Concluding Remarks

Fragility analysis has been performed on pipes under the influence of seismic wave hazard and fault displacement hazard. Fragility data for other components (e.g., tanks and tunnels) are taken from the literature. Ongoing work is on generation of fragility surface of a damaged water supply system using Monte Carlo simulation and hydraulic analysis.

Life cycle seismic hazard analysis and cost benefit analysis will be performed on the damaged system in order to optimize the retrofitting scheme for the water supply system.

Acknowledgements

This research was carried out under the supervision of Professor M.D. Grigoriu, and primarily supported by the Earthquake Engineering Research Centers Program of the National Science Foundation, under award number EEC-9701471 to the Multidisciplinary Center for Earthquake Engineering Research.

References

ALA (2001): American lifelines alliance. *Seismic Fragility Formulations for Water Systems*. ASCE.

Mavroeidis GP, Papageorgiou AS (2003): A mathematical representation of near-fault ground motions. *Bulletin of the Seismological Society of America*, **93** (3), 1099-1131

O'Rourke TD, Grigoriu MD, and Khater MM (1985): Seismic response of buried pipelines, *Pressure Vessel and Piping Technology - A Decade of Progress*. C. Sundararajan, Ed., ASME, New York, NY, 281-323.

Papageorgiou AS, Aki K (1983a): A specific barrier model for the quantitative description of inhomogeneous faulting and the prediction of strong ground motion. Part I, description of the model. *Bulletin of the Seismological Society of America*, **73** (3), 693-722

Papageorgiou AS, Aki K (1983b): A specific barrier model for the quantitative description of inhomogeneous faulting and the prediction of strong ground motion. Part II, application of the model. *Bulletin of the Seismological Society of America*, **73** (4), 953-978

Production Staff

- Jane E. Stoye, Managing Editor
- Michelle A. Zuppa, Layout and Design

Cover Images

Cover Images (from top left, then clockwise): A user interface of the Java-Powered Virtual Laboratory for conducting structural dynamic analysis discussed by Yong Gao, University of Illinois at Urbana-Champaign; Group photograph from the 2003 Tri-Center Field Mission to Italy; the simulator at the University at Buffalo on which Hiram Badillo-Almaraz, University at Buffalo, performed seismic fragility testing of suspended ceiling systems ; Ali Ashrafi, New Jersey Institute of Technology, discusses issues of seismic response and retrofit for critical substation equipment like this typical substation; Participants on the Field Mission to Italy studied damage to the University of D'Aquila; Jale Tezcan, Rice University, discusses evolutionary power spectrum estimation using harmonic wavelets in this example from the Kocaeli, Turkey earthquake of 1999; Students at the 2003 SLC retreat pose at Taughannock Falls in Ithaca, NY; Michael Pollino, University at Buffalo, analyzes seismic retrofit of bridge steel truss pier anchorage connections such as in the Lion's Gate Bridge in Vancouver, British, Columbia.

Acknowledgements

This work was supported primarily by the Earthquake Engineering Research Centers Program of the National Science Foundation under NSF Award Number EEC-9701471.

Any opinions, findings and conclusions or recommendations expressed in this material are those of the author(s) and do not necessarily reflect those of the National Science Foundation.



MULTIDISCIPLINARY CENTER FOR EARTHQUAKE ENGINEERING RESEARCH

A National Center of Excellence in Advanced Technology Applications

University at Buffalo, State University of New York

Red Jacket Quadrangle ■ Buffalo, New York 14261

Phone: (716) 645-3391 ■ Fax: (716) 645-3399

E-mail: mceer@mceermail.buffalo.edu ■ WWW Site <http://mceer.buffalo.edu>



University at Buffalo *The State University of New York*